

Finite element discretization of two-phase flow model

7.1 Introduction

In this chapter we treat finite element methods for the two-phase flow model in (6.59). We use a nested family of multilevel triangulations $\{\mathcal{T}_h\}$ as explained in Sect. 3.1. In our applications these grids will be locally refined in a (small) neighborhood of the interface. In Sect. 7.2 we discuss a finite element method for discretization of the level set equation. In Sect. 7.3 it is explained how for a resulting approximation ϕ_h of the level set function ϕ a corresponding approximation Γ_h (= approximate zero level of ϕ_h) of the interface Γ can be constructed. Other important issues related to the level set function, such as re-initialization, are treated in Sect. 7.4. Results of experiments with numerical methods applied to the level set equation are given in Sect. 7.5. In Sect. 7.6 a method for discretization of the surface tension force f_Γ is presented. An error analysis of this method is given in Sect. 7.7 and results of numerical experiments with this method are presented in Sect. 7.8. In Sect. 7.9 we treat a special finite element space for the discretization of the pressure variable. Results of numerical experiments with this space are given in Sect. 7.10. Finally, in Sect. 7.11 we apply the methods treated in this chapter for the discretization of the two-phase flow model (6.59).

7.2 Discretization of the level set equation

The level set equation is of linear hyperbolic type. It is well-known that standard conforming finite element discretization methods are in general not very suitable for such partial differential equations, since these methods can be unstable. There is extensive literature on finite element techniques for hyperbolic problems. We do not give an overview here, but refer to monographs in which this topic is treated, e.g., [108, 211, 206]. One popular strategy is to combine standard finite element spaces with a stabilization technique. A fundamental

stabilization method, that is very often used in practice, is the *streamline-diffusion finite element method* (SDFEM). We will apply this method for the discretization of the level set equation. In Sect. 7.2.1 we explain the basic idea of the technique using a simple 1D problem. In Sect. 7.2.2 we apply this method for the discretization of the level set equation.

7.2.1 Introduction to stabilization

We consider the very simple one-dimensional (hyperbolic) problem

$$\begin{aligned} bu'(x) + u(x) &= f(x), & x \in I := (0, 1), & \quad b > 0 \text{ a given constant,} \\ u(0) &= 0. \end{aligned} \tag{7.1}$$

For the weak formulation we introduce the Hilbert spaces

$$H_1 = \{v \in H^1(I) : v(0) = 0\}, \quad H_2 = L^2(I).$$

The norm on H_1 is $\|v\|_1^2 = \|v\|_{L^2}^2 + \|v'\|_{L^2}^2$. We define the bilinear form

$$k(u, v) = \int_0^1 bu'v + uv \, dx$$

on $H_1 \times H_2$.

Theorem 7.2.1 *Take $f \in L^2(I)$. There exists a unique $u \in H_1$ such that*

$$k(u, v) = (f, v)_{L^2} \quad \text{for all } v \in H_2. \tag{7.2}$$

Moreover, $\|u\|_1 \leq c\|f\|_{L^2}$ holds with c independent of f .

Proof. The proof is based on an application of Theorem 15.1.1. The bilinear form $k(\cdot, \cdot)$ is continuous on $H_1 \times H_2$:

$$|k(u, v)| \leq b\|u'\|_{L^2}\|v\|_{L^2} + \|u\|_{L^2}\|v\|_{L^2} \leq \sqrt{2} \max\{1, b\}\|u\|_1\|v\|_{L^2},$$

for $u \in H_1, v \in H_2$. For $u \in H_1$ we have

$$\begin{aligned} \sup_{v \in H_2} \frac{k(u, v)}{\|v\|_{L^2}} &= \sup_{v \in H_2} \frac{(bu' + u, v)_{L^2}}{\|v\|_{L^2}} = \|bu' + u\|_{L^2} \\ &= (b^2\|u'\|_{L^2}^2 + \|u\|_{L^2}^2 + 2b(u', u)_{L^2})^{\frac{1}{2}}. \end{aligned}$$

Using $u(0) = 0$ we get $(u', u)_{L^2} = u(1)^2 - (u, u')_{L^2}$ and thus $(u', u)_{L^2} \geq 0$. Hence we get

$$\sup_{v \in H_2} \frac{k(u, v)}{\|v\|_{L^2}} \geq \min\{1, b\}\|u\|_1 \quad \text{for all } u \in H_1,$$

i.e., the inf-sup condition for $k(\cdot, \cdot)$ is satisfied. We now prove that if $v \in H_2$ is such that $k(u, v) = 0$ for all $u \in H_1$, this implies $v = 0$. Take $v \in H_2$ with $k(u, v) = 0$ for all $u \in H_1$. This implies $b \int_0^1 u'v \, dx = - \int_0^1 uv \, dx$ for all $u \in C_0^\infty(I)$ and thus $v \in H^1(I)$ with $v' = \frac{1}{b}v$ (weak derivative). Using this we obtain

$$\begin{aligned} - \int_0^1 uv \, dx &= b \int_0^1 u'v \, dx = bu(1)v(1) - b \int_0^1 uv' \, dx \\ &= bu(1)v(1) - \int_0^1 uv \, dx \quad \text{for all } u \in H_1, \end{aligned}$$

and thus $u(1)v(1) = 0$ for all $u \in H_1$. This implies $v(1) = 0$. Using this and $bv' - v = 0$ yields

$$\begin{aligned} \|v\|_{L^2}^2 &= (v, v)_{L^2} + (bv' - v, v)_{L^2} \\ &= b(v', v)_{L^2} = \frac{b}{2}(v(1)^2 - v(0)^2) = -\frac{b}{2}v(0)^2 \leq 0. \end{aligned}$$

This implies $v = 0$. Application of Theorem 15.1.1 yields existence and uniqueness of a solution $u \in H_1$ and $\|u\|_1 \leq c\|f\|_{L^2}$, which completes the proof. \square

Remark 7.2.2 The analysis in the proof above is essentially the same as that used in the proof of Proposition 6.3.1 to show that the operator $I + C : W_{\mathbf{w}} \rightarrow L^2(\Omega)$ is bijective. This operator corresponds to the bilinear form $(\phi, v) \rightarrow (\phi + \mathbf{w} \cdot \nabla \phi, v)_{L^2}$ on $W_{\mathbf{w}} \times L^2(\Omega)$, which is the higher dimensional generalization of the bilinear form $k(\cdot, \cdot)$ used in the proof above.

For the discretization of the well-posed variational problem (7.2) we use a Galerkin method with a standard finite element space. To simplify the notation we use a uniform grid and consider only linear finite elements. Let $h = \frac{1}{n}$, $x_i = ih$, $0 \leq i \leq n$, and

$$\mathbb{X}_h = \{ v \in C(I) : v(0) = 0, v_{|[x_i, x_{i+1}]} \in \mathcal{P}_1 \text{ for } 0 \leq i \leq n-1 \}.$$

Note that $\mathbb{X}_h \subset H_1$ and $\mathbb{X}_h \subset H_2$. The discretization is as follows:

$$\text{determine } u_h \in \mathbb{X}_h \text{ such that } k(u_h, v_h) = (f, v_h)_{L^2} \quad \text{for all } v_h \in \mathbb{X}_h. \quad (7.3)$$

For the error analysis of this method we apply Céa's lemma 15.1.3. It remains to verify the discrete inf-sup condition:

$$\exists \varepsilon_h > 0 : \sup_{v_h \in \mathbb{X}_h} \frac{k(u_h, v_h)}{\|v_h\|_{L^2}} \geq \varepsilon_h \|u_h\|_1 \quad \text{for all } u_h \in \mathbb{X}_h. \quad (7.4)$$

Related to this we give the following lemma:

Lemma 7.2.3 *The inf-sup property (7.4) holds with $\varepsilon_h = ch$, $c > 0$ independent of h .*

Proof. For $u_h \in \mathbb{X}_h$ we have $(u'_h, u_h)_{L^2} = \frac{1}{2}u_h(1)^2 \geq 0$ and thus

$$\sup_{v_h \in \mathbb{X}_h} \frac{k(u_h, v_h)}{\|v_h\|_{L^2}} \geq \frac{k(u_h, u_h)}{\|u_h\|_{L^2}} = \frac{b(u'_h, u_h)_{L^2} + \|u_h\|_{L^2}^2}{\|u_h\|_{L^2}} \geq \|u_h\|_{L^2}.$$

Now apply an inverse inequality, $\|v'_h\|_{L^2} \leq ch^{-1}\|v_h\|_{L^2}$ for all $v_h \in \mathbb{X}_h$, resulting in $\|u_h\|_{L^2} \geq \frac{1}{2}\|u_h\|_{L^2} + ch\|u'_h\|_{L^2} \geq ch\|u_h\|_1$ with a constant $c > 0$ independent of h . \square

It can be shown that the result in this lemma is sharp in the sense that the best (i.e. largest) inf-sup constant ε_h in (7.4) in general satisfies $\varepsilon_h \leq ch$. This indicates that the standard linear finite element method is *unstable* in the sense that the inf-sup constant deteriorates for $h \downarrow 0$. This instability can be observed in numerical experiments with the discretization (7.3) for this simple 1D problem.

We will show how a satisfactory discretization with the space \mathbb{X}_h of linear finite elements can be obtained by using the concept of *stabilization*.

If $u \in H_1$ satisfies (7.2), then

$$\int_0^1 (bu' + u)bv' dx = (f, bv')_{L^2} \quad \text{for all } v \in H_1 \tag{7.5}$$

also holds. We add this equation δ -times, with δ a parameter in $[0, 1]$, to the one in (7.2). Thus the solution $u \in H_1$ of (7.2) also satisfies

$$k_\delta(u, v) = f_\delta(v) \quad \text{for all } v \in H_1, \text{ with} \tag{7.6a}$$

$$k_\delta(u, v) := (bu' + u, \delta bv' + v)_{L^2}, \quad f_\delta(v) := (f, \delta bv' + v)_{L^2}. \tag{7.6b}$$

Note that for $\delta = 0$ we have the original bilinear form and that $\delta = 1$ results in a problem with a *symmetric* bilinear form. For $\delta \neq 1$ the bilinear form $k_\delta(\cdot, \cdot)$ is not symmetric. For all $\delta \in [0, 1]$ we have $f_\delta \in H'_1$. The stabilizing effect for $\delta > 0$ is seen from the ellipticity estimate:

$$\begin{aligned} k_\delta(u, u) &= \delta b^2 \int_0^1 (u')^2 dx + \int_0^1 u^2 dx + b(\delta + 1) \int_0^1 u' u dx \\ &\geq \delta b^2 |u|_1^2 + \|u\|_{L^2}^2 \quad \text{for all } u \in H_1. \end{aligned} \tag{7.7}$$

Note that for $\delta > 0$ the norm $|u|_1$ occurs in this stability estimate. The discrete problem is as follows:

$$\text{determine } u_h \in \mathbb{X}_h \text{ such that } k_\delta(u_h, v_h) = f_\delta(v_h) \quad \text{for all } v_h \in \mathbb{X}_h. \tag{7.8}$$

The discrete solution u_h depends on δ . Using the stability estimate (7.7), approximation properties of the finite element space \mathbb{X}_h and a variant of C ea's lemma the following (sharp) result on the discretization error can be proved:

Proposition 7.2.4 *Let $u \in H_1$ and $u_h \in \mathbb{X}_h$ be the solutions of (7.2) and (7.8), respectively, and assume that $u \in H^2(I)$. For all $\delta \in [0, 1]$ the error bound*

$$b\sqrt{\delta}|u - u_h|_1 + \|u - u_h\|_{L^2} \leq Ch[h + b\sqrt{\delta} + b \min\{1, \frac{h}{b\sqrt{\delta}}\}] \|u''\|_{L^2} \quad (7.9)$$

holds with a constant C independent of h , δ , b and u .

The term between square brackets in (7.9) is minimal for $h \leq b$ if we take

$$\delta = \delta_{\text{opt}} = \frac{h}{b}. \quad (7.10)$$

We consider three cases:

$\underline{\delta = 0}$ (no stabilization): Then we get $\|u - u_h\|_{L^2} \leq ch\|u''\|_{L^2}$. We can not control the discretization error in the stronger H^1 -norm.

$\underline{\delta = 1}$ (full stabilization): Then we obtain

$$|u - u_h|_1 \leq ch\|u''\|_{L^2}, \quad \|u - u_h\|_{L^2} \leq ch\|u''\|_{L^2}.$$

$\underline{\delta = \delta_{\text{opt}}}$ (optimal value): This results in

$$|u - u_h|_1 \leq ch\|u''\|_{L^2}, \quad \|u - u_h\|_{L^2} \leq ch^{\frac{3}{2}}\|u''\|_{L^2}. \quad (7.11)$$

Hence, in the latter case the bound for the norm $|\cdot|_1$ is the same as for $\delta = 1$, but we have an improvement in the L^2 -error bound. The best stability property, in the sense of (7.7), is for the case $\delta = 1$. A somewhat weaker stability property but a better approximation property is obtained for $\delta = \delta_{\text{opt}}$. For $\delta = \delta_{\text{opt}}$ we have a *good compromise between sufficient stability and high approximation quality*.

The concept of stabilization as explained in this section is a very general one. It can be applied in higher dimensions, using finite elements of degree larger than one and also if instead of a hyperbolic equation one has to discretize a convection-diffusion problem in which convection is dominating. An extensive analysis of stabilization techniques is given in [211].

7.2.2 Discretization of the level set equation by the streamline diffusion finite element method

In this section we treat a stabilization approach, the so-called streamline diffusion stabilization method (SDFEM), for the discretization (in space) of the level set equation (6.59c). This method is based on the same approach as presented for a relatively simple one-dimensional hyperbolic problem in the previous section.

We introduce the finite element space of continuous piecewise polynomial functions. Let $\mathcal{V}(\partial\Omega_{in})$ be the set of vertices on the inflow boundary $\partial\Omega_{in} :=$

$\{x \in \partial\Omega : \mathbf{u} \cdot \mathbf{n}_\Omega < 0\}$. Given the Dirichlet boundary data ϕ_D on $\partial\Omega_{in}$ we define, for $k \geq 1$, the (affine) finite element space

$$V_h(\phi_D) := \{v \in C(\Omega) : v|_T \in \mathcal{P}_k \ \forall T \in \mathcal{T}_h, \ v(x) = \phi_D(x) \ \forall x \in \mathcal{V}(\partial\Omega_{in})\}.$$

The choice of the boundary data ϕ_D will be addressed in Remark 7.5.1. We use the notation $V_h = V_h(0)$. The latter space is independent of t , whereas $V_h(\phi_D)$ depends on t if the boundary data ϕ_D are time dependent. Note that $V_h(\phi_D) = V_h$ holds if $\phi_D = 0$ or $\partial\Omega_{in} = \emptyset$. As we will see later on, for the quality of the curvature approximation of the interface it is important to use finite elements of *degree at least two* for the approximation of the level set function. As explained in Sect. 7.2.1, cf. (7.6), for the spatial discretization of the level set equation (6.59c) we use test functions $\hat{v}_h \in L^2(\Omega)$ of the form

$$\hat{v}_h|_T := v_h + \delta_T \mathbf{u} \cdot \nabla v_h, \quad T \in \mathcal{T}_h, \ v_h \in V_h. \quad (7.12)$$

The *streamline diffusion finite element* discretization of the level set equation is as follows:

Let $\phi_{0,h} \in V_h(\phi_D)$ be an approximation of the initial condition $\phi_0 = \phi(0)$. Determine $\phi_h(t) \in V_h(\phi_D)$ with $\phi_h(0) = \phi_{0,h}$ and such that

$$\sum_{T \in \mathcal{T}_h} \left(\frac{\partial \phi_h}{\partial t} + \mathbf{u} \cdot \nabla \phi_h, v_h + \delta_T \mathbf{u} \cdot \nabla v_h \right)_{L^2(T)} = 0 \quad \text{for all } v_h \in V_h, \quad (7.13)$$

and $t \in [0, T]$.

Note that compared to the standard Galerkin finite element discretization ($\delta_T = 0$ for all T) in (7.13) we have added a stabilizing term of the form $(\mathbf{u} \cdot \nabla \phi_h, \mathbf{u} \cdot \nabla v_h)_{L^2}$, which is the variational form of a diffusion acting only in the direction \mathbf{u} . This explains the name of this finite element method. Based on a theoretical error bound and numerical experiments for model problems the parameter δ_T is often taken as

$$\delta_T = c \frac{h_T}{\max\{\varepsilon_0, \|\mathbf{u}\|_{\infty, T}\}} \quad (7.14)$$

with a given small $\varepsilon_0 > 0$ and $c = \mathcal{O}(1)$. This streamline diffusion discretization is consistent in the following sense.

Lemma 7.2.5 *Let $\phi(t)$ be a solution of (6.59c). Then ϕ satisfies*

$$\sum_{T \in \mathcal{T}_h} \left(\frac{\partial \phi}{\partial t} + \mathbf{u} \cdot \nabla \phi, v_h + \delta_T \mathbf{u} \cdot \nabla v_h \right)_{L^2(T)} = 0 \quad \text{for all } v_h \in V_h,$$

for all $t \in [0, T]$.

Proof. This immediately follows from the fact that for the test functions \hat{v}_h as in (7.12) we have $\hat{v}_h \in L^2(\Omega)$. □

Matrix-vector representation

For the matrix-vector formulation of the semidiscrete problem (7.13) we use the standard nodal basis in V_h , which is denoted by $\{\xi_i\}_{i=1,\dots,N_{V_h}}$. Hence, for all i we have $\xi_i(x) = 0$ for all $x \in \mathcal{V}(\partial\Omega_{in})$. The vector representation of $v_h \in V_h(\phi_D)$ is given by

$$v_h = \sum_{i=1}^{N_{V_h}} v_i \xi_i + b_h, \quad v_i \in \mathbb{R}, \quad (7.15)$$

with $b_h = b_h(x, t) \in V_h(\phi_D)$ such that $b_h(x, t) = \phi_D(x, t)$ for all $x \in \mathcal{V}(\partial\Omega_{in})$ and $b_h(x_i, t) = 0$ at all other vertices $x_i, i = 1, \dots, N_{V_h}$. We define the matrices $\mathbf{E} = \mathbf{E}(\mathbf{u}) \in \mathbb{R}^{N_{V_h} \times N_{V_h}}$ and $\mathbf{H} = \mathbf{H}(\mathbf{u}) \in \mathbb{R}^{N_{V_h} \times N_{V_h}}$:

$$\mathbf{E}_{ij} := \sum_{T \in \mathcal{T}_h} (\xi_j, \xi_i + \delta_T \mathbf{u} \cdot \nabla \xi_i)_{L^2(T)} \quad (\text{stabilized mass matrix}),$$

$$\mathbf{H}_{ij} := \sum_{T \in \mathcal{T}_h} (\mathbf{u} \cdot \nabla \xi_j, \xi_i + \delta_T \mathbf{u} \cdot \nabla \xi_i)_{L^2(T)} \quad (\text{stabilized convection}),$$

$$\mathbf{b}_i = \sum_{T \in \mathcal{T}_h} \left(\frac{\partial b_h}{\partial t} + \mathbf{u} \cdot \nabla b_h, \xi_i + \delta_T \mathbf{u} \cdot \nabla \xi_i \right)_{L^2(T)} \quad (\text{boundary data}),$$

for $1 \leq i, j \leq N_{V_h}$. Thus, using

$$\phi_h(t) = \sum_{i=1}^{N_{V_h}} \phi_i(t) \xi_i + b_h, \quad \vec{\phi}(t) := (\phi_1(t), \dots, \phi_{N_{V_h}}(t)),$$

and $\vec{\phi}_0$ the vector representation of the initial value $\phi_{0,h} - b_h(\cdot, 0) \in V_h$ we can reformulate (7.13) in matrix-vector notation:

Find $\vec{\phi}(t) \in \mathbb{R}^{N_{V_h}}$ with $\vec{\phi}(0) = \vec{\phi}_0$ and for all $t \in [0, T]$

$$\mathbf{E}(\mathbf{u}) \frac{d\vec{\phi}}{dt}(t) + \mathbf{H}(\mathbf{u}) \vec{\phi}(t) = -\mathbf{b}(t). \quad (7.16)$$

Note that in general the velocity field \mathbf{u} depends on t and thus the matrices $\mathbf{E}(\mathbf{u})$ and $\mathbf{H}(\mathbf{u})$ are time dependent. In practice, the velocity field \mathbf{u} will be replaced by a finite element approximation \mathbf{u}_h .

Time discretization

The discretization in (7.13), or in (7.16), can be combined with standard time discretization techniques (method of lines). If the velocity \mathbf{u} depends on t then for the method of lines approach the formulation in (7.16) is more natural,

since in (7.13) the test functions \hat{v}_h then depend on t . The θ -schema applied to (7.16) results in

$$\begin{aligned} \frac{\vec{\phi}^{n+1} - \vec{\phi}^n}{\Delta t} &= -\theta \mathbf{E}(\vec{\mathbf{u}}^{n+1})^{-1} (\mathbf{H}(\vec{\mathbf{u}}^{n+1}) \vec{\phi}^{n+1} + \mathbf{b}(t_{n+1})) \\ &\quad - (1 - \theta) \mathbf{E}(\vec{\mathbf{u}}^n)^{-1} (\mathbf{H}(\vec{\mathbf{u}}^n) \vec{\phi}^n + \mathbf{b}(t_n)). \end{aligned}$$

This can be reformulated in a computationally more favorable form using a new variable

$$\vec{\mathbf{w}}^k = -\mathbf{E}(\vec{\mathbf{u}}^k)^{-1} (\mathbf{H}(\vec{\mathbf{u}}^k) \vec{\phi}^k + \mathbf{b}(t_k)),$$

which satisfies (for $\theta \neq 0$)

$$\theta \vec{\mathbf{w}}^{n+1} = \frac{\vec{\phi}^{n+1} - \vec{\phi}^n}{\Delta t} - (1 - \theta) \vec{\mathbf{w}}^n,$$

resulting in

$$\begin{aligned} \mathbf{E}(\vec{\mathbf{u}}^{n+1}) \frac{\vec{\phi}^{n+1} - \vec{\phi}^n}{\Delta t} &= -\theta (\mathbf{H}(\vec{\mathbf{u}}^{n+1}) \vec{\phi}^{n+1} + \mathbf{b}(t_{n+1})) \\ &\quad + (1 - \theta) \mathbf{E}(\vec{\mathbf{u}}^{n+1}) \vec{\mathbf{w}}^n. \end{aligned} \quad (7.17)$$

Discretization error bound

A discretization error analysis of the fully discrete problem (7.17) for the general case of a time-dependent velocity field \mathbf{u} is not known, yet. For the case of a *stationary* and divergence free velocity field $\mathbf{u} = \mathbf{u}(x)$ an error analysis has recently been given in [59]. We outline the main result of that analysis. We assume that the Dirichlet data ϕ_D are also independent of t . Instead of a local stability parameter $\delta = \delta_T$ we assume quasi-uniformity of the triangulation and use one global parameter $\delta = h \|\mathbf{u}\|_{L^\infty(\Omega)}^{-1}$. For a stationary velocity field \mathbf{u} the matrices $\mathbf{E}(\mathbf{u})$ and $\mathbf{H}(\mathbf{u})$ are independent of t and the scheme (7.17) is the matrix-vector representation of the following discrete problem, cf. (7.13): let $\phi_h^0 := \phi_{0,h} \in V_h(\phi_D)$ be an approximation of the initial condition $\phi_0 = \phi(0)$; for $n \geq 0$ determine $\phi_h^n \in V_h(\phi_D)$ such that

$$\left(\frac{\phi_h^{n+1} - \phi_h^n}{\Delta t} + \mathbf{u} \cdot \nabla (\theta \phi_h^{n+1} + (1 - \theta) \phi_h^n), v_h + \delta \mathbf{u} \cdot \nabla v_h \right)_{L^2} = 0, \quad (7.18)$$

for all $v_h \in V_h$. In [59] an analysis for $\theta \in (0, 1]$ is presented. Here we restrict to the Crank-Nicolson method, i.e., $\theta = \frac{1}{2}$. In the analysis it is assumed that the solution ϕ is sufficiently smooth, such that higher order derivatives are bounded. Let $N\Delta t = T$, i.e. ϕ_h^N is the numerical approximation of $\phi(\cdot, T)$. The following error bound can be shown to hold:

$$\|\phi_h^N - \phi(\cdot, T)\|_{L^2} + \sqrt{\delta} \|\mathbf{u} \cdot \nabla (\phi_h^N - \phi(\cdot, T))\|_{L^2} \leq cT(h^{k+\frac{1}{2}} + \Delta t^2), \quad (7.19)$$

with a constant c that depends on the smoothness of the data ϕ_D and of the solution ϕ but not on $T, h, \Delta t$. In [59] this result is proved for the case of homogeneous inflow data $\phi_D = 0$, but the analysis can easily be extended to the inhomogeneous case $\phi_D \neq 0$, cf. [169]. As in the analysis presented for the simple hyperbolic problem in Sect. 7.2, the bound in (7.19) reflects that due to the stabilization not only the L^2 -norm of the error but also its derivative in streamline direction can be controlled. The estimate (7.19) is similar to the one given in (7.11). The term Δt^2 in the error bound is of optimal order. The term $h^{k+\frac{1}{2}}$ is optimal for the error in the streamline derivative (recall: $\delta \sim h$) and suboptimal (by a factor \sqrt{h}) for the L^2 -norm of the error.

7.3 Construction of an approximate interface Γ_h

As we will see further on, at several places (e.g., in the discretization of the surface tension force functional $f_\Gamma(\mathbf{v})$) we will need an approximation $\Gamma_h(t)$ of the interface $\Gamma(t)$. In this section we discuss a simple method for constructing such an approximation.

Assume that for a fixed $t \in [0, T]$ we have a finite element approximation $\phi_h(\cdot, t) \in V_h = \mathbb{X}_h^2$ of the level set function $\phi(x, t)$. To simplify the notation, in the remainder of this section we write $\phi(x, t) =: \phi(x)$, $\phi_h(x, t) =: \phi_h(x)$. In Sect. 7.4.1 we address the issue of re-initialization of the level set function, which is introduced to assure that ϕ (or ϕ_h) remains, in a neighborhood of the interface, close to a signed distance function. Thus ϕ and its approximation $\phi_h \in V_h$ can be assumed to be close to a signed distance function. Let $\tilde{\Gamma}_h$ be the zero level of ϕ_h and

$$\mathcal{T}_h^\Gamma := \left\{ T \in \mathcal{T}_h : \text{meas}_2(T \cap \tilde{\Gamma}_h) > 0 \right\} \tag{7.20}$$

the collection of tetrahedra which contain the approximate interface $\tilde{\Gamma}_h$. Let $\mathcal{T}_{h'}^\Gamma$ be the collection of tetrahedra obtained by one further regular refinement of all $T \in \mathcal{T}_h^\Gamma$ (subdivision of each tetrahedron in 8 child tetrahedra, cf. Fig. 3.1). Furthermore, $I(\phi_h)$ is the continuous piecewise linear function on $\mathcal{T}_{h'}^\Gamma$ which interpolates ϕ_h at all vertices of all tetrahedra in $\mathcal{T}_{h'}^\Gamma$. Note that the degrees of freedom of the P_1 finite element functions on $\mathcal{T}_{h'}^\Gamma$ (located at the vertices) coincide with the degrees of freedom of the P_2 finite element functions on \mathcal{T}_h^Γ (located at the vertices and midpoints of edges).

The approximation Γ_h of the interface Γ is defined by

$$\Gamma_h := \{ x \in \Omega : I(\phi_h)(x) = 0 \}. \tag{7.21}$$

Hence, Γ_h consists of piecewise planar segments $\Gamma_T \subset \Gamma_h$, where

$$\Gamma_T := T \cap \Gamma_h \tag{7.22}$$

for $T \in \mathcal{T}_{h'}^\Gamma$.

The *interface mesh size parameter* h_Γ is the maximal diameter of these segments. Thus h_Γ is approximately the maximal diameter of the tetrahedra in $\mathcal{T}_{h'}^\Gamma$, i.e., $2h_\Gamma$ is approximately the maximal diameter of the tetrahedra in \mathcal{T}_h that are close to the interface. In our applications we use local refinement close to the interface, which implies $h_\Gamma \ll h$. In Fig. 7.1 we illustrate this construction for the two-dimensional case. An illustration for a 3D case is given in Fig. 7.5. Note that in general the segments of Γ_h are not aligned with the faces of the tetrahedral triangulation $\mathcal{T}_{h'}^\Gamma$.

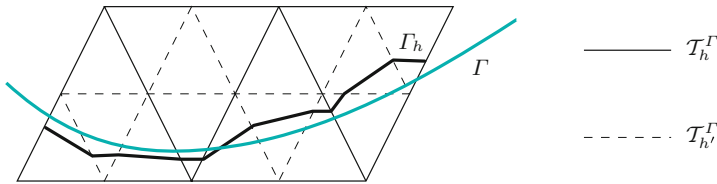


Fig. 7.1. Construction of approximate interface for 2D case.

Each of the planar segments Γ_T of Γ_h is either a triangle or a quadrilateral, depending on the sign pattern of ϕ_h on the corresponding $T \in \mathcal{T}_{h'}^\Gamma$, cf. Fig. 7.2. By construction the vertices of a planar segment Γ_T are located on those edges of T along which ϕ_h changes its sign. If there are two positive and two negative values of ϕ_h on the vertices of T , then the corresponding interface segment Γ_T is a quadrilateral. In all other cases Γ_T is a triangle. The quadrilaterals can (formally) be divided into two triangles. Thus Γ_h consists of a set of triangular faces, which is denoted by \mathcal{F}_h .

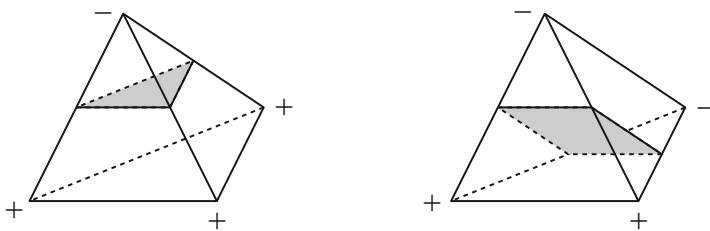


Fig. 7.2. Sign pattern of ϕ_h on $T \in \mathcal{T}_{h'}^\Gamma$ and corresponding interface segment $\Gamma_T = T \cap \Gamma$ (in gray): either a triangle or a quadrilateral.

Special cases may occur if some of the values of ϕ_h on the vertices of T are equal to zero (or below a given tolerance). Let $0 \leq n_0 \leq 4$ be the number of these (close to) zero values. In the following we discuss the shape of Γ_T in all the cases $n_0 = 0, 1, 2, 3, 4$.

- $n_0 = 0$ is not a special case, the situation is as depicted in Fig. 7.2 which was discussed in the foregoing paragraph.
- For $n_0 = 1, 2$ we distinguish two cases: If the other $4 - n_0$ non-zero values have the same sign, then Γ_T is a point ($n_0 = 1$) or a line segment ($n_0 = 2$) and can be ignored as $\text{meas}_2(\Gamma_T) = 0$. Otherwise the non-zero values are of different sign yielding $3 - n_0$ edges with a change of sign, as a simple case differentiation shows. Thus Γ_T has 3 vertices, hence Γ_T is a triangle.
- In the case $n_0 = 3$ the interface segment Γ_T is equal to a face of T . Then one has to take care that this face is not counted twice when computing a surface integral on Γ_h using an assembling strategy over $T \in \mathcal{T}_h^I$.
- If $n_0 = 4$ then either the intersection of $T \in \mathcal{T}_h^I$ with Γ_h is empty (cf. for example the left upper triangle in Fig. 7.1) or there is a degeneration, namely $\Gamma_T = T$, i.e. the interface segment is three-dimensional. Of course, the latter makes not much sense. Such a situation typically indicates that the grid is too coarse to represent the interface properly, cf. Fig. 7.3.

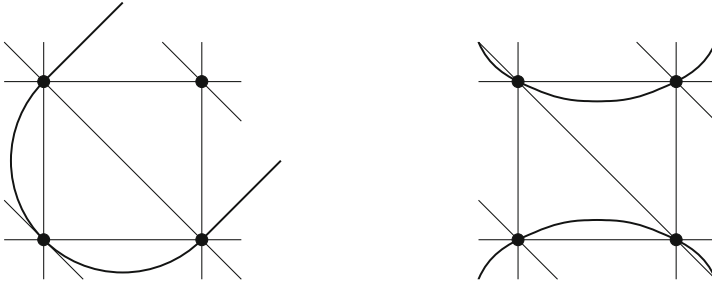


Fig. 7.3. 2D examples for interface degeneration such that the interface reconstruction fails. Left: curvature κ too large compared to grid resolution ($|\kappa| \geq \frac{2}{h}$). Right: distance d between interfaces too small compared to grid resolution ($d \leq h$).

If a situation as on the right in Fig. 7.3 occurs, then in the interface reconstruction special measures have to be taken to handle the (almost) topological singularity.

For an example in which Γ is a sphere, the resulting polygonal approximations Γ_h for $h = \frac{1}{5}$ and $h = \frac{1}{10}$ are shown in Fig. 7.4. A detail of such a polygonal interface approximation is shown in Fig. 7.5.

7.3.1 Error in approximation of Γ by Γ_h

We assume a fixed sufficiently smooth interface Γ , which is the zero level of ϕ , and a mesh size h_Γ that is sufficiently small such that degenerations as in Fig. 7.3 do not occur. We analyze the quality of Γ_h as an approximation

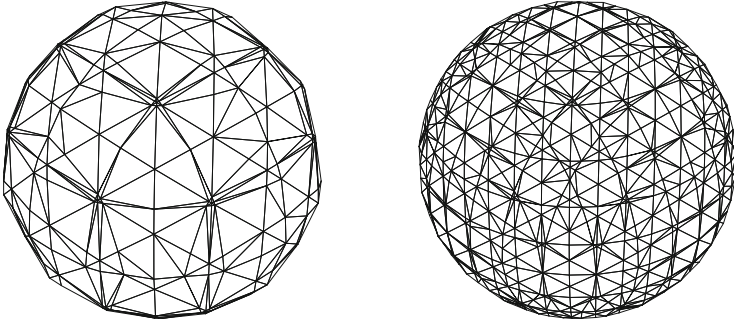


Fig. 7.4. Approximate interface Γ_h for an example with a sphere, on a coarse grid (left) and after one refinement (right).

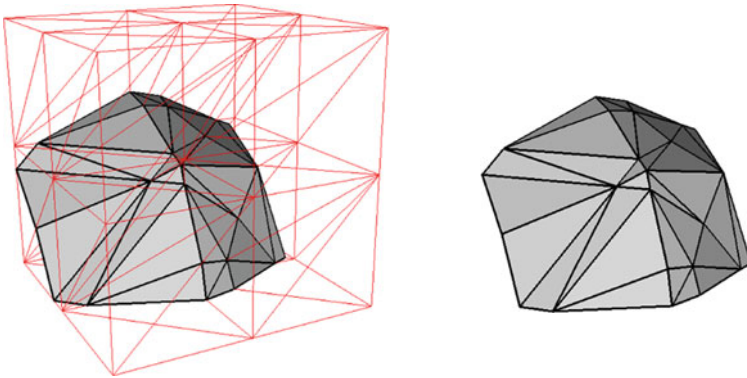


Fig. 7.5. Detail of the interface triangulation Γ_h . On the left, also the outer triangulation \mathcal{T}_h^Γ is shown.

of Γ . For this we first introduce some notation and further assumptions. Let $U := \{x \in \mathbb{R}^3 : \text{dist}(x, \Gamma) < c\}$ be a sufficiently small neighborhood of Γ . We define \mathcal{T}_h^Γ as in (7.20), i.e., the collection of tetrahedra which intersect the zero level $\tilde{\Gamma}_h$ of ϕ_h , and assume that $\mathcal{T}_h^\Gamma \subset U$. Let d be the signed distance function

$$d : U \rightarrow \mathbb{R}, \quad |d(x)| := \text{dist}(x, \Gamma) \quad \text{for all } x \in U.$$

Thus Γ is the zero level set of d . Note that $\mathbf{n}_\Gamma = \nabla d$ on Γ . We define $\mathbf{n}(x) := \nabla d(x)$ for $x \in U$. Thus $\mathbf{n} = \mathbf{n}_\Gamma$ on Γ and $\|\mathbf{n}(x)\| = 1$ for all $x \in U$. Here and in the remainder of this section $\|\cdot\|$ denotes the Euclidean norm on \mathbb{R}^3 . We introduce a local orthogonal coordinate system by using the projection $\mathbf{p} : U \rightarrow \Gamma$:

$$\mathbf{p}(x) = x - d(x)\mathbf{n}(x) \quad \text{for all } x \in U.$$

We assume that the decomposition $x = \mathbf{p}(x) + d(x)\mathbf{n}(x)$ is unique for all $x \in U$. Note that

$$\mathbf{n}(x) = \mathbf{n}(\mathbf{p}(x)) \quad \text{for all } x \in U.$$

The unit normal on Γ_h (pointing outward from Ω_1) is denoted by \mathbf{n}_h . Using these preliminaries we can derive the following approximation result.

Theorem 7.3.1 *Assume that $\phi \in H_\infty^2(U)$ and that for $c_1, c_0 > 0$*

$$c_0 \leq \|\nabla\phi(x)\| \leq c_1 \quad \text{for all } x \in U. \quad (7.23)$$

Furthermore, we assume that the approximation $\phi_h \in V_h = \mathbb{X}_h^2$ of ϕ satisfies

$$\|\phi_h - \phi\|_{L^\infty(U)} + h_\Gamma \|\phi_h - \phi\|_{H_\infty^1(U)} \leq ch_\Gamma^m \|\phi\|_{H_\infty^m(U)}, \quad m = 1, 2. \quad (7.24)$$

Then the following holds:

$$|d(x)| \leq ch_\Gamma^2 \quad \text{for all } x \in \Gamma_h, \quad (7.25a)$$

$$\|\mathbf{n}(x) - \mathbf{n}_h(x)\| \leq ch_\Gamma \quad \text{for all } x \in \Gamma_h. \quad (7.25b)$$

Proof. Let I be the linear interpolation operator corresponding to \mathcal{T}_h^Γ , used in (7.21), and define the piecewise linear function $\tilde{\phi}_h = I\phi_h$. Recall that $\Gamma_h = \{x \in \mathbb{R}^3 : \tilde{\phi}_h(x) = 0\}$. Using standard properties of I and the error bound in (7.24) one obtains

$$\begin{aligned} \|\tilde{\phi}_h - \phi\|_{L^\infty(\mathcal{T}_h^\Gamma)} &\leq \|I(\phi_h - \phi)\|_{L^\infty(\mathcal{T}_h^\Gamma)} + \|I\phi - \phi\|_{L^\infty(\mathcal{T}_h^\Gamma)} \\ &\leq \|\phi_h - \phi\|_{L^\infty(U)} + ch_\Gamma^2 \|\phi\|_{H_\infty^2(U)} \\ &\leq ch_\Gamma^2 \|\phi\|_{H_\infty^2(U)}. \end{aligned}$$

Due to $\tilde{\phi}_h(x) = 0$ for $x \in \Gamma_h$ this yields

$$|\phi(x)| \leq ch_\Gamma^2 \quad \text{for } x \in \Gamma_h. \quad (7.26)$$

Take $x \in \Gamma_h$ and introduce the notation $y = \mathbf{p}(x) = x - d(x)\mathbf{n}(x) = x - d(x)\mathbf{n}(y) \in \Gamma$. For suitable s with $|s| \leq |d(x)|$ and $\tilde{y} = y + s\mathbf{n}(y)$ we get

$$\begin{aligned} \phi(x) &= \phi(x) - \phi(y) = \phi(y + d(x)\mathbf{n}(y)) - \phi(y) \\ &= d(x)\nabla\phi(y + s\mathbf{n}(y)) \cdot \mathbf{n}(y) = d(x)\nabla\phi(\tilde{y}) \cdot \mathbf{n}(y) \\ &= d(x)((\nabla\phi(\tilde{y}) - \nabla\phi(y)) \cdot \mathbf{n}(y) + \|\nabla\phi(y)\|). \end{aligned} \quad (7.27)$$

Due to (7.23) we have $\|\nabla\phi(y)\| \geq c_0$. We assume that U is sufficiently small such that $\|\nabla\phi(\tilde{y}) - \nabla\phi(y)\| \leq \|\phi\|_{H_\infty^2(U)}|d(x)| \leq \frac{1}{2}c_0$ holds. Hence we obtain from (7.27) that $|\phi(x)| \geq \frac{1}{2}c_0|d(x)|$ holds, and using (7.26) yields

$$|d(x)| \leq c|\phi(x)| \leq ch_\Gamma^2, \quad x \in \Gamma_h,$$

i.e., the result in (7.25a). We also have, using Assumption (7.24)

$$\begin{aligned} \|\tilde{\phi}_h - \phi\|_{H_\infty^1(\mathcal{T}_h^\Gamma)} &\leq \|I(\phi_h - \phi)\|_{H_\infty^1(\mathcal{T}_h^\Gamma)} + \|I\phi - \phi\|_{H_\infty^1(\mathcal{T}_h^\Gamma)} \\ &\leq c\|\phi_h - \phi\|_{H_\infty^1(U)} + ch_\Gamma\|\phi\|_{H_\infty^2(U)} \leq ch_\Gamma\|\phi\|_{H_\infty^2(U)}. \end{aligned}$$

This implies

$$\|\nabla\tilde{\phi}_h(x)\| = \|\nabla\phi(x)\| + \mathcal{O}(h), \quad x \in \Gamma_h.$$

Using this, we obtain for $x \in \Gamma_h$ (not on an edge) and $y = \mathbf{p}(x) \in \Gamma$

$$\begin{aligned} \|\mathbf{n}(x) - \mathbf{n}_h(x)\| &= \|\mathbf{n}(y) - \mathbf{n}_h(x)\| = \left\| \frac{\nabla\phi(y)}{\|\nabla\phi(y)\|} - \frac{\nabla\tilde{\phi}_h(x)}{\|\nabla\tilde{\phi}_h(x)\|} \right\| \\ &\leq \left\| \frac{\nabla\phi(y)}{\|\nabla\phi(y)\|} - \frac{\nabla\phi(x)}{\|\nabla\phi(x)\|} \right\| + \left\| \frac{\nabla\phi(x)}{\|\nabla\phi(x)\|} - \frac{\nabla\tilde{\phi}_h(x)}{\|\nabla\tilde{\phi}_h(x)\|} \right\|. \end{aligned}$$

For the first term we obtain, from a Taylor expansion, Assumption (7.23) and $\|x - y\| \leq ch_\Gamma^2$:

$$\left\| \frac{\nabla\phi(y)}{\|\nabla\phi(y)\|} - \frac{\nabla\phi(x)}{\|\nabla\phi(x)\|} \right\| \leq ch_\Gamma^2.$$

For the second term we get

$$\begin{aligned} \left\| \frac{\nabla\phi(x)}{\|\nabla\phi(x)\|} - \frac{\nabla\tilde{\phi}_h(x)}{\|\nabla\tilde{\phi}_h(x)\|} \right\| &= \left\| \frac{\nabla\phi - \nabla\tilde{\phi} \frac{\|\nabla\phi\|}{\|\nabla\tilde{\phi}_h\|}}{\|\nabla\phi\|} \right\| \\ &\leq c_0^{-1} \left| \frac{\|\nabla\phi(x)\|}{\|\nabla\tilde{\phi}_h(x)\|} - 1 \right| \cdot \|\nabla\tilde{\phi}_h(x)\| + c_0^{-1} \|\nabla\tilde{\phi}_h(x) - \nabla\phi(x)\| \leq ch_\Gamma, \end{aligned}$$

which completes the proof. \square

The results in (7.25a) and (7.25b) give (satisfactory) quantitative results on the approximation quality of Γ_h . The result in (7.25b) implies that the tangent planes are close in a certain sense, and that “zigzag” effects in the approximation Γ_h do not occur. These bounds will play a crucial role in the analysis of the surface tension force discretization in Sect. 7.7. We comment on the assumptions in (7.23) and (7.24). Due to re-initialization, in a neighborhood of the interface the level set function ϕ is close to a signed distance function and thus $\|\nabla\phi\| \approx 1$ can be expected to hold. We claim that the assumption on the discretization error bound in (7.24) is also reasonable. Due to the re-initialization it is reasonable to assume that ϕ is (very) smooth. Hence, using quadratic finite elements, an optimal order discretization method would have an error bound of the form (7.24) with $m = 3$. We do not know whether the SDFEM applied to the hyperbolic level set equation is of optimal order. In (7.24), however, we only assume an h_Γ^2 error bound (instead of the optimal h_Γ^3

bound) to be satisfied. The only rigorous discretization error bounds for the level set equation known to us are given in [59], cf. the discussion in Sect. 7.2.2, in particular the result in (7.19). For quadratic finite elements and a suitable time step Δt the latter result yields a bound $ch_\Gamma^{2\frac{1}{2}}$. The discretization error, however, is measured in a weaker norm as the one used in (7.24).

For a sufficiently smooth level set function ϕ and an approximation $\phi_h \in \mathbb{X}_h^2$ one could consider the case in which the approximation error bound in (7.24) even holds for an $m \in (2, 3]$. Such a stronger assumption, however, would not improve the bounds in (7.25). This is due to the fact that *linear* interpolation is used in the construction of Γ_h . In the proof this is reflected by the terms $\|I\phi - \phi\|_{L^\infty(\mathcal{T}_h^\Gamma)}$ and $\|I\phi - \phi\|_{H_\infty^1(\mathcal{T}_h^\Gamma)}$ for which the optimal error bounds are of the form ch_Γ^2 and ch_Γ , respectively. Below we present a result which shows that by using ϕ_h , instead of $I\phi_h$, a better normal approximation than the one in (7.25b) can be obtained. This result will be crucial in the discretization of the surface tension force treated in Sect. 7.6.

Lemma 7.3.2 *Assume that $\phi \in H^3(U)$ and that (7.23) holds. Furthermore, we assume that $\phi_h \in \mathbb{X}_h^2$ satisfies*

$$\|\phi_h - \phi\|_{H_\infty^1(U)} \leq ch_\Gamma^p, \quad \text{for a } p \in (0, 2]. \tag{7.28}$$

For $x \in U$ define $\tilde{\mathbf{n}}_h(x) := \frac{\nabla \phi_h(x)}{\|\nabla \phi_h(x)\|}$. The following holds:

$$\|\mathbf{n}(x) - \tilde{\mathbf{n}}_h(x)\| \leq ch_\Gamma^p \quad \text{for all } x \in \Gamma_h. \tag{7.29}$$

Proof. We use similar arguments as in the proof of Theorem 7.3.1. For $x \in \Gamma_h$ (not on an edge)

$$\begin{aligned} \|\mathbf{n}(x) - \tilde{\mathbf{n}}_h(x)\| &= \|\mathbf{n}(y) - \tilde{\mathbf{n}}_h(x)\| = \left\| \frac{\nabla \phi(y)}{\|\nabla \phi(y)\|} - \frac{\nabla \phi_h(x)}{\|\nabla \phi_h(x)\|} \right\| \\ &\leq \left\| \frac{\nabla \phi(y)}{\|\nabla \phi(y)\|} - \frac{\nabla \phi(x)}{\|\nabla \phi(x)\|} \right\| + \left\| \frac{\nabla \phi(x)}{\|\nabla \phi(x)\|} - \frac{\nabla \phi_h(x)}{\|\nabla \phi_h(x)\|} \right\|. \end{aligned}$$

Using a Taylor expansion and $\|x - y\| \leq ch_\Gamma^2$, we obtain a bound ch_Γ^2 , for the first term. Since $\|\nabla \phi_h(x) - \nabla \phi(x)\| \leq ch_\Gamma^p$, the second term can be bounded by ch_Γ^p using the same arguments as in the proof of Theorem 7.3.1. \square

Let $\tilde{\Gamma}_h$ be the zero level set of $\phi_h \in \mathbb{X}_h^2$. This zero level is difficult to compute; therefore, in practice we use its piecewise planar approximation Γ_h . For $x \in \tilde{\Gamma}_h$, the quantity $\tilde{\mathbf{n}}_h(x)$ is the unit outward normal on $\tilde{\Gamma}_h$. Note that, for a given $\phi_h \in \mathbb{X}_h^2$ and $x \in U$ it is easy to compute the quantity $\tilde{\mathbf{n}}_h(x)$. In the sense as in Theorem 7.3.1 and Lemma 7.3.2, $\tilde{\mathbf{n}}_h(x)$ is a better approximation to the normal $\mathbf{n}(x)$ than $\mathbf{n}_h(x)$.

7.4 Corrections of the level set function

During the evolution of the level set function ϕ or of its finite element approximation ϕ_h , which is driven by the velocity field \mathbf{u} , the property of ϕ (ϕ_h) being close to a signed distance function is lost. This has undesirable effects, which can be avoided by using a re-initialization technique as explained in Sect. 7.4.1. In general the (spatial and temporal) discretizations of the level set equation are such that mass conservation is not guaranteed on the discrete level (only for $h, \Delta t \downarrow 0$). This issue of loss of mass is briefly addressed in Sect. 7.4.2.

7.4.1 Re-initialization

Assume that the initial data $\phi_0(x)$, $x \in \Omega$, for the level set equation are such that (locally, close to the initial interface) ϕ_0 is a signed distance function to $\Gamma(0)$. Then in general during the evolution of the level set function ϕ the property of ϕ being close to a (signed) distance function is lost, which has undesirable effects. For example, an accurate spatial discretization of ϕ becomes hard in regions where ϕ has a very strong variation, and the problem of finding the zero level set of ϕ becomes ill conditioned in regions where ϕ is very flat. Therefore, often level set methods are combined with a re-initialization (also called “reparametrization”) technique.

Assume that for a given $t_0 \in [0, T]$ an approximation $\phi_h(\cdot)$ of the level set function $\phi(\cdot, t_0)$ is known. Given this ϕ_h a re-initialization method results in $\tilde{\phi}_h$ such that:

1. The zero level of $\tilde{\phi}_h$ is (approximately) equal to that of ϕ_h .
2. The function $\tilde{\phi}_h$ is close to a signed distance function: $\|\nabla\tilde{\phi}_h\| \approx 1$ (close to the interface).

The function $\tilde{\phi}_h$ is then used as re-initialization in the evolution of the level set function: $\tilde{\phi}_h$ is taken as “initial” data to solve the level set equation for $t \geq t_0$.

Different re-initialization techniques are known in the literature, cf. [221, 222, 148, 266, 205]. A popular method is based on solving the Eikonal equation

$$\|\nabla\psi\| = 1$$

by introducing a pseudo-time evolution as follows. Let ϕ_h be the given approximation of the level set function, and consider the first order partial differential equation for $\psi = \psi(x, \tau)$:

$$\begin{aligned} \frac{\partial\psi}{\partial\tau} &= S_\alpha(\phi_h)(1 - \|\nabla\psi\|), & \tau \geq 0, \quad x \in \Omega, \\ \psi(\cdot, 0) &= \phi_h, \end{aligned} \tag{7.30}$$

with

$$S_\alpha(\zeta) = \frac{\zeta}{\sqrt{\zeta^2 + \alpha^2}}, \quad \zeta \in \mathbb{R},$$

where α is a regularization parameter ($0 < \alpha \ll 1$). The function S_α is a smoothed sign function. Due to $S_\alpha(0) = 0$ the zero level set of ψ remains equal to that of ϕ_h . A stationary solution $\psi(x) = \lim_{\tau \rightarrow \infty} \psi(x, \tau)$ of (7.30) solves the Eikonal equation and thus ψ is a signed distance function. The equation (7.30) can be reformulated in the more convenient form

$$\frac{\partial \psi}{\partial \tau} + \mathbf{w}(\psi) \cdot \nabla \psi = S_\alpha(\phi_h) \quad \text{with } \mathbf{w}(\psi) := S_\alpha(\phi_h) \frac{\nabla \psi}{\|\nabla \psi\|}. \quad (7.31)$$

In practice, the equation (7.31) is discretized in space and time and for sufficiently large $\tau_f > 0$ one can use the computed discrete solution $\tilde{\phi}_h := \psi_h(\cdot, \tau_f)$ as a re-initialization of ϕ_h . For a further discussion of this re-initialization method we refer to the literature [231, 230, 240]. Using this technique one faces the following difficulties. Firstly, the method contains control parameters α and τ_f and there are no good practical criteria on how to select these. Secondly, the partial differential equation (7.31) is nonlinear and hyperbolic; accurate discretization of this type of partial differential equation is rather difficult. Finally, the invariance property of the zero level holds for the stationary solution $\psi(x, \tau)$ of the continuous problem in (7.30), but after discretization it is usually lost. It may well happen that the difference between the zero levels of ϕ_h and $\psi_h(\cdot, \tau_f)$ is “large”.

Another technique for re-initialization is the Fast Marching Method (cf. [157, 220]). In [148] a survey and comparison of different re-initialization methods is given, where (for a certain class of problems) the Fast Marching Method turns out to be the most accurate and efficient one. In our level set method we use a variant of the Fast Marching Method that is explained in detail below.

Fast Marching Method (FMM)

In our level set method we have a piecewise quadratic function $\phi_h \in V_h = \mathbb{X}_h^2$ for which a re-initialization should be determined. We first describe the FMM applied to a piecewise *linear* function and then explain how this method is applied to the piecewise quadratic ϕ_h .

Let ψ_h be a piecewise linear function on the tetrahedral triangulation \mathcal{T}_h . The zero level of ψ_h is denoted by Γ_h . This zero level consists of planar segments Γ_T :

$$\Gamma_h = \bigcup_{T \in \mathcal{T}_h^\Gamma} \Gamma_T, \quad \text{with } \Gamma_T := \Gamma_h \cap T, \quad (7.32)$$

and \mathcal{T}_h^Γ the collection of all tetrahedra that have a nonempty intersection with Γ_h . The planar segment Γ_T is either a triangle or a quadrilateral, cf. Fig. 7.2. We introduce some notation. For $T \in \mathcal{T}_h$, $\mathcal{V}(T)$ is the set of the four vertices of T . More general, for a collection of tetrahedra \mathcal{S} , the set of all

vertices contained in \mathcal{S} is denoted by $\mathcal{V}(\mathcal{S})$. We write $\mathcal{V} := \mathcal{V}(\mathcal{T}_h)$. Furthermore, for $v \in \mathcal{V}$, $\mathcal{T}(v)$ is the set of all tetrahedra which have v as a vertex:

$$\mathcal{T}(v) = \{ T \in \mathcal{T}_h : v \in \mathcal{V}(T) \}.$$

We also need the recursively defined larger neighborhoods:

$$\mathcal{T}^1(v) := \mathcal{T}(v), \quad \mathcal{T}^{k+1}(v) = \{ T \in \mathcal{T}_h : \mathcal{V}(T) \cap \mathcal{V}(\mathcal{T}^k(v)) \neq \emptyset \}, \quad k \geq 1.$$

Finally, for $v \in \mathcal{V}$, $\mathcal{N}(v)$ is the collection of all neighboring vertices of v (i. e., for each $w \in \mathcal{N}(v)$ there is an edge in \mathcal{T}_h connecting v and w):

$$\mathcal{N}(v) := \left(\bigcup_{T \in \mathcal{T}(v)} \mathcal{V}(T) \right) \setminus \{v\}.$$

As input for the FMM we need \mathcal{T}_h , the zero level set Γ_h and $\text{sign}(\psi_h(v))$, $v \in \mathcal{V}$. Thus only $\text{sign}(\psi_h(v))$ is needed, and not $\psi_h(v)$ itself. The FMM consists of two phases: The *initialization phase*, where the values at vertices close to the interface are determined, and the *extension phase*, where the information is propagated from the interface to the vertices in the far field.

Initialization phase. We define the set of vertices corresponding to \mathcal{T}_h^Γ :

$$\mathcal{V}_\Gamma := \mathcal{V}(\mathcal{T}_h^\Gamma) = \{ v \in \mathcal{V}(T) : T \in \mathcal{T}_h^\Gamma \}. \quad (7.33)$$

The aim of the initialization phase is to define a discrete (approximate) distance function $\hat{d}(v)$ for each $v \in \mathcal{V}_\Gamma$. To this end, we present two possible strategies, a geometry-based approach and a weighted scaling approach.

We first consider the geometry-based approach. For $v \in \mathcal{V}_\Gamma$ and $T \in \mathcal{T}(v) \cap \mathcal{T}_h^\Gamma$ let Γ_T be the planar segment as in (7.32). This segment is either a triangle or a quadrilateral. In the latter case Γ_T can be subdivided into two triangles. If Δ is a triangle in \mathbb{R}^3 and $p \in \mathbb{R}^3$ then the distance between Δ and p

$$d(p, \Delta) := \min_{x \in \Delta} \|p - x\|, \quad (7.34)$$

can be computed using elementary geometry, for example as follows. If $\Delta = \text{conv}\{v_1, v_2, v_3\}$ and $\mathbf{A} = (v_2 - v_1, v_3 - v_1)$ one first solves the 3×2 least squares problem $\|\mathbf{A}z - (p - v_1)\| \rightarrow \min$. This results in the orthogonal projection of p on the plane that contains Δ . If this orthogonal projection is contained in the triangle Δ then the residual of the least squares problem equals $d(p, \Delta)$. Otherwise, $d(p, \Delta) = \text{dist}(p, \partial\Delta)$, and thus the distance of p to the three edges of Δ has to be determined.

Hence, for arbitrary $v \in \mathcal{V}_\Gamma$, $T \in \mathcal{T}_h^\Gamma$ we can compute

$$d_T(v) := d(v, \Gamma_T).$$

For a given $k \geq 1$ the (approximate) distance between v and Γ_h is defined by

$$\hat{d}(v) := \min_{T \in \mathcal{T}^k(v) \cap \mathcal{T}_h^T} d_T(v) = \min_{x \in \Gamma_h \cap \mathcal{T}^k(v)} \|v - x\| \quad \text{for } v \in \mathcal{V}_\Gamma. \quad (7.35)$$

In practice we typically use $k = 2$. Properties of the geometry based initialization are discussed in Remark 7.4.3.

Another approach is based on a scaling of the level set function at the vertices $v \in \mathcal{V}_\Gamma$. One motivation for this approach comes from the following observation. If one wants to guarantee that the approximated interface Γ_h is not moved by re-initialization, then the only choice is $\hat{d}(v) = \alpha^{-1} \phi_h(v)$ for $v \in \mathcal{V}_\Gamma$ with a suitable scalar $\alpha > 0$. Achieving the (distance) property $\|\nabla \hat{d}\| \approx 1$ by scaling with a *single* scalar, however, is not possible in general. Consider, for example, the case of a level set function ϕ_h which has a large gradient $\|\nabla \phi_h\| \approx 10^3$ in one part of \mathcal{T}_h^T and a small gradient $\|\nabla \phi_h\| \approx 10^{-3}$ in another part.

This leads to the idea to use a vertex-dependent scalar α_v , i. e., to define

$$\hat{d}(v) = \alpha_v^{-1} \phi_h(v), \quad v \in \mathcal{V}_\Gamma. \quad (7.36)$$

We propose to use

$$\alpha_v := \frac{\sum_{T \in \mathcal{T}(v)} \int_T \|\nabla \phi_h\| dx}{\sum_{T \in \mathcal{T}(v)} \int_T 1 dx}, \quad v \in \mathcal{V}_\Gamma, \quad (7.37)$$

i. e., α_v is an average of the gradients of ϕ_h on $\mathcal{T}(v)$. Compared to the geometry-based approach described above there is no need to reconstruct Γ_h from ϕ_h , allowing for a relatively simple implementation of the method. A comparison of both methods in a numerical example is given in Sect. 7.5.2. After completion of the initialization phase the values $\{(v, \hat{d}(v)) : v \in \mathcal{V}_\Gamma\}$ determine an approximate distance grid function for the vertices $v \in \mathcal{V}_\Gamma$.

Extension phase. The second phase consists of a greedy algorithm in which the approximate distance function \hat{d} is extended to neighbor vertices of \mathcal{V}_Γ and then to neighbors of neighbors, etc. To explain this more precisely we introduce two sets of vertices.

The first set $\hat{\mathcal{V}} \subset \mathcal{V}$ contains the vertices where the values of the approximate distance function $\hat{d} : \mathcal{V} \rightarrow \mathbb{R}$ have already been computed. As initialization we take $\hat{\mathcal{V}} := \mathcal{V}_\Gamma$. We call $\hat{\mathcal{V}}$ the *finalized set*.

The second one is the set of so-called *active* vertices $\mathcal{A} \subset \mathcal{V} \setminus \hat{\mathcal{V}}$, which consists of vertices $v \notin \hat{\mathcal{V}}$ that have a neighboring vertex in $\hat{\mathcal{V}}$:

$$\mathcal{A} := \left\{ v \in \mathcal{V} \setminus \hat{\mathcal{V}} : \mathcal{N}(v) \cap \hat{\mathcal{V}} \neq \emptyset \right\}. \quad (7.38)$$

\mathcal{A} is called the *active set*. After the initialization phase, the initial active set \mathcal{A}_0 is given by

$$\mathcal{A}_0 := \{ v \in \mathcal{V} \setminus \mathcal{V}_\Gamma : \mathcal{N}(v) \cap \mathcal{V}_\Gamma \neq \emptyset \}. \quad (7.39)$$

For $v \in \mathcal{A}$ we define an approximate distance function in a similar way as in the initialization phase. Since its values may change if the finalized and

active set are updated, we denote it by $\tilde{d} : \mathcal{A} \rightarrow \mathbb{R}$. We emphasize that \tilde{d} has tentative character in contrast to \hat{d} , which will be the final outcome of the algorithm. The construction of \tilde{d} is described in the following.

Take $v \in \mathcal{A}$ and $T \in \mathcal{T}(v)$ with $\mathcal{V}(T) \cap \hat{\mathcal{V}} \neq \emptyset$. Note that such a T exists if \mathcal{A} is nonempty. There are three possible cases, namely $|\mathcal{V}(T) \cap \hat{\mathcal{V}}| \in \{1, 2, 3\}$.

- If $|\mathcal{V}(T) \cap \hat{\mathcal{V}}| = 1$, say $\mathcal{V}(T) \cap \hat{\mathcal{V}} = \{w\}$, we define

$$\tilde{d}_T(v) := \hat{d}(w) + \|v - w\|.$$

- For the other two cases, i.e., $\mathcal{V}(T) \cap \hat{\mathcal{V}} = \{w_i\}_{1 \leq i \leq m}$ with $m = 2$ or $m = 3$, we use a distance function to the line segment $W = \text{conv}(w_1, w_2)$ (for $m = 2$) or the triangle $W = \text{conv}(w_1, w_2, w_3)$ (for $m = 3$), which is denoted by $d(v, W)$. In the case $m = 3$, this is the distance function as in (7.34). Let $P_W : \mathbb{R}^3 \rightarrow W$ be such that $d(v, W) = \|v - P_W v\|$. We define

$$\tilde{d}_T(v) := \hat{d}(P_W v) + \|v - P_W v\| = \hat{d}(P_W v) + d(v, W).$$

The value $\hat{d}(P_W v)$ is determined by linear interpolation of the *known* values $\hat{d}(w_j)$, $1 \leq j \leq m$. This is well-defined since $w_j \in \hat{\mathcal{V}}$ for $1 \leq j \leq m$ and \hat{d} is already defined on $\hat{\mathcal{V}}$.

The tentative approximate distance function $\tilde{d} : \mathcal{A} \rightarrow \mathbb{R}$ at active vertices $v \in \mathcal{A}$ is defined by

$$\tilde{d}(v) := \min \left\{ \tilde{d}_T(v) : T \in \mathcal{T}(v) \text{ with } \mathcal{V}(T) \cap \hat{\mathcal{V}} \neq \emptyset \right\}. \quad (7.40)$$

The complete re-initialization method is as follows:

Algorithm 7.4.1 (Fast Marching Method)

1. Initialization: \mathcal{V}_T as in (7.33), compute $\hat{d}(\mathcal{V}_T)$ as in (7.35) (or (7.36)).
2. Initialize finalized set $\hat{\mathcal{V}} := \mathcal{V}_T$ and active set $\mathcal{A} := \mathcal{A}_0$, cf. (7.39).
3. For the initial active set \mathcal{A}_0 , compute $\tilde{d}(\mathcal{A}_0)$ as in (7.39), (7.40).
4. While $\mathcal{A} \neq \emptyset$, repeat the following steps:
 - a) Determine $v_{\min} \in \mathcal{A}$ such that $\tilde{d}(v_{\min}) = \min_{v \in \mathcal{A}} \tilde{d}(v)$.
 - b) Update finalized set $\hat{\mathcal{V}} := \hat{\mathcal{V}} \cup \{v_{\min}\}$ and define $\hat{d}(v_{\min}) := \tilde{d}(v_{\min})$.
 - c) Update active set $\mathcal{A} := (\mathcal{A} \cup \tilde{\mathcal{N}}) \setminus \{v_{\min}\}$ where $\tilde{\mathcal{N}} := \mathcal{N}(v_{\min}) \setminus \hat{\mathcal{V}}$.
 - d) (Re)compute $\tilde{d}(v)$ for $v \in \tilde{\mathcal{N}}$.
5. For all $v \in \mathcal{V}$, set $\hat{d}(v) := \text{sign}(\psi_h(v)) \cdot \tilde{d}(v)$.

After this re-initialization we have $\hat{\mathcal{V}} = \mathcal{V}$ and a grid function $\hat{d}(v)$, $v \in \mathcal{V}$, which uniquely determines a continuous piecewise linear approximate signed

distance function. This function is defined to be the re-initialization of ψ_h , denoted by $\hat{\psi}_h$. The zero level set of $\hat{\psi}_h$ is denoted by $\hat{\Gamma}_h$. Below, in Remark 7.4.3 we discuss important approximation properties of the re-initialization $\hat{\psi}_h$ and its zero level.

Remark 7.4.2 (Complexity) The number of (arithmetic) operations for the initialization phase (steps 1–3 in Algorithm 7.4.1) is $\mathcal{O}(|\mathcal{V}_\Gamma| + |\mathcal{A}_0|)$. For the extension phase (steps 4–5 in Algorithm 7.4.1) the sorting and updating in the steps 4.a)-c) can be realized with $\mathcal{O}(\log |\mathcal{A}|)$ complexity using a heap data structure for \mathcal{A} . Step 4 is repeated $N_\mathcal{V} := |\mathcal{V} \setminus \mathcal{V}_\Gamma|$ times, and thus this FMM has an overall complexity of the order $\mathcal{O}(N_\mathcal{V} \log N_\mathcal{V})$.

Remark 7.4.3 (Approximation properties) A detailed analysis of the FMM in Algorithm 7.4.1 using the geometry-based initialization phase (7.35) is given in [123]. We outline some main results. By construction each $T \in \mathcal{T}_h^\Gamma$ contains a segment of the new zero level $\hat{\Gamma}_h$ and thus $\text{dist}(\Gamma_h, \hat{\Gamma}_h) \leq h_\Gamma$ holds. In practice, however, one typically observes $\text{dist}(\Gamma_h, \hat{\Gamma}_h) \ll h_\Gamma$, which can be explained by the results from [123]. We use notation and assumptions as in Sect. 7.3.1. We assume that Γ_h approximates a smooth interface Γ and define d to be the signed distance function to Γ . The approximation error is assumed to be sufficiently small in the following sense:

$$|d(x)| \leq ch_\Gamma^2 \quad \text{for all } x \in \Gamma_h, \quad (7.41a)$$

$$\|\mathbf{n}(x) - \mathbf{n}_h(x)\| \leq ch_\Gamma \quad \text{for all } x \in \Gamma_h. \quad (7.41b)$$

In our setting these are reasonable assumptions, cf. Theorem 7.3.1. The approximate interface Γ_h is the zero level of the given piecewise linear function ψ_h . Let d_h be the signed distance function to Γ_h . After the initialization phase, for $v \in \mathcal{V}_\Gamma$ the re-initialization $\hat{\psi}_h(v)$ is determined by the function \hat{d} in (7.35): $\hat{\psi}_h(v) = \text{sign}(\psi_h(v))\hat{d}(v)$ for $v \in \mathcal{V}_\Gamma$. Note that \hat{d} in (7.35) depends on $k \geq 1$. It is obvious that for k sufficiently large we have

$$\hat{\psi}_h(v) = d_h(v) \quad \text{for all } v \in \mathcal{V}_\Gamma, \quad (7.42)$$

i.e. at the vertices in \mathcal{V}_Γ we have determined the *exact* signed distance to Γ_h . For the theoretical analysis we assume that (7.42) holds. Based on experience, in computations we take $k = 2$. Note that a larger k value induces higher computational costs for the re-initialization.

Based on the assumptions in (7.41), (7.42) one can derive the following results:

$$|d(x)| \leq ch_\Gamma^2 \quad \text{for all } x \in \hat{\Gamma}_h, \quad (7.43a)$$

$$\|\nabla \hat{\psi}_h - \mathbf{n}\|_{L^\infty(\mathcal{T}_h^\Gamma)} \leq ch_\Gamma. \quad (7.43b)$$

The result in (7.43a) shows that in the re-initialization the accuracy of the zero level set as an approximation of Γ is maintained. Due to $\|\mathbf{n}\| = 1$, we conclude from (7.43b) that $\|\nabla \hat{\psi}_h(x)\| = 1 + \mathcal{O}(h_\Gamma)$ for $x \in \mathcal{T}_h^\Gamma$, i.e., $\hat{\psi}_h$ is, at least in

a neighborhood of its zero level, close to a signed distance function. These approximation properties of the re-initialization are illustrated in a numerical experiment in Sect. 7.5.2.

Application of FMM to a piecewise quadratic function

Let $\phi_h \in \mathbb{X}_h^2$ be a piecewise quadratic function corresponding to the triangulation \mathcal{T}_h . The regular refinement of \mathcal{T}_h is denoted by $\mathcal{T}_{h'} := \{T' \in \mathcal{K}(T) : T \in \mathcal{T}_h\}$ and $I(\phi_h)$ is the continuous piecewise linear function on $\mathcal{T}_{h'}$ that interpolates ϕ_h at all vertices of all tetrahedra in $\mathcal{T}_{h'}$. The approximate interface Γ_h is the zero level of $I(\phi_h)$. We can apply the FMM given above to the function $I(\phi_h)$, which results in the function $\widehat{I(\phi_h)}$ that is piecewise linear on $\mathcal{T}_{h'}$. The values at the vertices of this function uniquely define a piecewise *quadratic* function on \mathcal{T}_h , which is denoted by $\hat{\phi}_h =: FMM(\phi_h)$ and is defined to be the re-initialization of ϕ_h .

Remark 7.4.4 There is a need for re-initialization, only if the size of the gradient of ϕ_h is “too small” or “too large”. One possibility to quantify this is the following. For $c > 1$ define the subset

$$V_c := \left\{ \phi_h \in \mathbb{X}_h^2 : \|\nabla\phi_h\|_{L^2(T)} < c|T|^{\frac{1}{2}} \quad \forall T \in \mathcal{T}_{h'} \right\} \\ \cap \left\{ \phi_h \in \mathbb{X}_h^2 : \frac{1}{c}|T|^{\frac{1}{2}} < \|\nabla\phi_h\|_{L^2(T)} \quad \forall T \in \mathcal{T}_{h'} \right\}.$$

In practice we take $c \in [5, 10]$ and apply the FMM only if $\phi_h \notin V_c$. This defines a re-initialization mapping $\text{ReInit} : \mathbb{X}_h^2 \rightarrow \mathbb{X}_h^2$:

$$\text{ReInit}(\phi_h) = \begin{cases} \phi_h & \text{if } \phi_h \in V_c, \\ \hat{\phi}_h = FMM(\phi_h) & \text{otherwise.} \end{cases} \quad (7.44)$$

The FMM is such that $\|\nabla\hat{\phi}_h\|$ is close to one, in particular we have (for c not too close to one) $\hat{\phi}_h \in V_c$. Hence one can expect $\text{ReInit}(\text{ReInit}(\phi_h)) = \text{ReInit}(\phi_h)$ to hold for all $\phi_h \in \mathbb{X}_h^2$. Furthermore, one can check that the re-initialization mapping ReInit is *continuous* on V_c .

7.4.2 Mass conservation

Due to immiscibility the mass of the phase contained in $\Omega_i(t)$ is constant. Using the incompressibility of the phases, it follows that the volume $V_i(t) := \int_{\Omega_i(t)} 1 \, dx$ is conserved, i.e. $\frac{d}{dt} V_i(t) = 0$ for $i = 1, 2$. Due to $\overline{\Omega_1(t)} \cup \overline{\Omega_2(t)} = \overline{\Omega}$ it suffices to consider $i = 1$ (or $i = 2$). For the level set function the quantity $\int_{\Omega_i(t)} \phi(x, t) \, dx$ is conserved:

$$\frac{d}{dt} \int_{\Omega_i(t)} \phi(x, t) \, dx = 0, \quad i = 1, 2, \quad (7.45)$$

which follows from the Reynolds' transport theorem and $\operatorname{div} \mathbf{u} = 0$. There is, however, no natural relation between this conservation property and mass conservation. The VOF method for interface capturing is based on a discretization of a transport equation for the characteristic function corresponding to Ω_1 (denoted by χ_1) and thus this method has a natural discrete mass conservation property. Recall the transport equation for χ_1 :

$$\frac{\partial}{\partial t} \int_W \chi_1 dx + \int_{\partial W} \chi_1 \mathbf{u} \cdot \mathbf{n} ds = 0, \quad W \subset \Omega,$$

cf. (6.26) (\mathbf{n} is the outward unit normal on ∂W). Applying a conservative finite volume method to this problem results in a discretization $\tilde{\chi}_1(x, t_n)$ of $\chi_1(x, t_n)$, for which

$$\int_{\Omega} \tilde{\chi}_1(x, t_n) - \tilde{\chi}_1(x, t_{n-1}) dx = 0, \quad n = 1, \dots, \frac{T}{\Delta t},$$

holds. Hence the volume conservation property holds on the discrete level.

In general the (temporal and spatial) discretization of the level set equation do *not* guarantee a volume conservation property. Also the FMM for re-initialization of the level set function is not volume-conserving. This is a disadvantage of the level set method compared to the VOF method. Since for $\Delta t \downarrow 0$, $h \downarrow 0$ the discrete level set function converges to the exact solution ϕ of the level set equation, one may expect that the amount of change in volume is reduced if the time step and mesh size are taken smaller. For the SDFEM method combined with Crank-Nicolson time discretization this is analyzed in [169]. The analysis is based on a discretization error bound

$$\|\phi_h^N - \phi(\cdot, T)\|_{L^2} \leq cT(h^{k+\frac{1}{2}} + \Delta t^2), \quad (7.46)$$

for the finite element approximation $\phi_h^N(x)$, cf. (7.19). Let $V_1(\phi_h^N)$ be the numerical approximation of the exact volume $V_1(T) = V_1(0) = V_1$, i.e., $V_1(\phi_h^N) = \int_{\Omega_{1,h}^N} 1 dx$, with $\Omega_{1,h}^N := \{x \in \Omega : \phi_h^N(x) < 0\}$. In [169] it is shown that from the discretization error bound (7.46) and with $\Delta t \sim h^{\frac{1}{2}k+\frac{1}{4}}$ one can derive the volume error estimate

$$|V_1(\phi_h^N) - V_1| \leq ch^k.$$

This estimate shows how the volume error can be controlled by reducing the mesh size.

In recent years there have appeared studies in which modifications of the level set method are presented that have better volume conservation properties. Often these modifications are based on combining the level set approach with a VOF technique. We do not treat this topic here, but refer to the literature, e.g. [229, 203, 87, 196].

In the literature also the following very simple (but less satisfactory) strategy, which guarantees volume conservation for the level set method, can be found. Let $V_1(0) = \int_{\Omega_1(0)} 1 \, dx$ be the volume of Ω_1 at $t = 0$, that is assumed to be known. For a given $t > 0$, let $\phi_h(x) \approx \phi(x, t)$ be a computed approximation of the level set function and introduce

$$\Omega_{1,h}(t) := \{x \in \Omega : \phi_h(x, t) < 0\}, \quad V_1(\phi_h; t) := \int_{\Omega_{1,h}(t)} 1 \, dx.$$

We assume that the quantity $V_1(\phi_h; t)$ can easily be determined (sufficiently accurate). In our applications, where ϕ_h is piecewise quadratic on \mathcal{T}_h , we use the interpolation $I(\phi_h)$, which is piecewise linear on the refined triangulation $\mathcal{T}_{h'}$ and take

$$\Omega_{1,h}(t) := \{x \in \Omega : I(\phi_h(\cdot, t))(x) < 0\}.$$

Then $\partial\Omega_{1,h}(t) = \Gamma_h(t)$ and the integral $\int_{\Omega_{1,h}(t)} 1 \, dx$ can be determined exactly (apart from rounding errors) using a simple quadrature rule on tetrahedra. In general one has no volume conservation, i.e. there may be a significant difference between $V_1(0)$ and $V_1(\phi_h; t)$. Due to the fact that ϕ_h is close to a signed distance function, a shift of the interface over a distance δ in outward normal direction can be realized (approximately) if one subtracts δ from the approximate level set function ϕ_h . For (exact!) volume conservation one has to find $\delta \in \mathbb{R}$ such that

$$V_1(\phi_h - \delta; t) - V_1(0) = 0$$

holds. In a method for computing a zero of this scalar function it is important to keep the number of evaluations of $V_1(\cdot; t)$ low. In our numerical simulations we use the Anderson-Björck method [14] to solve this equation. Let δ^* be a solution of this problem. We then set $\phi_h^{\text{new}} := \phi_h - \delta^*$ and discard ϕ_h .

Note that this strategy only works if Ω_1 consists of a single component. If there are multiple components, volume must be preserved for each of them. In this case the algorithm can be modified to shift ϕ_h only locally.

Clearly, using this simple strategy we have optimal volume conservation for the discrete level set function. Nevertheless, this approach is not very satisfactory since it introduces an additional discretization error source which is very hard to control.

7.5 Numerical experiments with the level set equation

In this section we present results of two numerical experiments to illustrate the performance of the discretization method for the level set equation and of the fast marching re-initialization technique.

7.5.1 Discretization using the SDFEM

We take $\Omega = [0, 1]^3$ and the ball $\Omega_1 := \{x \in \mathbb{R}^3 : \|x - x_M\| < 0.2\}$ with center $x_M = (\frac{1}{2}, \frac{1}{4}, \frac{1}{2})$. We use the stationary velocity field

$$\hat{\mathbf{u}}(x) = c(y) \cdot (y_2, -y_1, 0)$$

where $y := x - (\frac{1}{2}, \frac{1}{2}, \frac{1}{2})$ and

$$c(y) = \begin{cases} 4\|y\|(0.5 - \|y\|) & \text{if } \|y\| \leq \frac{1}{2}, \\ 0 & \text{otherwise.} \end{cases}$$

Hence, $\hat{\mathbf{u}}$ is a circular velocity field, cf. Fig. 7.6 for an illustration of $\hat{\mathbf{u}}$. Furthermore, $\hat{\mathbf{u}} = 0$ on $\partial\Omega$ holds. We consider the time interval $[0, T_{\text{end}}]$ and define the velocity field

$$\mathbf{u}(x, t) = \begin{cases} \hat{\mathbf{u}}(x) & t \leq \frac{1}{2}T_{\text{end}}, \\ -\hat{\mathbf{u}}(x) & t > \frac{1}{2}T_{\text{end}}. \end{cases}$$

We consider the level set equation

$$\frac{\partial\phi}{\partial t} + \mathbf{u} \cdot \nabla\phi = 0 \quad \text{in } \Omega, \quad t \in [0, T_{\text{end}}],$$

with initial condition $\phi(x, 0) = d(x)$, where d is the signed distance function to $\Gamma(0) := \partial\Omega_1$. In Fig. 7.7, for $T_{\text{end}} = 20$, an illustration of the computed zero level of $\phi(x, t)$ at different times is shown. Clearly, $\phi(x, T_{\text{end}}) = d(x)$, $x \in \Omega$, holds. Thus the exact solution is known for $t = T_{\text{end}}$.

The initial tetrahedral triangulation is obtained by subdividing Ω into 8 subcubes, each of which is subdivided into six tetrahedra. Then repeated global regular refinement is applied to this initial triangulation. This results in nested triangulations \mathcal{T}_{h_ℓ} with mesh size parameter $h_\ell = (\frac{1}{2})^\ell$. On each triangulation we apply a method of lines discretization.

For the space discretization we use the SDFEM with quadratic finite elements. Due to $\mathbf{u} = 0$ on $\partial\Omega$ we do not need boundary conditions for ϕ . Therefore we can use the finite space $V_h := \mathbb{X}_h^2$ of piecewise quadratic finite elements, without any boundary conditions.

Remark 7.5.1 In other problems we usually have $\mathbf{u} \neq 0$ on $\partial\Omega$. In that case, in the weak formulation of the level set equation in (6.59c) we use a trial space with Dirichlet boundary conditions on the inflow boundary $\partial\Omega_{\text{in}}$ to make this hyperbolic problem well-posed. We discuss a possible choice of these (artificial) boundary conditions. Let $\phi_0 = \phi_0(x)$, $x \in \Omega$, be the initialization for the level set function. The Dirichlet data for the level set function can be taken as follows:

$$\phi_D(x, t) = \phi_0(x) - \mathbf{u}(x, 0) \cdot \nabla\phi_0(x) t, \quad x \in \partial\Omega_{\text{in}}, \quad t \in [0, t_0]. \quad (7.47)$$

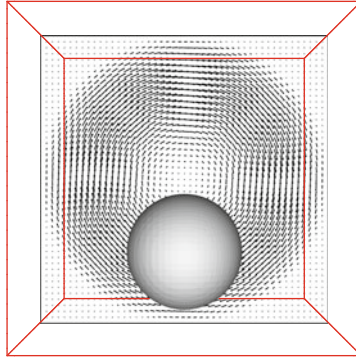


Fig. 7.6. Interface $\Gamma(0)$. Also shown is the velocity field $\hat{\mathbf{u}}$ on the slice $x_3 = 0$.

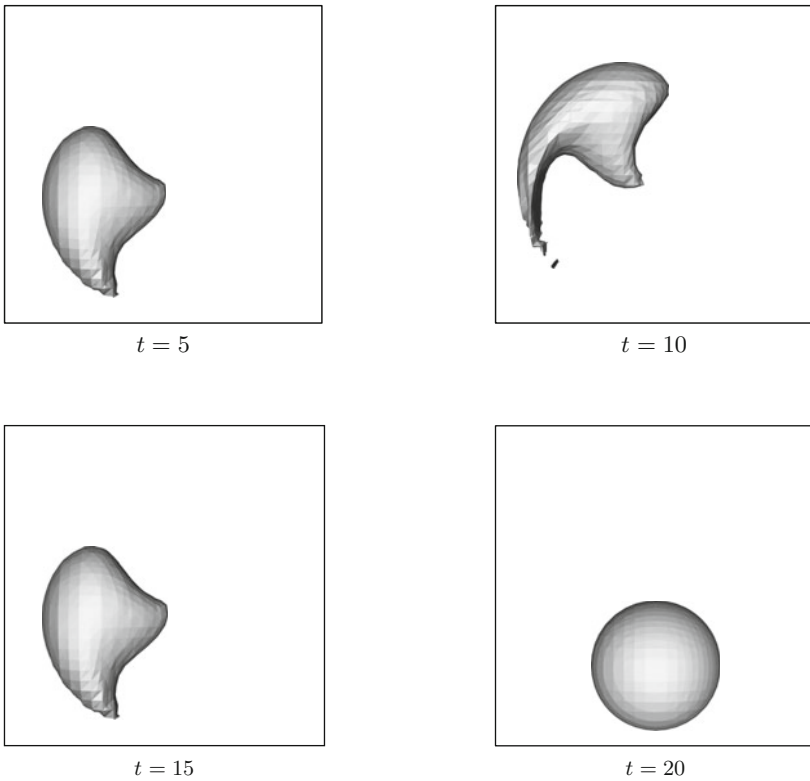


Fig. 7.7. Computed interface at different times.

These data are used until $t = t_0$, the point in time at which a re-initialization is applied. The re-initialization results in a modified level set function $\tilde{\phi}_h(x)$ and for $t \in (t_0, t_1]$ Dirichlet boundary data are defined as in (7.47) but with ϕ_0 replaced by $\tilde{\phi}_h$ and $\mathbf{u}(x, 0)$ replaced by $\mathbf{u}(x, t_0)$, etc. Note that this Dirichlet boundary condition is time dependent. We explain the heuristics leading to a boundary condition as in (7.47). For this we assume the inflow boundary $\partial\Omega_{in}$ to be planar and $\mathbf{u}(x, 0)$, $x \in \partial\Omega_{in}$, to be normal to the inflow boundary, i.e. $\mathbf{u}(x, 0) = -\|\mathbf{u}(x, 0)\|\mathbf{n}(x)$, with \mathbf{n} the outward pointing unit normal on the boundary. The initial data ϕ_0 are extrapolated linearly by $\phi_0(x + \alpha\mathbf{n}(x)) := \phi_0(x) + \alpha \frac{\partial\phi_0(x)}{\partial n} = \phi_0(x) + \alpha\mathbf{n}(x) \cdot \nabla\phi_0(x)$, $\alpha \geq 0$. This defines initial data in the inflow region, outside the domain Ω . The velocity field \mathbf{u} has a natural constant extension given by $\mathbf{u}(x + \alpha\mathbf{n}(x), 0) := \mathbf{u}(x, 0)$, $x \in \partial\Omega_{in}$, $\alpha \geq 0$. Solving the level set equation, which describes transport of the initial data by the velocity field \mathbf{u} , results in

$$\phi(x, t) = \phi_0(x - t\mathbf{u}(x, 0)) = \phi_0(x) - t\mathbf{u}(x, 0) \cdot \nabla\phi_0(x), \quad x \in \partial\Omega_{in}, \quad t \geq 0,$$

which is the boundary condition proposed in (7.47).

The streamline diffusion finite element method is as explained in Sect. 7.2.2: Determine $\phi_h(t) \in V_h$ with $\phi_h(0) = d_h$ and such that

$$\sum_{T \in \mathcal{T}_h} \left(\frac{\partial\phi_h}{\partial t} + \mathbf{u} \cdot \nabla\phi_h, v_h + \delta_T \mathbf{u} \cdot \nabla v_h \right)_{L^2(T)} = 0 \quad \text{for all } v_h \in V_h,$$

and $t \in [0, T_{\text{end}}]$. Here d_h is the nodal interpolation of the initial condition d in the finite element space V_h . For the parameter δ_T in this method we take, cf. (7.14),

$$\delta_T = SD \frac{h_T}{\max\{10^{-3}, \|\mathbf{u}\|_{\infty, T}\}},$$

with a constant SD that is varied below. The resulting system of ordinary differential equations (7.16) is discretized using the implicit Euler or Crank-Nicolson method with a time step size Δt . Because in this experiment we want to study the accuracy of the discretization method, we do *not* use re-initialization of the level set function. In the Crank-Nicolson method we do *not* apply any volume correction procedure. In the implicit Euler method, however, the results without volume correction turn out to be very poor. Therefore we applied the simple method described in Sect. 7.4.2 at $t = 4, 8, \dots, 20$. The space and time discretization results in an approximation $\phi_h^n \in V_h$ of $\phi(\cdot, t_n)$, $t_n := n\Delta t$. Let N be such that $N\Delta t = T_{\text{end}}$, i.e. ϕ_h^N is an approximation of $\phi(\cdot, T_{\text{end}}) = d$. The approximate zero level of ϕ_h^n is constructed as explained in Sect. 7.3 and is denoted by $\Gamma_h(t_n)$. This approximate interface consists of a set $\{\Gamma_T : T \in \mathcal{T}_h^I\}$ of planar segments $\Gamma_T = T \cap \Gamma_h$, $T \in \mathcal{T}_h^I$.

We now turn to a quantitative evaluation of the discretization method. Since $\Gamma(T_{\text{end}}) = \Gamma(0)$ and d is the signed distance function to the *exact* initial

zero level $\Gamma(0)$, as a measure for the quality of $\Gamma_h(t_n) \approx \Gamma(0)$, $n = 0, n = N$, we introduce

$$\|d\|_{L^2(\Gamma_h(t_n))} := \sqrt{\sum_{\Gamma_T \subset \Gamma_h(t_n)} \int_{\Gamma_T} d(x)^2 dx}, \quad n = 0, n = N. \quad (7.48)$$

As a second error measure we use the global $L^2(\Omega)$ error,

$$\|d - \phi_h^n\|_{L^2(\Omega)} = \sqrt{\sum_{T \in \mathcal{T}_h} \int_T |d(x) - \phi_h^n(x)|^2 dx}, \quad n = 0, n = N, \quad (7.49)$$

which can be determined accurately using suitable quadrature. Note that for $n = 0$ we have $\phi_h^0 = d_h$ and in these error quantities only the interpolation error $d - d_h$ and the approximation of the zero level of the interpolant d_h plays a role. In Table 7.1 we give these quantities for $n = 0$ and different grid sizes h_ℓ .

ℓ	$\ d\ _{L^2(\Gamma_h(0))}$	order	ℓ	$\ d - \phi_h^0\ _{L^2(\Omega)}$	order
1	1.77 E-2	-	1	4.90 E-2	-
2	3.90 E-3	2.18	2	1.28 E-2	1.94
3	9.37 E-4	2.06	3	3.27 E-3	1.97
4	2.31 E-4	2.02	4	8.17 E-4	2.00
5	5.82 E-5	1.99	5	2.04 E-4	2.00

Table 7.1. Approximation errors for different mesh sizes $h = h_\ell$.

These results are consistent with the expected h_ℓ^2 convergence.

The quality of the space and time discretization is measured by these quantities for $n = N$. We only consider the implicit Euler method, since for the Crank-Nicolson method this test case is not representative, cf. Remark 7.5.2. Results for $T_{\text{end}} = 20$ and several mesh and time step sizes are given in Table 7.2 and Table 7.3. Note that for $SD = 0$ there is no stabilization in the spatial finite element discretization.

A first (surprising) observation is that the method without stabilization ($SD = 0$) produces very good results. One observes an $\mathcal{O}(\Delta t)$ error behavior if the time step is reduced. For $\Delta t = 2^{-6}$ one obtains close to optimal errors; for example, for $\ell = 3$ we have $\|d\|_{L^2(\Gamma_h(20))} = 1.07 \text{ E-3}$ and $\|d - \phi_h^N\|_{L^2(\Omega)} = 4.21 \text{ E-3}$, which have to be compared with the interpolation errors 9.37 E-4 and 3.27 E-3 of the initial data from Table 7.1. The performance of the method with stabilization is worse. In case of the stabilization with $SD = \frac{1}{2}$ we do not observe an $\mathcal{O}(\Delta t)$ error reduction behavior. Furthermore, for Δt “small” the error is dominated by the spatial discretization error and stagnates at a level higher than the interpolation error level. An explanation of this behavior is a topic for further research.

	$\ell = 3$		$\ell = 4$	
Δt	$SD = 0$	$SD = \frac{1}{2}$	$SD = 0$	$SD = \frac{1}{2}$
2^{-1}	1.34 E-2	1.42 E-2	1.40 E-2	1.32 E-2
2^{-2}	7.04 E-3	1.03 E-2	7.24 E-3	7.34 E-3
2^{-3}	3.87 E-3	8.84 E-3	3.87 E-3	4.55 E-3
2^{-4}	2.20 E-3	8.31 E-3	2.04 E-3	3.27 E-3
2^{-5}	1.39 E-3	8.11 E-3	1.05 E-3	2.80 E-3
2^{-6}	1.07 E-3	8.02 E-3	5.64 E-4	2.66 E-3

Table 7.2. Implicit Euler: error $\|d\|_{L^2(\Gamma_h(20))}$ for different $h = h_\ell$ and Δt

	$\ell = 3$		$\ell = 4$	
Δt	$SD = 0$	$SD = \frac{1}{2}$	$SD = 0$	$SD = \frac{1}{2}$
2^{-1}	3.77 E-2	4.15 E-2	3.61 E-2	3.72 E-2
2^{-2}	2.14 E-2	2.54 E-2	1.96 E-2	2.06 E-2
2^{-3}	1.22 E-2	1.66 E-2	1.03 E-2	1.13 E-2
2^{-4}	7.54 E-3	1.23 E-2	5.49 E-3	6.62 E-3
2^{-5}	5.27 E-3	1.02 E-2	3.12 E-3	4.37 E-3
2^{-6}	4.21 E-3	9.29 E-3	1.94 E-3	3.33 E-3

Table 7.3. Implicit Euler: error $\|d - \phi_h^N\|_{L^2(\Omega)}$ for different $h = h_\ell$ and Δt

Remark 7.5.2 Consider a system of ODEs of the form $y'(t) + F(t)y(t) = 0$, $y(0) = y_0$, $t \in [0, T_{\text{end}}]$ with $F(t) = A$ for $t \in [0, \frac{1}{2}T_{\text{end}}]$, $F(t) = -A$ for $t \in (\frac{1}{2}T_{\text{end}}, T_{\text{end}}]$ and $A \in \mathbb{R}^{n \times n}$ a given matrix. We apply the Crank-Nicolson method with a time step size $\Delta t = T_{\text{end}}/N$ and N even, resulting in approximations y^n of $y(t_n)$, $n = 1, 2, \dots, N$. One easily checks that, due to the special symmetry in the problem and in the Crank-Nicolson method, we have $y^N = y(0)$, i.e., the initial condition is exactly reproduced. In our test example we have such a symmetry in the spatially discretized problem (for the case $SD = 0$). Therefore, if we repeat the numerical experiment described above using the Crank-Nicolson method instead of the implicit Euler method we obtain $\|d\|_{L^2(\Gamma_h(20))} = \|d - \phi_h^N\|_{L^2(\Omega)} = 0$ for the case $SD = 0$ and very small errors for the case $SD = \frac{1}{2}$.

In order to compare the Crank-Nicolson method to the implicit Euler method we performed an experiment in which only the time discretization error is measured. On a fixed triangulation with mesh size $h = \frac{1}{8}$ we applied the SDFEM with $SD = 0.1$. We take $T_{\text{end}} = 20$ and on the time interval $[0, 10]$ the resulting system of ODEs is solved with a “small” time step $\frac{1}{10}2^{-5}$ resulting in a reference solution at $t = 10$ denoted by $\tilde{\phi}_h \approx \phi(\cdot, 10)$. Note that for $t \in [0, 10]$ the droplet is transported with the velocity field $\hat{\mathbf{u}}$ and does not move back to the initial position. Hence the symmetry property addressed in Remark 7.5.2 does not hold. The system of ODEs is solved using

both the Crank-Nicolson and the implicit Euler method for time step sizes $\Delta t = 2^{-k}$, $k = 0, \dots, 5$. The computed result at $t = 10$ is denoted by $\phi_h^{\frac{1}{2}N}$. In the Tables 7.4 and 7.5 we give the errors $\|\tilde{\phi}_h - \phi_h^{\frac{1}{2}N}\|_{L^2(\Omega)}$. These results show the expected rate of convergence, namely $\mathcal{O}(\Delta t)$ for the Euler method and $\mathcal{O}(\Delta t^2)$ for the Crank-Nicolson method.

Δt	2^0	2^{-1}	2^{-2}	2^{-3}	2^{-4}	2^{-5}
$\ell = 3$	2.88 E-2	1.54 E-2	7.85 E-3	3.93 E-3	1.96 E-3	9.65 E-4

Table 7.4. Implicit Euler: discretization error $\|\tilde{\phi}_h - \phi_h^{\frac{1}{2}N}\|_{L^2(\Omega)}$.

Δt	2^0	2^{-1}	2^{-2}	2^{-3}	2^{-4}	2^{-5}
$\ell = 3$	1.42 E-3	3.87 E-4	9.82 E-5	2.82 E-5	6.14 E-6	1.53 E-6

Table 7.5. Crank-Nicolson: discretization error $\|\tilde{\phi}_h - \phi_h^{\frac{1}{2}N}\|_{L^2(\Omega)}$.

7.5.2 Re-initialization by the Fast Marching Method

In this section we present some quantitative results related to the quality of the Fast Marching re-initialization method. More results are presented in [123]. We consider the cubic domain $\Omega = (-1, 1)^3$ and the quadratic level set function

$$\phi(x) = \|x\|^2 - r^2, \quad x \in \Omega, \quad r = 0.6.$$

The zero level of ϕ , denoted by Γ , is given by the sphere centered at the origin with radius r . On Γ we have $\|\nabla\phi\| = 2r = 1.2$. The signed distance function to Γ is denoted by $d(x)$. The domain Ω is subdivided into 8 subcubes, each subdivided into 6 tetrahedra. This defines the level $\ell = 0$ triangulation. The level $\ell \geq 1$ triangulation \mathcal{T}_{h_ℓ} is obtained by ℓ local refinements in the neighborhood $\{x \in \Omega : |d(x)| \leq 0.1\}$. The level ℓ triangulation has local mesh size parameter $h_{\Gamma,\ell} = (\frac{1}{2})^\ell$. To the quadratic function ϕ on a given triangulation $\mathcal{T}_h = \mathcal{T}_{h_\ell}$ we apply the FMM as discussed at the end of Sect. 7.4.1. As output of the initialization phase in the FMM one obtains an approximate signed distance function, denoted by $\hat{\psi}_h$, which is piecewise linear on $\mathcal{T}_{h'}$ ($h' = \frac{1}{2}h$; we use notation as in Sect. 7.4.1). The zero level of $\hat{\psi}_h$, which is contained in $\mathcal{T}_{h'}$, defines the new approximate interface denoted by $\hat{\Gamma}_h$. Let $\hat{\mathcal{F}}$ denote the set of triangles forming $\hat{\Gamma}_h$, i. e., $\hat{\Gamma}_h = \bigcup_{F \in \hat{\mathcal{F}}} F$, and $\hat{\mathcal{P}} = \left\{ v \in \hat{\Gamma}_h : v \text{ is vertex of triangle } F \in \hat{\mathcal{F}} \right\}$ the set of their vertices.

To measure the quality of this re-initialization we computed the quantities

$$e_{h,\infty} := \max_{v \in \hat{\mathcal{P}}} |d(v) - \hat{\psi}_h(v)| = \max_{v \in \hat{\mathcal{P}}} |d(v)|, \quad (7.50a)$$

$$\nabla e_{h,\infty} := \max_{T \in \mathcal{T}_h^r} \left\{ \|\nabla d(c) - \nabla \hat{\psi}_h(c)\| : c \text{ barycenter of } T \right\}. \quad (7.50b)$$

An important parameter in the geometry-based initialization phase is k , cf. (7.35). Below we consider $k = 1$ and $k = 2$. The results are compared to the scaling approach, cf. (7.36). In Tables 7.6 and 7.7 we present values of $e_{h,\infty}$ and $\nabla e_{h,\infty}$, respectively, for different levels ℓ and the different initialization strategies. Using the geometry-based initialization phase, for $k = 1$ we do

ℓ	geom, $k = 1$	order	geom, $k = 2$	order	scale	order
1	5.49 E-2	–	5.49 E-2	–	3.55 E-2	–
2	1.34 E-2	2.03	1.34 E-2	2.03	1.01 E-2	1.81
3	3.62 E-3	1.89	3.62 E-3	1.89	2.55 E-3	1.99
4	9.04 E-4	2.00	9.04 E-4	2.00	6.60 E-4	1.95
5	3.18 E-4	1.51	2.27 E-4	2.00	1.66 E-4	1.99
6	1.42 E-4	1.17	5.67 E-5	2.00	4.16 E-5	1.99

Table 7.6. Error measures $e_{h,\infty}$ for different initialization approaches and $h = h_\ell$.

not observe second order convergence for $e_{h,\infty}$. Moreover, we see a stagnation for $\nabla e_{h,\infty}$, meaning that the re-initialized interface does not get smoother on finer grids which renders the choice $k = 1$ unfeasible. Taking $k = 2$ instead, we do get quadratic convergence for $e_{h,\infty}$ and linear convergence for $\nabla e_{h,\infty}$, showing that the choice $k = 2$ should be preferred. The same convergence properties hold for the scaling approach which is less expensive in terms of computational effort. The results confirm the theoretical error bounds discussed in Remark 7.4.3. We briefly comment on this. Take $T \in \mathcal{T}_h^r$ and let I_T be the linear interpolation operator on T that interpolates at the vertices of T . For $x \in T$ we have $(d - \hat{\psi}_h)(x) = I_T(d - \hat{\psi}_h)(x) + \mathcal{O}(h_T^2)$. The results in the fifth column in Table 7.6 indicate $|I_T(d - \hat{\psi}_h)(x)| \leq ch_T^2$ uniformly in T and $x \in \Gamma_T = \Gamma \cap T$. Hence for $x \in \hat{\Gamma}_h$, i.e. $\hat{\psi}_h(x) = 0$, we get $|d(x)| \leq ch_T^2$, which is the same as the bound in (7.43a). Since $\nabla d = \mathbf{n}$ the results in the fifth column in Table 7.7 are consistent with the error bound given in (7.43b).

7.6 Discretization of the surface tension functional

In this section we explain how the localized surface tension force term $f_\Gamma(\mathbf{v})$ in (6.59a) can be approximated. We use the approach presented in [23, 93, 126].

Let \mathbf{V}_h be the finite element space that is used for the discretization of the velocity unknown. In our simulations we use for \mathbf{V}_h the standard conforming space of continuous piecewise quadratic functions. Applying the Galerkin

ℓ	geom, $k = 1$	order	geom, $k = 2$	order	scale	order
1	3.07 E-1	–	2.09 E-1	–	1.87 E-1	–
2	2.70 E-1	0.19	1.34 E-1	0.64	1.03 E-1	0.87
3	1.73 E-1	0.64	7.12 E-2	0.91	5.62 E-2	0.87
4	3.78 E-1	-1.13	3.69 E-2	0.95	2.79 E-2	1.01
5	4.69 E-1	-0.31	1.80 E-2	1.04	1.42 E-2	0.98
6	5.11 E-1	-0.12	8.95 E-3	1.01	7.04 E-3	1.01

Table 7.7. Error measures $\nabla e_{h,\infty}$ for different initialization approaches and $h = h_\ell$.

discretization to the variational (momentum) equation (6.59a) results in a *surface tension functional* of the form

$$f_\Gamma(\mathbf{v}_h) = -\tau \int_\Gamma \kappa \mathbf{v}_h \cdot \mathbf{n} \, ds, \quad \mathbf{v}_h \in \mathbf{V}_h. \tag{7.51}$$

In many numerical simulations of two-phase flows, the discretization of the curvature κ is a very delicate problem. This is related to the fact that κ contains *second* derivatives. One way to express these second derivatives is by means of the Laplace-Beltrami characterization of the mean curvature, cf. (14.9):

$$-\Delta_\Gamma \text{id}_\Gamma(x) = \kappa(x)\mathbf{n}(x), \quad x \in \Gamma. \tag{7.52}$$

In the variational formulation we have the possibility to lower the order of differentiation by shifting one of the derivatives to the test function, as is shown in Lemma 14.1.2. Using this, we see that (7.51) can be rewritten as follows:

$$f_\Gamma(\mathbf{v}_h) = -\tau \int_\Gamma \nabla_\Gamma \text{id}_\Gamma \cdot \nabla_\Gamma \mathbf{v}_h \, ds, \quad \mathbf{v}_h \in \mathbf{V}_h. \tag{7.53}$$

In this variational setting it is natural to use the expression on the right-hand side in (7.53) as a starting point for the discretization. This idea is used in, for example, [93, 23, 116, 126, 147, 177]. In this discretization we use the approximation Γ_h of Γ . Given this approximate interface Γ_h ,

the localized force term $f_\Gamma(\mathbf{v}_h)$ is approximated by

$$f_{\Gamma_h}(\mathbf{v}_h) := -\tau \int_{\Gamma_h} \nabla_{\Gamma_h} \text{id}_{\Gamma_h} \cdot \nabla_{\Gamma_h} \mathbf{v}_h \, ds, \quad \mathbf{v}_h \in \mathbf{V}_h. \tag{7.54}$$

In Sect. 7.7 we will derive a bound for the error quantity

$$\|f_\Gamma - f_{\Gamma_h}\|_{\mathbf{V}'_h} = \sup_{\mathbf{v}_h \in \mathbf{V}_h} \frac{f_\Gamma(\mathbf{v}_h) - f_{\Gamma_h}(\mathbf{v}_h)}{\|\mathbf{v}_h\|_1}, \tag{7.55}$$

with f_{Γ_h} as in (7.54). Note that this quantity is essential in the analysis of discretization errors in velocity and pressure, cf. Corollary 7.10.5 (Strang-lemma).

Remark 7.6.1 Assume that Γ is sufficiently smooth. Then

$$f_\Gamma(\mathbf{v}) = -\tau \int_\Gamma \kappa \mathbf{v} \cdot \mathbf{n} \, ds \tag{7.56}$$

is a bounded linear functional on $\mathbf{V}_0 = H_0^1(\Omega)^3$. From Lemma 14.1.2 it follows that for this functional we have the *equivalent* representation

$$f_\Gamma : \mathbf{v} \rightarrow -\tau \int_\Gamma \nabla_\Gamma \text{id}_\Gamma \cdot \nabla_\Gamma \mathbf{v} \, ds. \tag{7.57}$$

Such an equivalence, however, does *not* hold for f_{Γ_h} . Because Γ_h is not sufficiently smooth, a partial integration result as in Lemma 14.1.2 does not hold. The linear functional

$$\mathbf{v} \rightarrow -\tau \int_{\Gamma_h} \nabla_{\Gamma_h} \text{id}_{\Gamma_h} \cdot \nabla_{\Gamma_h} \mathbf{v} \, ds$$

is *not* necessarily bounded on \mathbf{V}_0 . Due to this, in (7.54) and (7.55) we only consider $\mathbf{v}_h \in \mathbf{V}_h$.

We also introduce a modified (improved) variant of the functional f_{Γ_h} . Define the orthogonal projection

$$\mathbf{P}_h(x) := \mathbf{I} - \mathbf{n}_h(x)\mathbf{n}_h(x)^T \quad \text{for } x \in \Gamma_h, \text{ } x \text{ not on an edge,}$$

where \mathbf{n}_h is the unit normal on Γ_h (pointing outward from Ω_1). The tangential derivative along Γ_h can be written as $\nabla_{\Gamma_h} g = \mathbf{P}_h \nabla g$. Note that

$$\nabla_{\Gamma_h} \text{id}_{\Gamma_h} = \mathbf{P}_h \nabla \text{id}_{\Gamma_h} = (\mathbf{P}_h e_1, \mathbf{P}_h e_2, \mathbf{P}_h e_3)^T,$$

with e_i the i -th standard basis vector in \mathbb{R}^3 . Thus the functional f_{Γ_h} can be written as

$$\begin{aligned} f_{\Gamma_h}(\mathbf{v}_h) &= -\tau \int_{\Gamma_h} \mathbf{P}_h \nabla \text{id}_{\Gamma_h} \cdot \nabla_{\Gamma_h} \mathbf{v}_h \, ds \\ &= -\tau \sum_{i=1}^3 \int_{\Gamma_h} \mathbf{P}_h e_i \cdot \nabla_{\Gamma_h} v_i \, ds, \quad v_i := (\mathbf{v}_h)_i. \end{aligned} \tag{7.58}$$

The discrete interface Γ_h is constructed as the zero level of $I\phi_h$, where ϕ_h is a piecewise *quadratic* function, cf. Sect. 7.3. This piecewise quadratic function contains better information about the curvature of Γ than its piecewise linear interpolation $I\phi_h$ that is used for the construction of Γ_h . An improved projection $\tilde{\mathbf{P}}_h$ based on ϕ_h can be defined as follows:

$$\tilde{\mathbf{n}}_h(x) := \frac{\nabla \phi_h(x)}{\|\nabla \phi_h(x)\|}, \quad \tilde{\mathbf{P}}_h(x) := \mathbf{I} - \tilde{\mathbf{n}}_h(x)\tilde{\mathbf{n}}_h(x)^T, \quad x \in \Gamma_h. \tag{7.59}$$

Hence an obvious modification is given by

$$\begin{aligned}
 \tilde{f}_{\Gamma_h}(\mathbf{v}_h) &= -\tau \int_{\Gamma_h} \tilde{\mathbf{P}}_h \nabla \text{id}_{\Gamma_h} \cdot \nabla_{\Gamma_h} \mathbf{v}_h \, ds \\
 &= -\tau \sum_{i=1}^3 \int_{\Gamma_h} \tilde{\mathbf{P}}_h e_i \cdot \nabla_{\Gamma_h} v_i \, ds, \quad v_i := (\mathbf{v}_h)_i \quad (7.60) \\
 &= -\tau \int_{\Gamma_h} \text{tr}(\tilde{\mathbf{P}}_h \nabla_{\Gamma_h} \mathbf{v}_h) \, ds.
 \end{aligned}$$

In Sect. 7.7 it is shown that this discretization of the surface tension force is (significantly) better than the one in (7.54), namely with an error bound $\mathcal{O}(h)$ instead of $\mathcal{O}(\sqrt{h})$. This is confirmed by numerical experiments in Sect. 7.8.

7.6.1 Treatment of general surface tension tensors

In the previous section we restricted ourselves to the case of a *constant* surface tension coefficient τ , i.e. with an interface condition of the form

$$[\boldsymbol{\sigma} \mathbf{n}_\Gamma] = -\tau \kappa \mathbf{n}_\Gamma = \text{div}_\Gamma(\tau \mathbf{P}).$$

We now consider the more general case with an interface condition of the form

$$[\boldsymbol{\sigma} \mathbf{n}_\Gamma] = \text{div}_\Gamma(\boldsymbol{\sigma}_\Gamma), \quad (7.61)$$

and an interface stress tensor $\boldsymbol{\sigma}_\Gamma$ such that $\boldsymbol{\sigma}_\Gamma = \boldsymbol{\sigma}_\Gamma \mathbf{P}$ holds. A variable surface tension coefficient corresponds to $\boldsymbol{\sigma}_\Gamma = \tau \mathbf{P}$, resulting in $\text{div}_\Gamma(\boldsymbol{\sigma}_\Gamma) = -\tau \kappa \mathbf{n}_\Gamma + \nabla_\Gamma \tau$, cf. Remark 1.1.3. In the Boussinesq-Scriven model treated in Sect. 1.1.5 the interface stress tensor $\boldsymbol{\sigma}_\Gamma$ is as in (1.36). In the weak formulation, instead of the surface tension functional $f_\Gamma(\mathbf{v}) = -\tau \int_\Gamma \kappa \mathbf{n} \cdot \mathbf{v} \, ds$ we then have the generalization

$$f_\Gamma(\mathbf{v}) = \int_\Gamma \text{div}_\Gamma(\boldsymbol{\sigma}_\Gamma) \cdot \mathbf{v} \, ds.$$

We can rewrite this using the partial integration identity (14.17), resulting in the general surface tension functional

$$f_\Gamma(\mathbf{v}) = - \int_\Gamma \text{tr}(\boldsymbol{\sigma}_\Gamma \nabla_\Gamma \mathbf{v}) \, ds = - \sum_{i=1}^3 \int_\Gamma (e_i^T \boldsymbol{\sigma}_\Gamma) \nabla_\Gamma v_i \, ds, \quad (7.62)$$

with $\mathbf{v} = (v_1, v_2, v_3)^T$. We consider the case of a variable surface tension coefficient, i.e., $\boldsymbol{\sigma}_\Gamma = \tau \mathbf{P}$. For the discretization of the corresponding surface tension functional, as in the previous section we approximate Γ by Γ_h and \mathbf{P} by $\tilde{\mathbf{P}}_h$. Thus we obtain the following generalization of (7.60):

$$\tilde{f}_{\Gamma_h}(\mathbf{v}_h) = - \int_{\Gamma_h} \tau \operatorname{tr}(\tilde{\mathbf{P}}_h \nabla_{\Gamma_h} \mathbf{v}) \, ds = - \sum_{i=1}^3 \int_{\Gamma_h} \tau \tilde{\mathbf{P}}_h e_i \cdot \nabla_{\Gamma_h} v_i \, ds. \quad (7.63)$$

Comparing (7.60) (constant τ) and (7.63) (variable τ) we observe that the only difference is that in case of a constant surface tension coefficient the term τ can be taken out of the integral. Below, in Sect. 7.7, we present an error analysis only for the case that τ is *constant*, in which the discretization (7.63) reduces to (7.60). If τ is a smooth function then an error analysis for the generalization (7.63) can be derived along the same lines as for the constant coefficient case presented in Sect. 7.7. Results of numerical experiments with this discrete variable surface tension functional are given in [184] and in Sect. 11.5.3.

7.7 Analysis of the Laplace-Beltrami discretization

In this section we derive a bound for

$$\sup_{\mathbf{v}_h \in \mathbf{V}_h} \frac{f_{\Gamma}(\mathbf{v}_h) - f_{\Gamma_h}(\mathbf{v}_h)}{\|\mathbf{v}_h\|_1}, \quad (7.64)$$

where f_{Γ_h} is the discretization of the surface tension force as in (7.54). We also derive a bound for this error measure with f_{Γ_h} replaced by \tilde{f}_{Γ_h} as in (7.60). For $\mathbf{V}_h = V_h^3$ we take the finite element space of piecewise quadratics:

$$V_h = \{ v \in C(\Omega) : v|_T \in \mathcal{P}_2 \quad \text{for all } T \in \mathcal{T}_h \}. \quad (7.65)$$

The choice of this finite element space is not essential in our analysis. The results also hold if for V_h we take another conforming piecewise polynomial finite element space.

7.7.1 Preliminaries

Properties of Γ and of Γ_h

We recall some notation and definitions from Sect. 7.3. The function d is the signed distance function

$$d : U \rightarrow \mathbb{R}, \quad |d(x)| := \operatorname{dist}(x, \Gamma) \quad \text{for all } x \in U.$$

Thus Γ is the zero level set of d . We assume $d < 0$ on the interior of Γ (that is, in Ω_1) and $d > 0$ on the exterior. Note that $\mathbf{n}_{\Gamma} = \nabla d$ on Γ . We define $\mathbf{n}(x) := \nabla d(x)$ for all $x \in U$. Thus $\mathbf{n} = \mathbf{n}_{\Gamma}$ on Γ and $\|\mathbf{n}(x)\| = 1$ for all $x \in U$.

The Hessian of d is denoted by \mathbf{H} :

$$\mathbf{H}(x) = \nabla^2 d(x) \in \mathbb{R}^{3 \times 3} \quad \text{for all } x \in U. \quad (7.66)$$

The eigenvalues of $\mathbf{H}(x)$ are denoted by $\kappa_1(x), \kappa_2(x)$ and 0. For $x \in \Gamma$ the eigenvalues $\kappa_i(x)$, $i = 1, 2$, are the *principal curvatures*, and $\kappa(x) = \kappa_1(x) + \kappa_2(x)$ is the *mean curvature*, cf. Chap. 14.

In the analysis we always assume that the following (technical) assumption is satisfied, namely that the neighborhood U of Γ is sufficiently small in the following sense. We assume that U is a strip of width $\delta > 0$ with

$$\delta^{-1} > \max_{i=1,2} \|\kappa_i(x)\|_{L^\infty(\Gamma)}. \quad (7.67)$$

We define the orthogonal projection:

$$\mathbf{P}(x) = \mathbf{I} - \mathbf{n}(x)\mathbf{n}(x)^T \quad \text{for } x \in U. \quad (7.68)$$

From $\nabla(\mathbf{n}(x)^T \mathbf{n}(x)) = 0$ it follows that $(\nabla \mathbf{n}(x))\mathbf{n}(x) = \nabla^2 d(x)\mathbf{n}(x) = 0$ holds for all $x \in U$. Hence we obtain the following:

$$\mathbf{P}(x)\mathbf{H}(x) = \mathbf{H}(x)\mathbf{P}(x) = \mathbf{H}(x) \quad \text{for all } x \in U.$$

We introduce assumptions on the approximate interface Γ_h . We emphasize, that although we use the notation Γ_h , *this interface must not necessarily be constructed using the method explained in Sect. 7.3*. Our analysis below is presented in a more general setting. In Remark 7.7.3 we explain how the concrete interface construction that is discussed in Sect. 7.3 fits in this more general setting.

Let $\{\Gamma_h\}_{h>0}$ be a family of polygonal approximations of Γ . We assume that each Γ_h is contained in U and consists of a set \mathcal{F}_h of *triangular faces*:

$$\Gamma_h = \bigcup_{F \in \mathcal{F}_h} F. \quad (7.69)$$

For $F_1, F_2 \in \mathcal{F}_h$ with $F_1 \neq F_2$ we assume that $F_1 \cap F_2$ is either empty or a common edge or a common vertex. The parameter h_Γ denotes the maximal diameter of the triangles in \mathcal{F}_h :

$$h_\Gamma = \max_{F \in \mathcal{F}_h} \text{diam}(F).$$

By $\mathbf{n}_h(x)$ we denote the outward pointing unit normal on Γ_h . This normal is piecewise constant with possible discontinuities at the edges of the triangles in \mathcal{F}_h . We recall the discrete analogon of the orthogonal projection \mathbf{P} :

$$\mathbf{P}_h(x) := \mathbf{I} - \mathbf{n}_h(x)\mathbf{n}_h(x)^T \quad \text{for } x \in \Gamma_h, \text{ } x \text{ not on an edge.}$$

The tangential derivative along Γ_h can be written as $\nabla_{\Gamma_h} g = \mathbf{P}_h \nabla g$.

Assumption 7.7.1 We need assumptions which guarantee that Γ_h is “sufficiently close” to Γ . Related to this we assume that $\Gamma_h \subset U$ and that the following holds:

$$|d(x)| \leq ch_\Gamma^2 \quad \text{for all } x \in \Gamma_h, \tag{7.70a}$$

$$\text{ess sup}_{x \in \Gamma_h} \|\mathbf{n}(x) - \mathbf{n}_h(x)\| \leq \min\{c_0, ch_\Gamma\}, \quad \text{with } c_0 < \sqrt{2}. \tag{7.70b}$$

Here c, c_0 denote generic constants independent of h_Γ .

Remark 7.7.2 For a given $x \in \Gamma_h$, let θ be the angle between $\mathbf{n}(x)$ and $\mathbf{n}_h(x)$. Then $\cos \theta = \mathbf{n}(x)^T \mathbf{n}_h(x)$, $\sin \theta = \|\mathbf{P}\mathbf{n}_h(x)\|$ and $\|\mathbf{n}(x) - \mathbf{n}_h(x)\|^2 = 2(1 - \cos \theta)$. Elementary manipulations show that the condition (7.70b) holds if and only if the following two conditions are satisfied:

$$\text{ess inf}_{x \in \Gamma_h} \mathbf{n}(x)^T \mathbf{n}_h(x) \geq c > 0, \tag{7.71a}$$

$$\text{ess sup}_{x \in \Gamma_h} \|\mathbf{P}(x)\mathbf{n}_h(x)\| \leq ch_\Gamma. \tag{7.71b}$$

Remark 7.7.3 Related to these assumptions we note the following. In Theorem 7.3.1 it is shown that under certain (reasonable) assumptions the construction explained in Sect. 7.3 results in a family $\{\Gamma_h\}$ that satisfies the conditions (7.70).

Extensions

We introduce extensions that will be used in the analysis below. The techniques that we use are from the paper [83]. For proofs of certain results we will refer to that paper.

As in Sect. 7.3 we define a locally (in a neighborhood of Γ) orthogonal coordinate system by using the projection $\mathbf{p} : U \rightarrow \Gamma$:

$$\mathbf{p}(x) = x - d(x)\mathbf{n}(x) \quad \text{for all } x \in U.$$

We assume that the decomposition $x = \mathbf{p}(x) + d(x)\mathbf{n}(x)$ is unique for all $x \in U$. Note that

$$\mathbf{n}(x) = \mathbf{n}(\mathbf{p}(x)) \quad \text{for all } x \in U.$$

We use an extension operator defined as follows. For a (scalar) function v defined on Γ we define

$$v_\Gamma^e(x) := v(x - d(x)\mathbf{n}(x)) = v(\mathbf{p}(x)) \quad \text{for all } x \in U,$$

i.e., v is extended along normals on Γ . We will also need extensions of functions defined on Γ_h . This is done again by extending along normals $\mathbf{n}(x)$. For v defined on Γ_h we define, for $x \in \Gamma_h$,

$$v_{\Gamma_h}^e(x + \alpha\mathbf{n}(x)) := v(x) \quad \text{for all } \alpha \in \mathbb{R} \quad \text{with } x + \alpha\mathbf{n}(x) \in U. \tag{7.72}$$

The projection \mathbf{p} and the extensions $v_\Gamma^e, v_{\Gamma_h}^e$ are illustrated in Fig. 7.8. In the following two lemmas some properties of these extensions are given. Proofs are elementary and can be found in [83]. In the remainder we assume that Assumption 7.7.1 is satisfied.

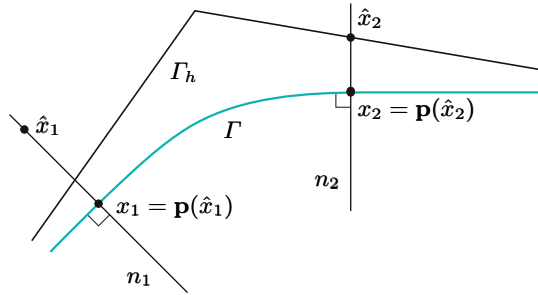


Fig. 7.8. Example of projection \mathbf{p} and construction of extension operators. n_1 and n_2 are straight lines perpendicular to Γ . For v defined on Γ we have $v_\Gamma^e \equiv v(x_1)$ on n_1 . For v_h defined on Γ_h we have $v_{\Gamma_h}^e \equiv v_h(\hat{x}_2)$ on n_2 .

Lemma 7.7.4 For v defined on Γ and sufficiently smooth the following holds:

$$\nabla_{\Gamma_h} v_\Gamma^e(x) = \mathbf{P}_h(x)(\mathbf{I} - d(x)\mathbf{H}(x))\mathbf{P}(x)\nabla_\Gamma v(\mathbf{p}(x)) \quad \text{a.e. on } \Gamma_h. \quad (7.73)$$

Proof. Given in Sect. 2.3 in [83]. □

In (7.73) (and also below) we have results “a.e. on Γ_h ” because quantities (derivatives, \mathbf{P}_h , etc.) are not well-defined on the edges of the triangulation Γ_h .

Lemma 7.7.5 For $x \in \Gamma_h$ (not on an edge) define

$$\mu(x) = [\prod_{i=1}^2 (1 - d(x)\kappa_i(x))] \mathbf{n}(x)^T \mathbf{n}_h(x), \quad (7.74)$$

$$\mathbf{A}(x) = \frac{1}{\mu(x)} \mathbf{P}(x) [\mathbf{I} - d(x)\mathbf{H}(x)] \mathbf{P}_h(x) [\mathbf{I} - d(x)\mathbf{H}(x)] \mathbf{P}(x). \quad (7.75)$$

Let $\mathbf{A}_{\Gamma_h}^e$ be the extension of \mathbf{A} as in (7.72). The following identity holds for functions v and ψ that are defined on Γ_h and are sufficiently smooth:

$$\int_{\Gamma_h} \nabla_{\Gamma_h} v \cdot \nabla_{\Gamma_h} \psi \, ds = \int_\Gamma \mathbf{A}_{\Gamma_h}^e \nabla_\Gamma v_{\Gamma_h}^e \cdot \nabla_\Gamma \psi_{\Gamma_h}^e \, ds. \quad (7.76)$$

Proof. Given in Sect. 2.3 in [83]. □

Due to the assumptions in (7.71a) and (7.67) we have $\text{ess inf}_{x \in \Gamma_h} \mu(x) > 0$ and thus $\mathbf{A}(x)$ is well defined and symmetric positive semi-definite.

A trace estimate

In the analysis of the discretization error in the next section we will need a bound for $\|\nabla_{\Gamma_h} v\|_{L^2(\Gamma_h)}$ in terms of $\|v\|_1$ for $v \in V_h$ (piecewise quadratics).

A possible approach is to apply an inverse inequality combined with a trace theorem, resulting in:

$$\|\nabla_{\Gamma_h} v\|_{L^2(\Gamma_h)} \leq c h_{\min}^{-1} \|v\|_{L^2(\Gamma_h)} \leq c h_{\min}^{-1} \|v\|_1 \quad \text{for all } v \in V_h. \quad (7.77)$$

This, however, turns out to be too crude. In order to be able to derive a better bound than the one in (7.77) we have to introduce some further assumptions which relate the approximations Γ_h of Γ to the outer tetrahedral triangulation \mathcal{T}_h that is used in the definition of the space V_h , cf. (7.65).

Assumption 7.7.6 Let $\{\mathcal{T}_h\}$ be the family of tetrahedral triangulations that is used in the finite element space V_h . We assume that to each interface triangulation $\Gamma_h = \cup_{F \in \mathcal{F}_h} F$ there can be associated a set of tetrahedra \mathcal{S}_h with the following properties:

For each $F \in \mathcal{F}_h$ there is a corresponding $S_F \in \mathcal{S}_h$ with $F \subset S_F$. (7.78a)

For $F_1, F_2 \in \mathcal{F}_h$ with $F_1 \neq F_2$ we have $\text{meas}_3(S_{F_1} \cap S_{F_2}) = 0$. (7.78b)

The family $\{\mathcal{S}_h\}_{h>0}$ is shape-regular. (7.78c)

$\exists c_0 > 0 : c_0 h \leq \text{diam}(S_F) \leq ch$ for all $F \in \mathcal{F}_h$, (quasi-uniformity). (7.78d)

For each $S_F \in \mathcal{S}_h$ there is a tetrahedron $T \in \mathcal{T}_h$ such that $S_F \subset T$. (7.78e)

Note that the set of tetrahedra \mathcal{S}_h has to be defined only close to the approximate interface Γ_h and that this set not necessarily forms a regular tetrahedral triangulation of Ω . Furthermore, it is *not* assumed that the family $\{\Gamma_h\}_{h>0}$ is shape-regular or quasi-uniform.

Remark 7.7.7 The construction in Sect. 7.3 is such that Assumption 7.7.6 is satisfied. We briefly explain this. Let \mathcal{T}_h^{Γ} be the collection of tetrahedra that have a nonempty intersection with the zero level of the piecewise quadratic level set function and assume that $(\mathcal{T}_h^{\Gamma})_{h>0}$ is quasi-uniform. Let $\mathcal{T}_{h'}^{\Gamma}$ be the triangulation obtained after one regular refinement of \mathcal{T}_h^{Γ} . Let Γ_h be as defined in (7.21). All $T \in \mathcal{T}_{h'}^{\Gamma}$ for which $\Gamma_T = T \cap \Gamma_h$ is a quadrilateral are further subdivided into two subtetrahedra such that for $T \cap \Gamma_h$ is always a triangle. The resulting triangulation is denoted by $\tilde{\mathcal{T}}_h^{\Gamma}$. With this Γ_h and $\mathcal{S}_h = \tilde{\mathcal{T}}_h^{\Gamma}$ the conditions formulated in Assumption 7.7.6 are satisfied.

In the following lemma we derive elementary properties of a standard affine mapping between a tetrahedron $S_F \in \mathcal{S}_h$ and the reference unit tetrahedron, which will be used in the proof of Theorem 7.7.9.

Lemma 7.7.8 Assume that the family $\{\Gamma_h\}_{h>0}$ is such that Assumption 7.7.6 is satisfied. Take $F \in \mathcal{F}_h$ and the corresponding $S_F \in \mathcal{S}_h$. Let \hat{S} be the reference unit tetrahedron and $L(x) = \mathbf{J}x + \mathbf{b}$ be an affine mapping such that $L(\hat{S}) = S_F$. Define $\hat{F} := L^{-1}(F)$. The following holds:

$$\|\mathbf{J}\|^2 \frac{\text{meas}_3(\hat{S})}{\text{meas}_3(S_F)} \leq c h^{-1}, \quad (7.79)$$

$$\|\mathbf{J}^{-1}\|^2 \frac{\text{meas}_2(F)}{\text{meas}_2(\hat{F})} \leq c, \tag{7.80}$$

with constants c independent of F and h .

Proof. Let $\rho(S_F)$ be the diameter of the maximal ball contained in S_F and similarly for $\rho(\hat{S})$. From standard finite element theory we have

$$\|\mathbf{J}\| \leq \frac{\text{diam}(S_F)}{\rho(\hat{S})}, \quad \|\mathbf{J}^{-1}\| \leq \frac{\text{diam}(\hat{S})}{\rho(S_F)}.$$

Using (7.78c) and (7.78d) we then get

$$\|\mathbf{J}\|^2 \frac{\text{meas}_3(\hat{S})}{\text{meas}_3(S_F)} \leq c \frac{\text{diam}(S_F)^2}{\text{meas}_3(S_F)} \leq c \text{diam}(S_F)^{-1} \leq ch^{-1},$$

and thus the result in (7.79) holds.

The vertices of $\hat{F} = L^{-1}(F)$ are denoted by \hat{V}_i , $i = 1, 2, 3$. Let $\hat{V}_1\hat{V}_2$ be a longest edge of \hat{F} and \hat{M} the point on this edge such that $\hat{M}\hat{V}_3$ is perpendicular to $\hat{V}_1\hat{V}_2$. Define $V_i := L(\hat{V}_i)$, $i = 1, 2, 3$, and $M := L(\hat{M})$. Then V_i , $i = 1, 2, 3$, are the vertices of F and M lies on the edge V_1V_2 . We then have

$$\begin{aligned} \text{meas}_2(\hat{F}) &= \frac{1}{2} \|\hat{V}_1 - \hat{V}_2\| \|\hat{V}_3 - \hat{M}\| = \frac{1}{2} \|\mathbf{J}^{-1}(V_1 - V_2)\| \|\mathbf{J}^{-1}(V_3 - M)\| \\ &\geq \frac{1}{2} \|\mathbf{J}\|^{-2} \|V_1 - V_2\| \|V_3 - M\| \geq c \frac{\rho(\hat{S})^2}{\text{diam}(S_F)^2} \text{meas}_2(F), \end{aligned}$$

with a constant $c > 0$. Thus we obtain

$$\|\mathbf{J}^{-1}\|^2 \frac{\text{meas}_2(F)}{\text{meas}_2(\hat{F})} \leq c \frac{\text{diam}(\hat{S})^2}{\rho(S_F)^2} \frac{\text{diam}(S_F)^2}{\rho(\hat{S})^2} \leq c,$$

which completes the proof. □

Theorem 7.7.9 *Assume that the family $\{\Gamma_h\}_{h>0}$ is such that Assumption 7.7.6 is satisfied. The following holds:*

$$\|\nabla_{\Gamma_h} v\|_{L^2(\Gamma_h)} \leq ch^{-\frac{1}{2}} \|v\|_1 \quad \text{for all } v \in V_h.$$

Proof. Note that

$$\|\nabla_{\Gamma_h} v\|_{L^2(\Gamma_h)}^2 = \sum_{F \in \mathcal{F}_h} \|\nabla_F v\|_{L^2(F)}^2.$$

Take $F \in \mathcal{F}_h$ and let S_F be the associated tetrahedron as explained above. Let \hat{S} be the reference unit tetrahedron and $L : \hat{S} \rightarrow S_F$ as in Lemma 7.7.8. Define $\hat{v} := v \circ L$. Using standard transformation rules and Lemma 7.7.8 we get

$$\begin{aligned}
 \|\nabla_F v\|_{L^2(F)}^2 &= \|\mathbf{P}_h \nabla v\|_{L^2(F)}^2 \leq \|\nabla v\|_{L^2(F)}^2 = \sum_{|\alpha|=1} \|\partial^\alpha v\|_{L^2(F)}^2 \\
 &\leq c \|\mathbf{J}^{-1}\|^2 \sum_{|\alpha|=1} \|(\partial^\alpha \hat{v}) \circ L^{-1}\|_{L^2(F)}^2 \\
 &\leq c \|\mathbf{J}^{-1}\|^2 \frac{\text{meas}_2(F)}{\text{meas}_2(\hat{F})} \sum_{|\alpha|=1} \|\partial^\alpha \hat{v}\|_{L^2(\hat{F})}^2 \leq c \sum_{|\alpha|=1} \|\partial^\alpha \hat{v}\|_{L^2(\hat{F})}^2 \\
 &\leq c \sum_{|\alpha|=1} \max_{x \in \hat{F}} |\partial^\alpha \hat{v}(x)|^2 \leq c \sum_{|\alpha|=1} \max_{x \in \hat{S}} |\partial^\alpha \hat{v}(x)|^2,
 \end{aligned}$$

with a constant c independent of F . From (7.78e) it follows that \hat{v} is a polynomial on \hat{S} of maximal degree 2. On $\mathcal{P}_2^* := \{p \in \mathcal{P}_2 : p(0) = 0\}$ we have, due to equivalence of norms:

$$\sum_{|\alpha|=1} \max_{x \in \hat{S}} |\partial^\alpha \hat{v}(x)|^2 \leq c \sum_{|\alpha|=1} \|\partial^\alpha \hat{v}\|_{L^2(\hat{S})}^2 \quad \text{for all } \hat{v} \in \mathcal{P}_2^*.$$

Because, for $\hat{v} \in \mathcal{P}_2$ and $|\alpha| = 1$, $\partial^\alpha \hat{v}$ is independent of $\hat{v}(0)$, the same inequality holds for all $\hat{v} \in \mathcal{P}_2$. Thus we get

$$\begin{aligned}
 \|\nabla_F v\|_{L^2(F)}^2 &\leq c \sum_{|\alpha|=1} \|\partial^\alpha \hat{v}\|_{L^2(\hat{S})}^2 \leq c \|\mathbf{J}\|^2 \sum_{|\alpha|=1} \|(\partial^\alpha v) \circ L\|_{L^2(\hat{S})}^2 \\
 &= c \|\mathbf{J}\|^2 \frac{\text{meas}_3(\hat{S})}{\text{meas}_3(S_F)} \sum_{|\alpha|=1} \|\partial^\alpha v\|_{L^2(S_F)}^2 \leq c h^{-1} \|\nabla v\|_{L^2(S_F)}^2,
 \end{aligned}$$

with a constant c independent of F and h . Using (7.78b) we finally obtain

$$\begin{aligned}
 \|\nabla_{\Gamma_h} v\|_{L^2(\Gamma_h)}^2 &\leq c h^{-1} \sum_{F \in \mathcal{F}_h} \|\nabla v\|_{L^2(S_F)}^2 \\
 &\leq c h^{-1} \int_{\Omega} (\nabla v)^2 dx \leq c h^{-1} \|v\|_1^2,
 \end{aligned}$$

which proves the result. \square

Remark 7.7.10 The analysis above also applies if instead of piecewise quadratics other piecewise polynomial finite element functions are used. Thus Theorem 7.7.9 also holds if for V_h we take another piecewise polynomial finite element space.

7.7.2 Error bounds for discrete surface tension functionals

In Sect. 7.6, for the surface tension functional

$$f_\Gamma(\mathbf{v}_h) = -\tau \int_\Gamma \nabla_\Gamma \text{id}_\Gamma \cdot \nabla_\Gamma \mathbf{v}_h ds = -\tau \sum_{i=1}^3 \int_\Gamma \nabla_\Gamma (\text{id}_\Gamma)_i \cdot \nabla_\Gamma (\mathbf{v}_h)_i ds$$

we introduced the discretizations

$$f_{\Gamma_h}(\mathbf{v}_h) = -\tau \sum_{i=1}^3 \int_{\Gamma_h} \nabla_{\Gamma_h}(\text{id}_{\Gamma_h})_i \cdot \nabla_{\Gamma_h}(\mathbf{v}_h)_i \, ds, \quad (7.81)$$

$$\tilde{f}_{\Gamma_h}(\mathbf{v}_h) = -\tau \sum_{i=1}^3 \int_{\Gamma_h} \tilde{\mathbf{P}}_h \nabla(\text{id}_{\Gamma_h})_i \cdot \nabla_{\Gamma_h}(\mathbf{v}_h)_i \, ds. \quad (7.82)$$

In this section we derive error bounds for these discretizations. It suffices to consider only one term in this sum, say the i -th. We write id_Γ and v for the *scalar* functions $(\text{id}_\Gamma)_i$ and $(\mathbf{v}_h)_i$, respectively, and id_{Γ_h} for $(\text{id}_{\Gamma_h})_i$. With this notation we have

$$\begin{aligned} \nabla_\Gamma \text{id}_\Gamma &= \mathbf{P} \nabla \text{id}_\Gamma = \mathbf{P} e_i \quad \text{on } \Gamma, & \nabla_{\Gamma_h} \text{id}_{\Gamma_h} &= \mathbf{P}_h \nabla \text{id}_{\Gamma_h} = \mathbf{P}_h e_i \quad \text{on } \Gamma_h, \\ \tilde{\mathbf{P}}_h \nabla \text{id}_{\Gamma_h} &= \tilde{\mathbf{P}}_h e_i \quad \text{on } \Gamma_h, \end{aligned}$$

where e_i denotes the i -th basis vector in \mathbb{R}^3 . For the i -th term in these functionals we introduce the notation (ignoring the scaling with $-\tau$):

$$\begin{aligned} g(v) &:= \int_\Gamma \nabla_\Gamma \text{id}_\Gamma \cdot \nabla_\Gamma v \, ds, \\ g_h(v) &:= \int_{\Gamma_h} \nabla_{\Gamma_h} \text{id}_{\Gamma_h} \cdot \nabla_{\Gamma_h} v \, ds, \\ \tilde{g}_h(v) &:= \int_{\Gamma_h} \tilde{\mathbf{P}}_h \nabla \text{id}_{\Gamma_h} \cdot \nabla_{\Gamma_h} v \, ds. \end{aligned}$$

For the analysis it is convenient to introduce yet another functional:

$$\hat{g}_h(v) := \int_{\Gamma_h} \nabla_{\Gamma_h} \text{id}_\Gamma^e \cdot \nabla_{\Gamma_h} v \, ds,$$

where id_Γ^e is the extension of id_Γ . Note that due to the occurrence of id_Γ the functional $\hat{g}_h(v)$ can not be used in practice. For the error $g(v) - g_h(v)$ we write $g(v) - g_h(v) = (g(v) - \hat{g}_h(v)) + (\hat{g}_h(v) - g_h(v))$, derive bounds for $|g(v) - \hat{g}_h(v)|$ and $|\hat{g}_h(v) - g_h(v)|$ and then apply a triangle inequality. The same is done for the error $g(v) - \tilde{g}_h(v)$.

We start with the term $|g(v) - \hat{g}_h(v)|$. A bound for this is derived, based on the following splitting:

$$\begin{aligned} &g(v) - \hat{g}_h(v) \\ &= \int_\Gamma \nabla_\Gamma \text{id}_\Gamma \cdot \nabla_\Gamma v \, ds - \int_{\Gamma_h} \nabla_{\Gamma_h} \text{id}_\Gamma^e \cdot \nabla_{\Gamma_h} v \, ds \\ &= \int_\Gamma \nabla_\Gamma \text{id}_\Gamma \cdot \nabla_\Gamma v \, ds - \int_\Gamma \mathbf{A}_{\Gamma_h}^e \nabla_\Gamma \text{id}_\Gamma \cdot \nabla_\Gamma v_{\Gamma_h}^e \, ds \quad (\text{cf. (7.76)}) \\ &= \int_\Gamma \nabla_\Gamma \text{id}_\Gamma \cdot \nabla_\Gamma (v - v_{\Gamma_h}^e) \, ds + \int_\Gamma (\mathbf{I} - \mathbf{A}_{\Gamma_h}^e) \nabla_\Gamma \text{id}_\Gamma \cdot \nabla_\Gamma v_{\Gamma_h}^e \, ds. \end{aligned} \quad (7.83)$$

In the lemma below we give bounds for the two terms in (7.83).

Lemma 7.7.11 *Let Assumption 7.7.1 be satisfied. The following holds for all $v \in V_h$:*

$$\left| \int_{\Gamma} \nabla_{\Gamma} \text{id}_{\Gamma} \cdot \nabla_{\Gamma} (v - v_{\Gamma_h}^e) ds \right| \leq c h_{\Gamma} \|v\|_{1,U}, \quad (7.84)$$

$$\left| \int_{\Gamma} (\mathbf{I} - \mathbf{A}_{\Gamma_h}^e) \nabla_{\Gamma} \text{id}_{\Gamma} \cdot \nabla_{\Gamma} v_{\Gamma_h}^e ds \right| \leq c h_{\Gamma}^2 \|\nabla_{\Gamma_h} v\|_{L^2(\Gamma_h)}. \quad (7.85)$$

Proof. (7.84)–(7.85) are proved in Lemmas 4.1 and 4.3 in [129]. \square

Using this we obtain a bound for the error $\|g - \hat{g}_h\|_{V_h}$:

Theorem 7.7.12 *Let the Assumptions 7.7.1 and 7.7.6 be satisfied. The following holds:*

$$\sup_{v \in V_h} \frac{|g(v) - \hat{g}_h(v)|}{\|v\|_1} \leq c h_{\Gamma}. \quad (7.86)$$

Proof. The result in Lemma 7.7.11 implies

$$|g(v) - \hat{g}_h(v)| \leq c h_{\Gamma} \|v\|_{1,U} + c h_{\Gamma}^2 \|\nabla_{\Gamma_h} v\|_{L^2(\Gamma_h)} \quad \text{for all } v \in V_h.$$

From Theorem 7.7.9 we obtain $\|\nabla_{\Gamma_h} v\|_{L^2(\Gamma_h)} \leq c h_{\Gamma}^{-\frac{1}{2}} \|v\|_1$. Furthermore, $\|v\|_{1,U} \leq \|v\|_1$ holds. Thus the result in (7.86) holds. \square

We now derive a bound for $|\hat{g}_h(v) - g_h(v)|$.

Lemma 7.7.13 *Let the Assumption 7.7.1 be satisfied. The following holds:*

$$|\hat{g}_h(v) - g_h(v)| \leq c h_{\Gamma} \|\nabla_{\Gamma_h} v\|_{L^2(\Gamma_h)} \quad \text{for all } v \in V_h. \quad (7.87)$$

Proof. From Lemma 7.7.4 we get, for $x \in \Gamma_h$ (not on an edge),

$$\begin{aligned} \nabla_{\Gamma_h} \text{id}_{\Gamma}^e(x) &= \mathbf{P}_h(x) (\mathbf{I} - d(x) \mathbf{H}(x)) \mathbf{P}(x) \nabla_{\Gamma} \text{id}_{\Gamma}(\mathbf{p}(x)) \\ &= \mathbf{P}_h(x) (\mathbf{I} - d(x) \mathbf{H}(x)) \mathbf{P}(x) e_i. \end{aligned}$$

We also have $\nabla_{\Gamma_h} \text{id}_{\Gamma_h} = \mathbf{P}_h \nabla \text{id}_{\Gamma_h} = \mathbf{P}_h e_i$. Hence,

$$\left| \int_{\Gamma_h} (\nabla_{\Gamma_h} \text{id}_{\Gamma}^e - \nabla_{\Gamma_h} \text{id}_{\Gamma_h}) \cdot \nabla_{\Gamma_h} v ds \right| \quad (7.88)$$

$$\begin{aligned} &= \left| \int_{\Gamma_h} (\mathbf{P}_h (\mathbf{I} - d \mathbf{H}) \mathbf{P} e_i - \mathbf{P}_h e_i) \cdot \nabla_{\Gamma_h} v ds \right| \\ &\leq c \text{ess sup}_{x \in \Gamma_h} \|\mathbf{P}_h(x) (\mathbf{I} - d(x) \mathbf{H}(x)) \mathbf{P}(x) - \mathbf{P}_h(x)\| \|\nabla_{\Gamma_h} v\|_{L^2(\Gamma_h)} \\ &\leq c \text{ess sup}_{x \in \Gamma_h} (\|\mathbf{P}_h(x) (\mathbf{I} - \mathbf{P}(x))\| \quad (7.89) \end{aligned}$$

$$+ |d(x)| \|\mathbf{P}_h(x) \mathbf{H}(x) \mathbf{P}(x)\|) \|\nabla_{\Gamma_h} v\|_{L^2(\Gamma_h)}. \quad (7.90)$$

Note that $|d(x)| \leq ch_T^2$ for $x \in \Gamma_h$, and

$$\text{ess sup}_{x \in \Gamma_h} \|\mathbf{P}_h(x)\mathbf{H}(x)\mathbf{P}(x)\| \leq \text{ess sup}_{x \in \Gamma_h} \|\mathbf{H}(x)\| \leq c.$$

For the term in (7.89) we have (dropping x in the notation):

$$\|\mathbf{P}_h(\mathbf{I} - \mathbf{P})\| = \|\mathbf{P}_h\mathbf{nn}^T\| = \|\mathbf{P}_h\mathbf{n}\| = \|\mathbf{P}_h(\mathbf{n} - \mathbf{n}_h)\| \leq \|\mathbf{n} - \mathbf{n}_h\| \leq ch_\Gamma.$$

In the last inequality we used Assumption 7.7.1. Using these results in (7.89)-(7.90) and the definitions of \hat{g}_h, g_h , we get

$$|\hat{g}_h(v) - g_h(v)| \leq ch_\Gamma \|\nabla_{\Gamma_h} v\|_{L^2(\Gamma_h)},$$

and thus the result is proved. □

This leads to a bound for the error $\|\hat{g}_h - g_h\|_{V'_h}$:

Theorem 7.7.14 *Let the Assumptions 7.7.1 and 7.7.6 be satisfied. The following holds:*

$$\sup_{v \in V_h} \frac{|\hat{g}_h(v) - g_h(v)|}{\|v\|_1} \leq c\sqrt{h_\Gamma}. \tag{7.91}$$

Proof. The result follows from Lemma 7.7.13 and Theorem 7.7.9. □

As a direct consequence we obtain a discretization error bound for f_{Γ_h} :

Corollary 7.7.15 *Let the Assumptions 7.7.1 and 7.7.6 be satisfied. For the surface tension force discretization f_{Γ_h} as defined in (7.81) the following holds:*

$$\sup_{\mathbf{v} \in \mathbf{V}_h} \frac{|f_\Gamma(\mathbf{v}_h) - f_{\Gamma_h}(\mathbf{v}_h)|}{\|\mathbf{v}_h\|_1} \leq \tau c\sqrt{h_\Gamma}.$$

Proof. It suffices to consider a bound for $\|g - g_h\|_{V'_h}$. From Theorem 7.7.12 and Theorem 7.7.14 it follows that

$$\|g - g_h\|_{V'_h} \leq \|g - \hat{g}_h\|_{V'_h} + \|\hat{g}_h - g_h\|_{V'_h} \leq ch_\Gamma + c\sqrt{h_\Gamma} \leq c\sqrt{h_\Gamma},$$

which implies the error bound for f_{Γ_h} . □

An upper bound $\mathcal{O}(\sqrt{h_\Gamma})$ as in Corollary 7.7.15 for the error in the approximation of the localized force term may seem rather pessimistic, because Γ_h is an $\mathcal{O}(h_T^2)$ accurate approximation of Γ . Numerical experiments in Sect. 7.8 and results in [115], however, indicate that the bound is sharp.

Along the same lines as presented above for f_{Γ_h} we now derive an error bound for \tilde{f}_{Γ_h} . It suffices to consider $|g(v) - \tilde{g}_h(v)|$. We use the triangle inequality

$$|g(v) - \tilde{g}_h(v)| \leq |g(v) - \hat{g}_h(v)| + |\hat{g}_h(v) - \tilde{g}_h(v)|.$$

The first term on the right-hand side is treated in Theorem 7.7.12. The next lemma gives a bound for the second term. In (7.92) we use the generalized normal $\tilde{\mathbf{n}}_h$ from (7.59).

Lemma 7.7.16 *Let Assumption 7.7.1 be satisfied. Furthermore, we assume that there exists $p > 0$ such that*

$$\|\mathbf{n}(x) - \tilde{\mathbf{n}}_h(x)\| \leq ch_\Gamma^p, \quad \text{for } x \in \Gamma_h. \quad (7.92)$$

Then the following holds:

$$|\hat{g}_h(v) - \tilde{g}_h(v)| \leq ch_\Gamma^{\min\{p,2\}} \|\nabla_{\Gamma_h} v\|_{L^2(\Gamma_h)} \quad \text{for all } v \in V_h.$$

Proof. We apply similar arguments as used in the proof of Lemma 7.7.13. We have

$$\nabla_{\Gamma_h} \text{id}_\Gamma^c(x) = \mathbf{P}_h(x)(\mathbf{I} - d(x)\mathbf{H}(x))\mathbf{P}(x)e_i$$

and $\tilde{\mathbf{P}}_h \nabla \text{id}_{\Gamma_h} = \tilde{\mathbf{P}}_h e_i$ on Γ_h . Hence,

$$\left| \int_{\Gamma_h} (\nabla_{\Gamma_h} \text{id}_\Gamma^c - \tilde{\mathbf{P}}_h \nabla \text{id}_{\Gamma_h}) \cdot \nabla_{\Gamma_h} v \, ds \right| \quad (7.93)$$

$$= \left| \int_{\Gamma_h} (\mathbf{P}_h(\mathbf{I} - d\mathbf{H})\mathbf{P}e_i - \mathbf{P}_h\tilde{\mathbf{P}}_h e_i) \cdot \nabla_{\Gamma_h} v \, ds \right|$$

$$\leq c \text{ess sup}_{x \in \Gamma_h} \|\mathbf{P}_h(x)(\mathbf{I} - d(x)\mathbf{H}(x))\mathbf{P}(x) - \mathbf{P}_h(x)\tilde{\mathbf{P}}_h(x)\| \|\nabla_{\Gamma_h} v\|_{L^2(\Gamma_h)}$$

$$\leq c \text{ess sup}_{x \in \Gamma_h} (\|\mathbf{P}_h(x)(\mathbf{P}(x) - \tilde{\mathbf{P}}_h(x))\| \quad (7.94)$$

$$+ |d(x)| \|\mathbf{P}_h(x)\mathbf{H}(x)\mathbf{P}(x)\|) \|\nabla_{\Gamma_h} v\|_{L^2(\Gamma_h)}. \quad (7.95)$$

As in the proof of Lemma 7.7.13 we have $\text{ess sup}_{x \in \Gamma_h} |d(x)| \|\mathbf{P}_h(x)\mathbf{H}(x)\mathbf{P}(x)\| \leq ch_\Gamma^2$. For the term in (7.94) we get (dropping x in the notation):

$$\|\mathbf{P}_h(\mathbf{P} - \tilde{\mathbf{P}}_h)\| \leq \|\mathbf{nn}^T - \tilde{\mathbf{n}}_h\tilde{\mathbf{n}}_h^T\|$$

$$\leq \|(\mathbf{n} - \tilde{\mathbf{n}}_h)\mathbf{n}^T\| + \|\tilde{\mathbf{n}}_h(\mathbf{n} - \tilde{\mathbf{n}}_h)^T\| = 2\|\mathbf{n} - \tilde{\mathbf{n}}_h\| \leq ch_\Gamma^p.$$

Combination of these estimates proves the result. \square

Remark 7.7.17 In Lemma 7.3.2 it is shown that for the approximate interface construction explained in Sect. 7.3 the assumption in (7.92) holds for $p \in (0, 2]$ if ϕ_h is an $\mathcal{O}(h_\Gamma^p)$ accurate (w.r.t $\|\cdot\|_{H_\infty^1}$) approximation of ϕ . For a piecewise quadratic level set approximation the optimal approximation quality is $\mathcal{O}(h_\Gamma^2)$, i.e., $p = 2$.

This leads to a bound for the error $\|\hat{g}_h - \tilde{g}_h\|_{V_h'}$:

Theorem 7.7.18 *Let the Assumptions 7.7.1, 7.7.6 and the one in (7.92) with $p \geq \frac{1}{2}$ be satisfied. The following holds:*

$$\sup_{v \in V_h} \frac{|\hat{g}_h(v) - \tilde{g}_h(v)|}{\|v\|_1} \leq ch_\Gamma. \quad (7.96)$$

Proof. The result follows from Lemma 7.7.16 and Theorem 7.7.9. □

As a direct consequence we obtain a discretization error bound for \tilde{f}_{Γ_h} :

Corollary 7.7.19 Let the assumptions as in Theorem 7.7.18 be satisfied. For the surface tension force discretization \tilde{f}_{Γ_h} as defined in (7.82) the following holds:

$$\sup_{\mathbf{v} \in \mathbf{V}_h} \frac{|f_{\Gamma}(\mathbf{v}_h) - \tilde{f}_{\Gamma_h}(\mathbf{v}_h)|}{\|\mathbf{v}_h\|_1} \leq \tau c h_{\Gamma}.$$

Proof. It suffices to consider a bound for $\|g - \tilde{g}_h\|_{V'_h}$. From Theorem 7.7.12 and Theorem 7.7.18 it follows that

$$\|g - \tilde{g}_h\|_{V'_h} \leq \|g - \hat{g}_h\|_{V'_h} + \|\hat{g}_h - \tilde{g}_h\|_{V'_h} \leq ch_{\Gamma},$$

which implies the error bound for \tilde{f}_{Γ_h} . □

This significant improvement ($\mathcal{O}(h_{\Gamma})$ compared to the $\mathcal{O}(\sqrt{h_{\Gamma}})$ error bound for the functional f_{Γ_h}) is confirmed by numerical experiments in the next section.

7.8 Numerical experiments with the Laplace-Beltrami discretization

In this section we present results of a numerical experiment which indicates that the $\mathcal{O}(\sqrt{h})$ bound in Corollary 7.7.15 is sharp. Furthermore, for the improved approximation \tilde{f}_{Γ_h} the $\mathcal{O}(h)$ bound will be confirmed numerically.

We consider the domain $\Omega := [-1, 1]^3$ with $\Omega_1 := \{x \in \Omega : \|x\| < R\}$. In our experiments we take $R = \frac{1}{2}$.

For the discretization a uniform tetrahedral mesh \mathcal{T}_0 is used where the vertices form a $6 \times 6 \times 6$ lattice, hence $h_0 = \frac{1}{5}$. This coarse mesh \mathcal{T}_0 is locally refined in the vicinity of $\Gamma = \partial\Omega_1$. This repeated refinement process yields the gradually refined meshes $\mathcal{T}_1, \mathcal{T}_2, \dots$ with *local* (i. e., close to the interface) mesh sizes $h_{\Gamma} = h_i = \frac{1}{5} \cdot 2^{-i}, i = 1, 2, \dots$. Part of the tetrahedral triangulation \mathcal{T}_4 is shown in Fig. 7.9. The corresponding finite element spaces $\mathbf{V}_i := \mathbf{V}_{h_i} = (V_{h_i})^3$ consist of vector functions where each component is a continuous piecewise quadratic function on \mathcal{T}_i .

The interface $\Gamma = \partial\Omega_1$ is a sphere and thus the curvature $\kappa = \frac{2}{R}$ is constant. If we discretize the flow problem using \mathbf{V}_i as discrete velocity space, we have to approximate the surface tension force

$$f_{\Gamma}(\mathbf{v}) = -\frac{2\tau}{R} \int_{\Gamma} \mathbf{n}_{\Gamma} \cdot \mathbf{v} \, ds = -\tau \int_{\Gamma} \nabla_{\Gamma} \text{id}_{\Gamma} \cdot \nabla_{\Gamma} \mathbf{v} \, ds, \quad \mathbf{v} \in \mathbf{V}_i. \quad (7.97)$$

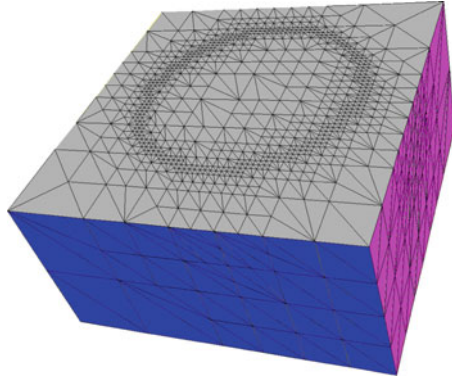


Fig. 7.9. Lower half part of the 4 times refined mesh \mathcal{T}_4 .

To simplify notation, we take a fixed $i \geq 0$ and the corresponding local mesh size parameter is denoted by $h = h_i$. For the construction of an approximate interface Γ_h we use the approach described in Sect. 7.3, starting with ϕ equal to the exact signed distance function to Γ .

The discrete approximation of the surface tension force is

$$f_{\Gamma_h}(\mathbf{v}) = -\tau \int_{\Gamma_h} \nabla_{\Gamma_h} \text{id}_{\Gamma_h} \cdot \nabla_{\Gamma_h} \mathbf{v} \, ds, \quad \mathbf{v} \in \mathbf{V}_i.$$

We are interested in, cf. Corollary 7.7.15,

$$\|f_\Gamma - f_{\Gamma_h}\|_{\mathbf{V}'_i} := \sup_{\mathbf{v} \in \mathbf{V}_i} \frac{f_\Gamma(\mathbf{v}) - f_{\Gamma_h}(\mathbf{v})}{\|\mathbf{v}\|_1}. \tag{7.98}$$

The evaluation of $f_\Gamma(\mathbf{v})$, for $\mathbf{v} \in \mathbf{V}_i$, requires the computation of integrals on curved triangles or quadrilaterals $\Gamma \cap T$ where T is a tetrahedron from the triangulation \mathcal{T}_i . We are not able to compute these exactly. Therefore, we introduce an artificial force term which, in this model problem with a known constant curvature, is computable and sufficiently close to f_Γ .

Lemma 7.8.1 For $\mathbf{v} \in \mathbf{V} = H_0^1(\Omega)^3$ define

$$\hat{f}_{\Gamma_h}(\mathbf{v}) := -\frac{2\tau}{R} \int_{\Gamma_h} \mathbf{n}_h \cdot \mathbf{v} \, ds,$$

where \mathbf{n}_h is the piecewise constant outward unit normal on Γ_h . Then the following inequality holds:

$$\|f_\Gamma - \hat{f}_{\Gamma_h}\|_{\mathbf{V}'} \leq ch. \tag{7.99}$$

Proof. Let $\Omega_{1,h} \subset \Omega$ be the domain enclosed by Γ_h , i.e., $\partial\Omega_{1,h} = \Gamma_h$. We define $D_h^+ := \Omega_1 \setminus \Omega_{1,h}$, $D_h^- := \Omega_{1,h} \setminus \Omega_1$ and $D_h := D_h^+ \cup D_h^-$. Due to Stokes' Theorem, for $\mathbf{v} \in \mathbf{V}$ we have

$$\begin{aligned}
 |f_\Gamma(\mathbf{v}) - \hat{f}_{\Gamma_h}(\mathbf{v})| &= \frac{2\tau}{R} \left| \int_{\Omega_1} \operatorname{div} \mathbf{v} \, dx - \int_{\Omega_{1,h}} \operatorname{div} \mathbf{v} \, dx \right| \\
 &= \frac{2\tau}{R} \left| \int_{D_h^+} \operatorname{div} \mathbf{v} \, dx - \int_{D_h^-} \operatorname{div} \mathbf{v} \, dx \right| \\
 &\leq \frac{2\tau}{R} \int_{D_h} |\operatorname{div} \mathbf{v}| \, dx.
 \end{aligned}$$

Using the Cauchy-Schwarz inequality, we get the estimate

$$|f_\Gamma(\mathbf{v}) - \hat{f}_{\Gamma_h}(\mathbf{v})| \leq c\sqrt{\operatorname{meas}_3(D_h)} \|\mathbf{v}\|_1 \quad \text{for all } \mathbf{v} \in \mathbf{V},$$

which results in

$$\|f_\Gamma - \hat{f}_{\Gamma_h}\|_{\mathbf{V}'} \leq c\sqrt{\operatorname{meas}_3(D_h)}. \tag{7.100}$$

Note that for the piecewise planar approximation Γ_h of the interface Γ we have $\operatorname{meas}_3(D_h) = \mathcal{O}(h^2)$ and thus (7.99) holds. \square

From Lemma 7.8.1 we obtain $\|f_\Gamma - \hat{f}_{\Gamma_h}\|_{\mathbf{V}'_j} \leq ch$ with a constant c independent of j . Thus we have

$$\|\hat{f}_{\Gamma_h} - f_{\Gamma_h}\|_{\mathbf{V}'_i} - ch \leq \|f_\Gamma - f_{\Gamma_h}\|_{\mathbf{V}'_i} \leq \|\hat{f}_{\Gamma_h} - f_{\Gamma_h}\|_{\mathbf{V}'_i} + ch. \tag{7.101}$$

The quantity $\|\hat{f}_{\Gamma_h} - f_{\Gamma_h}\|_{\mathbf{V}'_i}$ can be determined as follows. Since Γ_h is piecewise planar and $\mathbf{v} \in \mathbf{V}_i$ is a piecewise quadratic function, both $\hat{f}_{\Gamma_h}(\mathbf{v})$ and $f_{\Gamma_h}(\mathbf{v})$ can be computed exactly (up to machine accuracy) using suitable quadrature rules.

For the evaluation of the dual norm $\|\cdot\|_{\mathbf{V}'_i}$ we proceed as follows. Let $\{\boldsymbol{\xi}_j\}_{j=1,\dots,N}$ (with $N := \dim \mathbf{V}_i$) be the standard nodal basis in \mathbf{V}_i and $J_{\mathbf{V}_i} : \mathbb{R}^N \rightarrow \mathbf{V}_i$ the isomorphism $J_{\mathbf{V}_i} \mathbf{x} = \sum_{k=1}^N x_k \boldsymbol{\xi}_k$. Let \mathbf{M}_h be the mass matrix and \mathbf{A}_h the discrete Laplacian:

$$\begin{aligned}
 (\mathbf{M}_h)_{ij} &:= \int_{\Omega} \boldsymbol{\xi}_i \cdot \boldsymbol{\xi}_j \, dx, & 1 \leq i, j \leq N. \\
 (\mathbf{A}_h)_{ij} &:= \int_{\Omega} \nabla \boldsymbol{\xi}_i \cdot \nabla \boldsymbol{\xi}_j \, dx.
 \end{aligned}$$

Define $\mathbf{C}_h = \mathbf{A}_h + \mathbf{M}_h$. Note that for $\mathbf{v} = J_{\mathbf{V}_i} \mathbf{x} \in \mathbf{V}_i$ we have $\|\mathbf{v}\|_1^2 = \langle \mathbf{C}_h \mathbf{x}, \mathbf{x} \rangle$. Take $e \in \mathbf{V}'_i$ and define $\mathbf{e} \in \mathbb{R}^N$ by $\mathbf{e}_j := e(\boldsymbol{\xi}_j)$, $j = 1, \dots, N$. Due to

$$\|e\|_{\mathbf{V}'_i} = \sup_{\mathbf{v} \in \mathbf{V}_i} \frac{|e(\mathbf{v})|}{\|\mathbf{v}\|_1} = \sup_{\mathbf{x} \in \mathbb{R}^N} \frac{|\sum_{j=1}^N x_j e(\boldsymbol{\xi}_j)|}{\sqrt{\langle \mathbf{C}_h \mathbf{x}, \mathbf{x} \rangle}}$$

we obtain

$$\|e\|_{\mathbf{V}'_i} = \sup_{\mathbf{x} \in \mathbb{R}^N} \frac{\langle \mathbf{x}, \mathbf{e} \rangle}{\sqrt{\langle \mathbf{C}_h \mathbf{x}, \mathbf{x} \rangle}} = \|\mathbf{C}_h^{-1/2} \mathbf{e}\| = \sqrt{\langle \mathbf{C}_h^{-1} \mathbf{e}, \mathbf{e} \rangle}. \tag{7.102}$$

Thus for the computation of $\|e\|_{\mathbf{V}'_i}$ we proceed in the following way:

1. Compute $\mathbf{e} = (e(\boldsymbol{\xi}_j))_{j=1}^N$.
2. Solve the linear system $\mathbf{C}_h \mathbf{z} = \mathbf{e}$ up to machine accuracy.
3. Compute $\|e\|_{\mathbf{V}'_i} = \sqrt{\langle \mathbf{z}, \mathbf{e} \rangle}$.

We applied this strategy to $e := \hat{f}_{\Gamma_h} - f_{\Gamma_h}$. The results are given in the second column in Table 7.8. The numerical order of convergence in the third column of this table clearly indicates an $\mathcal{O}(\sqrt{h})$ behavior. Due to (7.101) this implies the same $\mathcal{O}(\sqrt{h})$ convergence behavior for $\|f_{\Gamma} - f_{\Gamma_h}\|_{\mathbf{V}'_i}$. This indicates that the $\mathcal{O}(\sqrt{h})$ bound in Corollary 7.7.15 is sharp.

The same procedure can be applied with f_{Γ_h} replaced by the modified (improved) approximate surface tension force

$$\tilde{f}_{\Gamma_h}(\mathbf{v}) = -\tau \sum_{i=1}^3 \int_{\Gamma_h} \tilde{\mathbf{P}}_h e_i \cdot \nabla_{\Gamma_h}(\mathbf{v})_i ds,$$

as defined in (7.82). This yields the results in the fourth column in Table 7.8. For this modification the numerical order of convergence is significantly better, namely at least first order in h . From (7.101) it follows that for $\|f_{\Gamma} - \tilde{f}_{\Gamma_h}\|_{\mathbf{V}'_i}$ we can expect $\mathcal{O}(h^p)$ with $p \geq 1$.

Summarizing, we conclude that the results of these numerical experiments confirm the theoretical $\mathcal{O}(\sqrt{h})$ error bound derived in the analysis in Sect. 7.7.2 and show that the modified approximation indeed leads to (much) better results.

Results of numerical experiments for a Stokes two-phase flow problem using both f_{Γ_h} and \tilde{f}_{Γ_h} are presented in Sect. 7.10.3.

i	$\ \hat{f}_{\Gamma_h} - f_{\Gamma_h}\ _{\mathbf{V}'_i}$	order	$\ \hat{f}_{\Gamma_h} - \tilde{f}_{\Gamma_h}\ _{\mathbf{V}'_i}$	order
0	1.79 E-1	–	1.32 E-1	–
1	1.40 E-1	0.35	4.43 E-2	1.57
2	1.03 E-1	0.45	1.46 E-2	1.61
3	7.22 E-2	0.51	5.06 E-3	1.52
4	5.02 E-2	0.53	1.78 E-3	1.51

Table 7.8. Error norms and numerical order of convergence for different refinement levels.

7.9 XFEM discretization of the pressure

If surface tension forces are present the pressure is *discontinuous* across the interface Γ . We show that standard finite element spaces have poor approximation properties for such functions with a jump across Γ and introduce

a so-called extended finite element space that is much better suited for discretization of the pressure variable. Most of the results presented in this section are from [128, 209].

In Sect. 7.9.1 we show, by means of a simple example, that if one uses standard finite element spaces for the discretization of a discontinuous function, then in general the approximation order (w.r.t. $\|\cdot\|_{L^2}$) is only $\mathcal{O}(\sqrt{h})$. In Sect. 7.9.2 we introduce *extended* finite element spaces, which are much better suited for the approximation of discontinuous functions. Some implementation issues related to XFEM are treated in Sect. 7.9.3. In Sect. 7.9.4 we present an analysis of the XFEM method. In Sect. 7.10 results of numerical experiments with this method are presented.

7.9.1 Approximation error for standard FE spaces

In this section we consider the approximation error

$$\inf_{q_h \in Q_h} \|q_h - p^*\|_{L^2}$$

for a few standard finite element spaces Q_h and explain why in general for a function p^* that is *discontinuous across* Γ_h one can expect no better bound for this approximation error than $c\sqrt{h}$. This serves as a motivation for an improved pressure finite element space as presented in Sect. 7.9.2. To explain the effect underlying the \sqrt{h} behavior of the error bound we analyze a concrete two-dimensional example as illustrated in Fig. 7.10. We take $\Omega = (0, 1)^2 \subset \mathbb{R}^2$ and define

$$\Omega_1 := \{x \in \Omega : x_1 \leq 1 - x_2\}, \quad \Omega_2 := \Omega \setminus \overline{\Omega}_1.$$

The interface Γ separating both subdomains from each other is given by

$$\Gamma = \{x \in \Omega : x_1 = 1 - x_2\}.$$

A family of 2D triangulations $\{\mathcal{T}_h\}_{h>0}$ is constructed as follows. The starting triangulation \mathcal{T}_0 consists of two triangles, namely the ones with vertices $\{(0, 0), (0, 1), (1, 1)\}$ and $\{(0, 0), (1, 0), (1, 1)\}$. Then a global regular refinement strategy (connecting the midpoints of edges) is applied repeatedly. This results in a nested sequence of triangulations \mathcal{T}_{h_k} , $k = 1, 2, \dots$, with mesh size $h_k = 2^{-k}$. In Fig. 7.10 the triangulation \mathcal{T}_{h_2} is shown. The set of triangles that contains the interface is given by (with $h := h_k$)

$$\mathcal{T}_h^\Gamma := \{T \in \mathcal{T}_h : \text{meas}_1(T \cap \Gamma) > 0\}.$$

In Fig. 7.10 the elements in $\mathcal{T}_{h_2}^\Gamma$ are colored gray.

For $h = h_k$ we consider the finite element spaces

$$\begin{aligned} Q_h^0 &:= \{p : \Omega \rightarrow \mathbb{R} : p|_T \in \mathcal{P}_0 \quad \text{for all } T \in \mathcal{T}_h\} && \text{(piecewise constants),} \\ Q_h^{1,\text{disc}} &:= \{p : \Omega \rightarrow \mathbb{R} : p|_T \in \mathcal{P}_1 \quad \text{for all } T \in \mathcal{T}_h\} && \text{(linear, discontinuous),} \\ Q_h^1 &:= \{p \in C(\Omega) : p|_T \in \mathcal{P}_1 \quad \text{for all } T \in \mathcal{T}_h\} && \text{(linear, continuous).} \end{aligned}$$

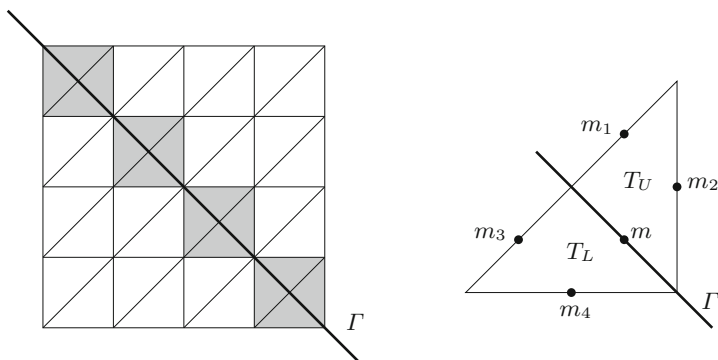


Fig. 7.10. Triangulation \mathcal{T}_{h_2} and a triangle $T \in \mathcal{T}_{h_k}^\Gamma$.

Note that

$$Q_h^j \subset Q_h^{1,\text{disc}} \quad \text{for } j = 0, 1. \quad (7.103)$$

We take p^* as follows: $p^*(x) = c_p > 0$ for all $x \in \Omega_1$, $p^*(x) = 0$ for all $x \in \Omega_2$. We study $\inf_{q_h \in Q_h} \|q_h - p^*\|_{L^2}$ for $Q_h \in \{Q_h^0, Q_h^{1,\text{disc}}, Q_h^1\}$. For $Q_h = Q_h^{1,\text{disc}}$ the identity

$$\inf_{q_h \in Q_h^{1,\text{disc}}} \|q_h - p^*\|_{L^2}^2 = \sum_{T \in \mathcal{T}_h^\Gamma} \min_{q \in \mathcal{P}_1} \|q - p^*\|_{L^2(T)}^2$$

holds. Take $T \in \mathcal{T}_h^\Gamma$. Using a quadrature rule on triangles that is exact for all polynomials of degree two we get, cf. Fig. 7.10,

$$\begin{aligned} \min_{q \in \mathcal{P}_1} \|q - p^*\|_{L^2(T)}^2 &= \min_{q \in \mathcal{P}_1} \left(\int_{T_L} (q - c_p)^2 dx dy + \int_{T_U} q^2 dx dy \right) \\ &= \frac{h^2}{12} \min_{q \in \mathcal{P}_1} \left((q(m_3) - c_p)^2 + (q(m_4) - c_p)^2 + (q(m) - c_p)^2 \right. \\ &\quad \left. + q(m_1)^2 + q(m_2)^2 + q(m)^2 \right) \\ &\geq \frac{h^2}{12} \min_{q \in \mathcal{P}_1} \left((q(m) - c_p)^2 + q(m)^2 \right) = \frac{1}{24} c_p^2 h^2. \end{aligned}$$

Thus we have

$$\inf_{q_h \in Q_h^{1,\text{disc}}} \|q_h - p^*\|_{L^2} \geq \left(\sum_{T \in \mathcal{T}_h^\Gamma} \frac{1}{24} c_p^2 h^2 \right)^{\frac{1}{2}} = \left(\frac{2}{h} \frac{1}{24} c_p^2 h^2 \right)^{\frac{1}{2}} = \frac{1}{2\sqrt{3}} c_p \sqrt{h}.$$

Due to (7.103) this yields

$$\inf_{q_h \in Q_h} \|q_h - p^*\|_{L^2} \geq \frac{1}{2\sqrt{3}} c_p \sqrt{h} \quad \text{for } Q_h \in \{Q_h^0, Q_h^{1,\text{disc}}, Q_h^1\}.$$

To derive an upper bound for the approximation error we choose a suitable $q_h \in Q_h$. First consider $Q_h = Q_h^0$ and take $q_h^0 \in Q_h^0$ as follows: $(q_h^0)|_T = c_p$ for all T with $\text{meas}_1(T \cap \Omega_1) > 0$, $q_h^0 = 0$ otherwise. With this choice we get

$$\|q_h^0 - p^*\|_{L^2} = \left(\sum_{T \in \mathcal{T}_h^T} \|q_h^0 - p^*\|_{L^2(T)}^2 \right)^{\frac{1}{2}} = \left(\sum_{T \in \mathcal{T}_h^T} c_p^2 \frac{1}{4} h^2 \right)^{\frac{1}{2}} = \frac{1}{\sqrt{2}} c_p \sqrt{h}.$$

For $Q_h \in \{Q_h^{1,\text{disc}}, Q_h^1\}$ we take $q_h^1 := I_h(p^*)$, where I_h is the nodal interpolation operator (note: $p^* = c_p$ on Γ). Elementary computations yield

$$\|q_h^1 - p^*\|_{L^2} = \left(\frac{1}{12} c_p^2 h \right)^{\frac{1}{2}} = \frac{1}{2\sqrt{3}} c_p \sqrt{h}.$$

Combination of these results yields

$$\frac{1}{2\sqrt{3}} c_p \sqrt{h} \leq \inf_{q_h \in Q_h} \|q_h - p^*\|_{L^2} \leq \frac{1}{\sqrt{2}} c_p \sqrt{h} \quad \text{for } Q_h \in \{Q_h^0, Q_h^{1,\text{disc}}, Q_h^1\}.$$

If instead of piecewise constants or piecewise linears we consider polynomials of higher degree, the approximation error still behaves like \sqrt{h} .

Similar examples, which have a \sqrt{h} approximation error behavior, can be constructed using these finite element spaces on tetrahedral triangulations in 3D.

7.9.2 Extended finite element method (XFEM)

The analysis in the previous section, which is confirmed by numerical experiments in Sect. 7.10, leads to the conclusion that there is a need for an improved finite element space for the discretization of the pressure. In this section we introduce such a space which is based on an idea presented in [181, 30]. In these papers a so-called *extended finite element method* (XFEM) is introduced in the context of crack formations in structure mechanics which has good approximation properties for interface type of problems. A recent review on XFEM techniques is given in [113, 114]. XFEM belongs to the class of partition of unity methods (PUM) [18, 19].

Here we apply the XFEM method to two-phase flow problems by constructing a suitable extended pressure finite element space. In this section we explain the method. For $k \geq 1$ fixed we introduce the standard finite element space

$$Q_h = Q_h^k = \{q \in C(\Omega) : q|_T \in \mathcal{P}_k \quad \text{for all } T \in \mathcal{T}_h\}.$$

We explain the construction of the XFEM space for $k = 1$. This technique can easily be generalized to $k \geq 1$. Define the index set $\mathcal{J} = \{1, \dots, n\}$, where $n = \dim Q_h$ is the number of degrees of freedom. Let $\mathcal{B} := \{q_j\}_{j \in \mathcal{J}}$ be the

nodal basis of Q_h , i. e. $q_j(x_i) = \delta_{i,j}$ for $i, j \in \mathcal{J}$ where $x_i \in \mathbb{R}^3$ denotes the vector of spatial coordinates of the i -th degree of freedom.

The idea of the XFEM method is to enrich the original finite element space Q_h by additional functions q_j^X for $j \in \mathcal{J}'$ where $\mathcal{J}' \subset \mathcal{J}$ is a given index set. An additional function q_j^X is constructed by multiplying the original nodal basis function q_j by a so called enrichment function Φ_j :

$$q_j^X(x) := q_j(x) \Phi_j(x). \quad (7.104)$$

This enrichment yields the extended finite element space

$$Q_h^X := Q_h \oplus \text{span} \{ q_j^X : j \in \mathcal{J}' \}.$$

This idea was introduced in [181] and further developed in [30] for different kinds of discontinuities (kinks, jumps), which may also intersect or branch. The choice of the enrichment function depends on the type of discontinuity. For representing jumps the Heaviside function is proposed to construct appropriate enrichment functions. Basis functions with kinks can be obtained by using the distance function as enrichment function [180].

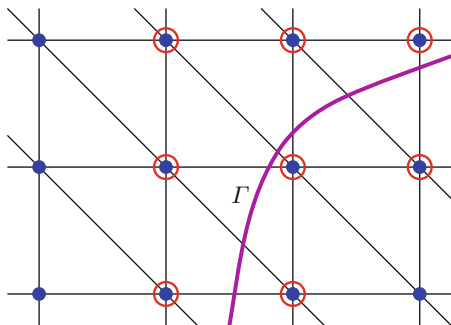


Fig. 7.11. Enrichment of P_1 finite elements in a 2D example. Dots represent degrees of freedom of original basis functions, circles indicate where additional functions are added in the vicinity of the interface Γ .

The index set of basis functions “close to the interface” is given by

$$\mathcal{J}_\Gamma := \{ j \in \mathcal{J} : \text{meas}_2(\Gamma \cap \text{supp } q_j) > 0 \},$$

cf. Fig. 7.11 for a 2D example.

Let $\phi : \Omega \rightarrow \mathbb{R}$ be an indicator function such that ϕ is negative in Ω_1 and positive in Ω_2 . For example the level set function could be used for ϕ . Let H be the Heaviside function and

$$H_\Gamma(x) := H(\phi(x)) = \begin{cases} 0 & x \in \Omega_1, \\ 1 & x \in \Omega_2. \end{cases}$$

Since we are interested in functions with a jump across the interface we define the enrichment function

$$\Phi_j^H(x) := H_\Gamma(x) - H_\Gamma(x_j), \quad j \in \mathcal{J}_\Gamma, \tag{7.105}$$

and a corresponding function

$$q_j^X := q_j \Phi_j^H, \quad j \in \mathcal{J}_\Gamma.$$

The second term in the definition of Φ_j^H is constant and may be omitted (as it doesn't introduce new functions in the function space), but ensures the nice property $q_j^X(x_i) = 0$ for all i , i.e., q_j^X vanishes in all degrees of freedom. As a consequence, we have $q_j^X \equiv 0$ in all T with $T \notin \mathcal{T}_h^\Gamma := \{T \in \mathcal{T}_h : \text{meas}_2(T \cap \Gamma) > 0\}$. In the following we will use the notation $q_j^\Gamma := q_j \Phi_j^H$ and the XFEM space is denoted by

$$Q_h^\Gamma := Q_h \oplus \text{span} \{ q_j^\Gamma : j \in \mathcal{J}_\Gamma \}. \tag{7.106}$$

We emphasize that the extended finite element space Q_h^Γ depends on the location of the interface Γ . In particular the dimension of Q_h^Γ may change if the interface moves. The shape of the extended basis functions for the 1D case is sketched in Fig. 7.12.

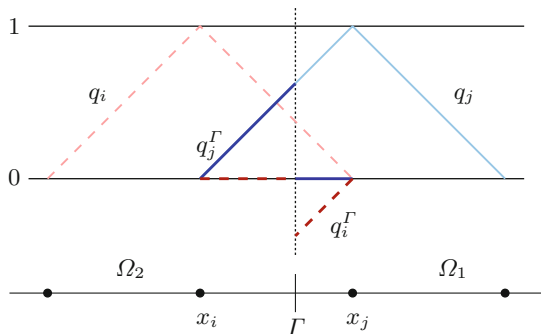


Fig. 7.12. Extended finite element basis functions q_i, q_i^Γ (dashed) and q_j, q_j^Γ (solid) for 1D case.

Remark 7.9.1 In [30] the XFEM is applied to problems from linear elasticity demonstrating the ability of the method to capture jumps and kinks. These discontinuities also branch or intersect in some of the examples, in this case more elaborate constructions of the enrichment functions are used.

In [66] the XFEM is also applied to a two-phase flow problem. In that paper discontinuous material properties ρ and μ , but *no surface tension forces*

are taken into account. Thus there is no jump in pressure, but the velocity solution exhibits a kink (i.e., a discontinuity in the derivative) at the interface. For the pressure and the level set function standard finite element spaces are used. The velocity field is discretized with an extended finite element space enriched by $\mathbf{v}_j^X(x) = \mathbf{v}_j(x) |d(x)|$ to capture the kinks at the interface. The location of the interface is captured by a level set approach. The level set function is used as an approximate signed distance function.

A similar idea of space enrichment in the context of two-phase flow simulations is also suggested in [177].

The same finite element space Q_h^Γ is also used in the “unfitted finite element method” that is introduced in [24] for a class of elliptic interface problems.

7.9.3 Modifications and implementation issues

In this section we discuss a few practical issues related to the application of XFEM to non-stationary Navier-Stokes two-phase flow problems.

As Q_h^Γ depends on the location of the interface Γ , the space Q_h^Γ changes if the interface moves. Thus the discretization of $b(\cdot, \cdot)$ has to be updated each time when the level set function has changed. In a Navier-Stokes code solving non-stationary two-phase flow problems this is nothing special since the mass and stiffness matrices depend on discontinuous material properties like density and viscosity and thus have to be updated as well. What is special about the extended pressure finite element space is the fact that the dimension of Q_h^Γ may vary, i.e., some extended pressure unknowns may appear or disappear when the interface is moving. This has to be taken into account by a suitable interpolation procedure for the extended pressure unknowns.

Let Γ_h be a piecewise planar approximation of the interface Γ as described in Sect. 7.3. For practical reasons we do not consider Q_h^Γ but the space $Q_h^{\Gamma_h}$, which is the extended pressure finite element space described above but with Γ replaced by its approximation Γ_h . We discuss how in the discretization of a two-phase flow problem the construction of the discrete problem changes if instead of (\mathbf{V}_h, Q_h) the pair $(\mathbf{V}_h, Q_h^{\Gamma_h})$ is used. For the velocity space \mathbf{V}_h we use the standard space of piecewise quadratics. The use of another finite element space $Q_h^{\Gamma_h}$ (instead of standard piecewise linears) influences only the evaluation of $b(\cdot, \cdot)$.

For a basis function $\xi_i \in \mathbf{V}_h$ and $j \in \mathcal{J}_\Gamma$ the evaluation of

$$b(\xi_i, q_j^{\Gamma_h}) = - \sum_{T' \in \mathcal{T}_{h'}} \int_{T'} q_j^{\Gamma_h} \operatorname{div} \xi_i \, dx$$

requires the computation of integrals with discontinuous integrands, as the extended pressure basis function $q_j^{\Gamma_h}$ has a jump across the interface. We sum over $T' \in \mathcal{T}_{h'}$ (and not $T \in \mathcal{T}_h$) because Γ_h is defined as in (7.21), i.e., Γ_h is piecewise planar corresponding to the refinement $\mathcal{T}_{h'}$ of \mathcal{T}_h . Let $T \in \mathcal{T}_h$

be a tetrahedron with $T \cap \text{supp } q_j^{\Gamma_h} \neq \emptyset$ and $T' \in \mathcal{T}_h'$, with $T' \subset T$ a child tetrahedron created by regular refinement of T . Define

$$T'_i := T' \cap \Omega_{i,h}, \quad i = 1, 2.$$

Using the definition of $q_j^{\Gamma_h}$, cf. (7.104), (7.105), we get

$$\begin{aligned} \int_{T'} q_j^{\Gamma_h} \operatorname{div} \boldsymbol{\xi}_i \, dx &= \int_{T'_2} q_j \operatorname{div} \boldsymbol{\xi}_i \, dx - H_{\Gamma}(x_j) \int_{T'} q_j \operatorname{div} \boldsymbol{\xi}_i \, dx \\ &= \begin{cases} \int_{T'_2} q_j \operatorname{div} \boldsymbol{\xi}_i \, dx & \text{if } x_j \in \Omega_{1,h}, \\ - \int_{T'_1} q_j \operatorname{div} \boldsymbol{\xi}_i \, dx & \text{if } x_j \in \Omega_{2,h}. \end{cases} \end{aligned} \tag{7.107}$$

The integrands in the right-hand side of (7.107) are polynomial on the polyhedral subdomains T'_1, T'_2 . For the computation of the integral over T'_i we distinguish two cases. The face $T' \cap \Gamma_h$ is either a triangle or a quadrilateral. In the first case one of the sets T'_1, T'_2 is tetrahedral; without loss of generality let T'_1 be tetrahedral. Then integration over T'_2 can be computed by

$$\int_{T'_2} G(x) \, dx = \int_{T'} G(x) \, dx - \int_{T'_1} G(x) \, dx.$$

In the second case both T'_1, T'_2 are non-tetrahedral, but can each be subdivided into three sub-tetrahedra, cf. Fig. 7.13. In *all cases* the integration over T'_i can be reduced to *integration on tetrahedra*, for which standard quadrature rules can be applied.

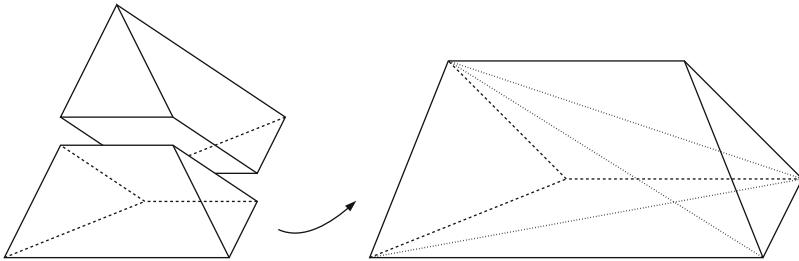


Fig. 7.13. Left: Parts of tetrahedron T' are non-tetrahedral, iff cutting face $T' \cap \Gamma_h$ is a quadrilateral. Right: Triangulation of the lower part into three tetrahedra.

Regarding stability, one has to treat carefully the situation where some extended basis functions q_j^{Γ} have a (very) “small” support. In such situations the resulting linear systems may become very ill-conditioned and the LBB-stability of the $(\mathbf{V}_h, Q_h^{\Gamma})$ pair is questionable, cf. the numerical experiment in Sect. 7.10.3. One obvious possibility to deal with this instability problem

is to skip the extended basis functions with relatively “small” contributions. What is meant by “small” will be specified now. In Sect. 7.9.4 we investigate which elements from the “added” space $\text{span} \{ q_j^F : j \in \mathcal{J}_\Gamma \}$ can be deleted without losing the optimal approximation quality of the extended finite element space. This leads to the following criterion, in which parameters $\tilde{c} > 0$ and $\alpha > 0$ are used. For $j \in \mathcal{J}_\Gamma$ we consider the following condition for the corresponding extended basis function q_j^F :

$$\|q_j^F\|_{l,T} \leq \tilde{c} h_T^\alpha \|q_j\|_{l,T} \quad \text{for all } T \in \mathcal{T}_h^F. \quad (7.108)$$

Here $l \in \{0, 1\}$ is the order of the Sobolev norm. We introduce the *reduced index set* $\tilde{\mathcal{J}}_\Gamma \subset \mathcal{J}_\Gamma$ by

$$\tilde{\mathcal{J}}_\Gamma := \{ j \in \mathcal{J}_\Gamma : (7.108) \text{ does not hold for } q_j^F \}$$

and the *reduced extended finite element space* \tilde{Q}_h^F

$$\tilde{Q}_h^F := Q_h \oplus \text{span} \{ q_j^F : j \in \tilde{\mathcal{J}}_\Gamma \}. \quad (7.109)$$

In other words, *only extended basis functions q_j^F are taken into account, for which (7.108) does not hold*. The criterion (7.108) quantifies what is meant by “small contributions”. In this modified space \tilde{Q}_h^F basis functions with very small supports are avoided and an approximation property of the following form can be shown to hold (Sect. 7.9.4):

$$\inf_{q \in \tilde{Q}_h^F} \|p - q\|_{l, \Omega_1 \cup \Omega_2} \leq c(h^{m-l} + h^{\alpha-l}) \|p\|_{m, \Omega_1 \cup \Omega_2}$$

for all $p \in H^m(\Omega_1 \cup \Omega_2)$ and integers l, m with $0 \leq l < m \leq 2$. Thus we maintain an optimal approximation error bound if in the criterion (7.108) we take $\alpha = m$. The choice of l and m depends on the norms in which the discretization error in the (pressure) variable p is measured. In our applications we use $l = 0$, $m = 2$, resulting in an optimal error bound $\mathcal{O}(h^2)$ for piecewise linear finite elements.

Numerical experiments, cf. Sect. 7.10.3, indicate that this reduction of the extended finite element has a significant influence on the LBB-stability of the (\mathbf{V}_h, Q_h^F) finite element pair.

Remark 7.9.2 Because $\|q_j\|_{l,T} \sim ch_T^{\frac{3}{2}-l}$ for $l = 0, 1$, the condition (7.108) can be replaced by

$$\|q_j^F\|_{l,T} \leq \hat{c} h_T^{\alpha + \frac{3}{2} - l} \quad \text{for all } T \in \mathcal{T}_h^F. \quad (7.110)$$

The constant \hat{c} may differ from \tilde{c} used in (7.108).

7.9.4 Analysis of XFEM

In this section we derive some properties of the XFEM method. We discuss the following topics: approximation quality, conditioning of a basis in the XFEM space and LBB-stability of the $(\mathbf{V}_h, Q_h^\Gamma)$ pair.

Approximation error bounds

For the approximation error bounds we consider the XFEM space Q_h^Γ with a given h -independent interface Γ . Note that in practice the space $Q_h^{\Gamma_h}$ is used; we do not consider this in the analysis, since it would lead to additional technical complications induced by the h -dependence of the interface.

For an integer $k \geq 0$ we define the space

$$H^k(\Omega_1 \cup \Omega_2) := \{ p \in L^2(\Omega) : p|_{\Omega_i} \in H^k(\Omega_i), i = 1, 2 \},$$

with the norm $\|p\|_{k, \Omega_1 \cup \Omega_2}^2 := \|p\|_{k, \Omega_1}^2 + \|p\|_{k, \Omega_2}^2$. We need *restriction* operators $R_i : L^2(\Omega) \rightarrow L^2(\Omega)$, $i = 1, 2$

$$R_i v = \begin{cases} v|_{\Omega_i} & \text{on } \Omega_i \\ 0 & \text{on } \Omega \setminus \Omega_i \end{cases} \tag{7.111}$$

(in L^2 sense). The extended finite element space Q_h^Γ can also be characterized by the following property: $v \in Q_h^\Gamma$ if and only if there exist functions $v_1, v_2 \in Q_h$ such that $v|_{\Omega_i} = v_i|_{\Omega_i}$, $i = 1, 2$. In other words:

$$Q_h^{\Gamma_h} = R_1 Q_h \oplus R_2 Q_h. \tag{7.112}$$

We present an approximation error bound for the XFEM space:

Theorem 7.9.3 For integers l, m with $0 \leq l < m \leq 2$ the following holds:

$$\inf_{q \in Q_h^\Gamma} \|p - q\|_{l, \Omega_1 \cup \Omega_2} \leq c h^{m-l} \|p\|_{m, \Omega_1 \cup \Omega_2} \tag{7.113}$$

for all $p \in H^m(\Omega_1 \cup \Omega_2)$.

Proof. We use extension operators $\mathcal{E}_i^m : H^m(\Omega_i) \rightarrow H^m(\Omega)$, $i = 1, 2$, with $(\mathcal{E}_i^m w)|_{\Omega_i} = w$ and $\|\mathcal{E}_i^m w\|_m \leq c \|w\|_{m, \Omega_i}$, cf. [256]. For $m = 1, 2$, let $I_h^m : H^m(\Omega) \rightarrow Q_h$ be a (quasi-)interpolation operator such that $\|w - I_h^m w\|_l \leq c h^{m-l} \|w\|_m$ for all $w \in H^m(\Omega)$, $0 \leq l < m \leq 2$ (for example, nodal interpolation if $m = 2$). Let $m \in \{1, 2\}$ and $p \in H^m(\Omega_1 \cup \Omega_2)$ be given. Define $q^* \in Q_h^\Gamma$ by

$$q^* = R_1 I_h^m \mathcal{E}_1^m R_1 p + R_2 I_h^m \mathcal{E}_2^m R_2 p. \tag{7.114}$$

For this approximation we obtain

$$\begin{aligned}
 & \|p - q^*\|_{l, \Omega_1 \cup \Omega_2}^2 \\
 &= \sum_{i=1}^2 \|p - q^*\|_{l, \Omega_i}^2 = \sum_{i=1}^2 \|p - I_h^m \mathcal{E}_i^m R_i p\|_{l, \Omega_i}^2 \\
 &= \sum_{i=1}^2 \|\mathcal{E}_i^m R_i p - I_h^m \mathcal{E}_i^m R_i p\|_{l, \Omega_i}^2 \leq \sum_{i=1}^2 \|\mathcal{E}_i^m R_i p - I_h^m \mathcal{E}_i^m R_i p\|_i^2 \\
 &\leq c h^{2(m-l)} \sum_{i=1}^2 \|\mathcal{E}_i^m R_i p\|_m^2 \leq c h^{2(m-l)} \sum_{i=1}^2 \|R_i p\|_{m, \Omega_i}^2 \\
 &= c h^{2(m-l)} \|p\|_{m, \Omega_1 \cup \Omega_2}^2,
 \end{aligned}$$

which proves the result. □

Hence, the XFEM space has optimal approximation quality for piecewise smooth functions p , for example $\inf_{q_h \in Q_h^\Gamma} \|q_h - p\|_{L^2} \leq c h^2$ if $p|_{\Omega_i} \in H^2(\Omega_i)$, $i = 1, 2$. Similar approximation results are given in [135]. In [209] also a result for the reduced XFEM space \tilde{Q}_h^Γ is derived. In the analysis a global inverse inequality is used and therefore in the following theorem we use the assumption that the family of triangulations is quasi-uniform.

Theorem 7.9.4 Assume that the family $\{\mathcal{T}_h\}_{h>0}$ is quasi-uniform. For integers l, m with $0 \leq l < m \leq 2$ the following holds, with \tilde{Q}_h^Γ defined as in (7.109):

$$\inf_{q \in \tilde{Q}_h^\Gamma} \|p - q\|_{l, \Omega_1 \cup \Omega_2} \leq c (h^{m-l} + h^{\alpha-l}) \|p\|_{m, \Omega_1 \cup \Omega_2} \tag{7.115}$$

for all $p \in H^m(\Omega_1 \cup \Omega_2)$.

Proof. Theorem 4 in [209]. □

Properties of a basis in the XFEM space

In this section we derive properties of a basis in the space $Q_h^{\Gamma_h}$. Note that now we consider $Q_h^{\Gamma_h}$ (instead of Q_h^Γ). We first introduce some further notation. The restriction R_i , $i = 1, 2$, is as in (7.111), but with Ω_i replaced by $\Omega_{i,h}$ (recall: Γ_h defines the interface between $\Omega_{1,h}$ and $\Omega_{2,h}$). The nodal basis in Q_h is denoted by $\{q_j\}_{j \in \mathcal{J}}$, $\mathcal{J} = \{1, \dots, n\}$. We introduce subsets of \mathcal{J} for which the corresponding basis functions have a nonzero intersection with Γ_h :

$$\begin{aligned}
 \mathcal{J}_1^{\Gamma_h} &:= \{k \in \mathcal{J} : x_k \in \Omega_{2,h} \text{ and } \text{supp}(q_k) \cap \Gamma_h \neq \emptyset\} \\
 \mathcal{J}_2^{\Gamma_h} &:= \{k \in \mathcal{J} : x_k \in \Omega_{1,h} \text{ and } \text{supp}(q_k) \cap \Gamma_h \neq \emptyset\}.
 \end{aligned}$$

Corresponding spaces are defined by

$$V_i^{\Gamma_h} := \text{span} \left\{ R_i q_k : k \in \mathcal{J}_i^{\Gamma_h} \right\}, \quad i = 1, 2.$$

To avoid technical difficulties in the analysis, we make the (reasonable) assumption that $\text{meas}_2(\Gamma_h \cap \partial T) = 0$ for all T , i.e., the interface Γ_h does not contain faces of the tetrahedra $T \in \mathcal{T}_h$. The extended finite element space Q_h^{Γ} can be represented as

$$Q_h^{\Gamma_h} = Q_h \oplus V_1^{\Gamma_h} \oplus V_2^{\Gamma_h}. \tag{7.116}$$

We will analyze the stability of the basis

$$\{q_k\}_{1 \leq k \leq n} \cup \{R_1 q_k\}_{k \in \mathcal{J}_1^{\Gamma_h}} \cup \{R_2 q_k\}_{k \in \mathcal{J}_2^{\Gamma_h}}. \tag{7.117}$$

We prove, cf. Theorem 7.9.7, that the *diagonally scaled mass matrix is uniformly* (w.r.t. h) *well-conditioned*. This holds independent of the size and the shape of the support of the basis functions $R_i q_k$. This immediately implies a similar result for the reduced XFEM space $\tilde{Q}_h^{\Gamma_h}$.

We first derive a strengthened Cauchy-Schwarz inequality between the spaces Q_h and $V_1^{\Gamma_h} \oplus V_2^{\Gamma_h}$. The collection of all vertices in the triangulation \mathcal{T}_h is denoted by $\mathcal{V} := \{x_k : k \in \mathcal{J}\}$. For each vertex $x \in \mathcal{V}$ let $\mathcal{T}(x)$ be the set of all tetrahedra in \mathcal{T}_h that have x as a vertex. Define $\mathcal{T}_R = \{T \in \mathcal{T}_h : T \cap \Gamma_h = \emptyset\}$. We introduce the assumption

$$\mathcal{T}(x) \cap \mathcal{T}_R \neq \emptyset \quad \text{for all } x \in \mathcal{V}. \tag{7.118}$$

For h sufficiently small this assumption is satisfied.

Lemma 7.9.5 *Assume that (7.118) holds. There exists a constant $c_{CS} < 1$ independent of h such that*

$$(v, w)_{L^2} \leq c_{CS} \|v\|_{L^2} \|w\|_{L^2} \quad \text{for all } v \in Q_h, w \in V_1^{\Gamma_h} \oplus V_2^{\Gamma_h}.$$

Proof. We use the notation $W = V_1^{\Gamma_h} \oplus V_2^{\Gamma_h}$. Let $P_W : L^2(\Omega) \rightarrow W$ be the L^2 -orthogonal projection on W . Let $\mathcal{V}(T)$ denote the set of vertices of T . Transformation to a unit tetrahedron yields the norm equivalence

$$c_1 \|v\|_{L^2(T)}^2 \leq |T| \sum_{x \in \mathcal{V}(T)} v(x)^2 \leq c_2 \|v\|_{L^2(T)}^2 \tag{7.119}$$

for all $T \in \mathcal{T}_h$, $v \in Q_h$, with constants $c_1 > 0$ and c_2 independent of h . Due to (7.118) we have that for each $x \in \mathcal{V}(T)$ there exists a tetrahedron $\hat{T} \in \mathcal{T}(x) \cap \mathcal{T}_R$ with $x \in \mathcal{V}(\hat{T})$. Let \mathcal{T}_R be as defined above and $\mathcal{T}_h^{\Gamma} := \mathcal{T}_h \setminus \mathcal{T}_R$ the set of all tetrahedra that have a nonzero intersection with Γ_h . We obtain for $v \in Q_h$ and $T \in \mathcal{T}_h^{\Gamma}$:

$$\begin{aligned} \|v\|_{L^2(T)}^2 &\leq c |T| \sum_{x \in \mathcal{V}(T)} v(x)^2 \\ &\leq c \sum_{x \in \mathcal{V}(T)} \sum_{\hat{T} \in \mathcal{T}(x) \cap \mathcal{T}_R} |\hat{T}| \sum_{y \in \mathcal{V}(\hat{T})} v(y)^2 \\ &\leq c \sum_{x \in \mathcal{V}(T)} \|v\|_{L^2(\mathcal{T}(x) \cap \mathcal{T}_R)}^2. \end{aligned}$$

Hence,

$$\|v\|_{L^2(\mathcal{T}_h^\Gamma)}^2 = \sum_{T \in \mathcal{T}_h^\Gamma} \|v\|_{L^2(T)}^2 \leq c \|v\|_{L^2(\mathcal{T}_R)}^2, \quad v \in Q_h,$$

holds with a constant c independent of h . This yields $\|v\|_{L^2}^2 = \|v\|_{L^2(\mathcal{T}_h^\Gamma)}^2 + \|v\|_{L^2(\mathcal{T}_R)}^2 \leq c \|v\|_{L^2(\mathcal{T}_R)}^2$ with c independent of h . Using this and $(P_W v)|_{\mathcal{T}_R} = 0$ we get, for $v \in Q_h$,

$$\|v - P_W v\|_{L^2} \geq \|v - P_W v\|_{L^2(\mathcal{T}_R)} = \|v\|_{L^2(\mathcal{T}_R)} \geq \hat{c} \|v\|_{L^2},$$

with a constant $\hat{c} > 0$ independent of h . Thus we get

$$\|P_W v\|_{L^2}^2 = \|v\|_{L^2}^2 - \|v - P_W v\|_{L^2}^2 \leq (1 - \hat{c}^2) \|v\|_{L^2}^2 =: c_{CS}^2 \|v\|_{L^2}^2$$

for all $v \in Q_h$. Hence, for $v \in Q_h$, $w \in W$,

$$\begin{aligned} (v, w)_{L^2} &= (v, P_W w)_{L^2} = (P_W v, w)_{L^2} \leq \|P_W v\|_{L^2} \|w\|_{L^2} \\ &\leq c_{CS} \|v\|_{L^2} \|w\|_{L^2}, \end{aligned}$$

which completes the proof. \square

The spaces $V_1^{\Gamma_h}$ and $V_2^{\Gamma_h}$ are (due to disjoint supports of functions from these spaces) L^2 -orthogonal. Thus we conclude that in the decomposition

$$Q_h^{\Gamma_h} = Q_h \oplus V_1^{\Gamma_h} \oplus V_2^{\Gamma_h}$$

we have a strengthened Cauchy-Schwarz inequality between Q_h and $V_1^{\Gamma_h} \oplus V_2^{\Gamma_h}$ and even orthogonality between $V_1^{\Gamma_h}$ and $V_2^{\Gamma_h}$.

For $v = w + w_1 + w_2 \in Q_h^{\Gamma_h}$, with $w \in Q_h$, $w_i \in V_i^{\Gamma_h}$, we have

$$\|v\|_{L^2}^2 \leq 2(\|w\|_{L^2}^2 + \|w_1 + w_2\|_{L^2}^2) = 2(\|w\|_{L^2}^2 + \|w_1\|_{L^2}^2 + \|w_2\|_{L^2}^2)$$

and

$$\begin{aligned} \|v\|_{L^2}^2 &= \|w\|_{L^2}^2 + \|w_1 + w_2\|_{L^2}^2 + 2(w, w_1 + w_2)_{L^2} \\ &\geq \|w\|_{L^2}^2 + \|w_1 + w_2\|_{L^2}^2 - 2c_{CS} \|w\|_{L^2} \|w_1 + w_2\|_{L^2} \\ &\geq (1 - c_{CS})(\|w\|_{L^2}^2 + \|w_1\|_{L^2}^2 + \|w_2\|_{L^2}^2). \end{aligned}$$

Hence we obtain

$$\begin{aligned} (1 - c_{CS})(\|w\|_{L^2}^2 + \|w_1\|_{L^2}^2 + \|w_2\|_{L^2}^2) \\ \leq \|v\|_{L^2}^2 \leq 2(\|w\|_{L^2}^2 + \|w_1\|_{L^2}^2 + \|w_2\|_{L^2}^2). \end{aligned} \tag{7.120}$$

We now turn to the conditioning of the mass matrix. A function $v \in Q_h^{\Gamma_h}$ is represented in the basis $\{q_k\}_{1 \leq k \leq n} \cup \{R_1 q_k\}_{k \in \mathcal{J}_1^{\Gamma_h}} \cup \{R_2 q_k\}_{k \in \mathcal{J}_2^{\Gamma_h}}$ as

$$v = \sum_{k=1}^n \alpha_k q_k + \sum_{i=1}^2 \sum_{k \in \mathcal{J}_i^{\Gamma_h}} \beta_k^{(i)} R_i q_k =: w + w_1 + w_2, \tag{7.121}$$

where $w \in Q_h$, $w_i \in V_i^{\Gamma_h}$, $i = 1, 2$. It is well-known (cf. also (7.119)) that for $w = \sum_{k=1}^n \alpha_k q_k$ we have

$$c_1 \sum_{k=1}^n \alpha_k^2 \|q_k\|_{L^2}^2 \leq \|w\|_{L^2}^2 \leq c_2 \sum_{k=1}^n \alpha_k^2 \|q_k\|_{L^2}^2, \tag{7.122}$$

with constants $c_1 > 0$ and c_2 independent of h , i.e., the nodal basis $\{q_k\}_{1 \leq k \leq n}$ of Q_h is uniformly in h well-conditioned (w.r.t. $\|\cdot\|_{L^2}$). We prove a similar result for the basis $\{R_i q_k\}_{k \in \mathcal{J}_i^{\Gamma_h}}$ of $V_i^{\Gamma_h}$.

Lemma 7.9.6 *For $w_i = \sum_{k \in \mathcal{J}_i^{\Gamma_h}} \beta_k^{(i)} R_i q_k$, $i = 1, 2$, the following holds:*

$$\frac{\sqrt{2}-1}{2\sqrt{2}} \sum_{k \in \mathcal{J}_i^{\Gamma_h}} (\beta_k^{(i)})^2 \|R_i q_k\|_{L^2}^2 \leq \|w_i\|_{L^2}^2 \leq 3 \sum_{k \in \mathcal{J}_i^{\Gamma_h}} (\beta_k^{(i)})^2 \|R_i q_k\|_{L^2}^2. \tag{7.123}$$

Proof. It suffices to consider $i = 1$. We write $w_1 = \sum_{k \in \mathcal{J}_1^{\Gamma_h}} \beta_k R_1 q_k$. For each $T \in \mathcal{T}_h^{\Gamma} = \mathcal{T}_h \setminus \mathcal{T}_R$ there are at most 3 k -values in $\mathcal{J}_1^{\Gamma_h}$ with $(R_1 q_k)|_T \neq 0$ and thus

$$\begin{aligned} \|w_1\|_{L^2}^2 &= \sum_{T \in \mathcal{T}_h^{\Gamma}} \left\| \sum_{k \in \mathcal{J}_1^{\Gamma_h}} \beta_k R_1 q_k \right\|_{L^2(T)}^2 \leq \sum_{T \in \mathcal{T}_h^{\Gamma}} \left(\sum_{k \in \mathcal{J}_1^{\Gamma_h}} |\beta_k| \|R_1 q_k\|_{L^2(T)} \right)^2 \\ &\leq 3 \sum_{T \in \mathcal{T}_h^{\Gamma}} \sum_{k \in \mathcal{J}_1^{\Gamma_h}} |\beta_k|^2 \|R_1 q_k\|_{L^2(T)}^2 = 3 \sum_{k \in \mathcal{J}_1^{\Gamma_h}} |\beta_k|^2 \|R_1 q_k\|_{L^2}^2, \end{aligned}$$

which proves the upper bound in (7.123). A proof of the lower bound is given in Lemma 3 in [209]. □

Using the norm equivalences in (7.120), (7.122) and (7.123) we derive a spectral result for the mass matrix using standard arguments. Let $m = m_h := n + |\mathcal{J}_1^{\Gamma_h}| + |\mathcal{J}_2^{\Gamma_h}|$ be the dimension of $Q_h^{\Gamma_h}$ and $J : \mathbb{R}^m \rightarrow Q_h^{\Gamma_h}$ the isomorphism defined by (7.121):

$$J\mathbf{z} = J(\vec{\alpha}, \vec{\beta}^{(1)}, \vec{\beta}^{(2)}) = v.$$

The mass matrix $\mathbf{M} \in \mathbb{R}^{m \times m}$ is given by

$$\langle \mathbf{M}\mathbf{z}, \mathbf{z} \rangle = (J\mathbf{z}, J\mathbf{z})_{L^2} \quad \text{for all } \mathbf{z} \in \mathbb{R}^m.$$

Here $\langle \cdot, \cdot \rangle$ denotes the Euclidean scalar product.

Define $\text{diag}(\mathbf{M}) =: \mathbf{D}_M$ with

$$\mathbf{D}_M = \begin{pmatrix} \mathbf{D} & \emptyset \\ \emptyset & \mathbf{D}_1 \\ \emptyset & \emptyset & \mathbf{D}_2 \end{pmatrix}, \quad \mathbf{D}_{k,k} = \|q_k\|_{L^2}^2, \quad 1 \leq k \leq n,$$

$$(\mathbf{D}_i)_{k,k} = \|R_i q_k\|_{L^2}^2, \quad k \in \mathcal{J}_i^{\Gamma_h}.$$

Theorem 7.9.7 *There are constants $c_1 > 0$ and c_2 independent of h such that*

$$c_1 \langle \mathbf{D}_M \mathbf{z}, \mathbf{z} \rangle \leq \langle \mathbf{M} \mathbf{z}, \mathbf{z} \rangle \leq c_2 \langle \mathbf{D}_M \mathbf{z}, \mathbf{z} \rangle \quad \text{for all } \mathbf{z} \in \mathbb{R}^m.$$

Proof. From (7.120), (7.122) and (7.123) we get

$$\begin{aligned} \langle \mathbf{M} \mathbf{z}, \mathbf{z} \rangle &= \|v\|_{L^2}^2 \leq 2(\|w\|_{L^2}^2 + \|w_1\|_{L^2}^2 + \|w_2\|_{L^2}^2) \\ &\leq 2 \left(c_2 \sum_{k=1}^n \alpha_k^2 \|q_k\|_{L^2}^2 + 3 \sum_{k \in \mathcal{J}_1^{\Gamma_h}} (\beta_k^{(1)})^2 \|R_1 q_k\|_{L^2}^2 + 3 \sum_{k \in \mathcal{J}_2^{\Gamma_h}} (\beta_k^{(2)})^2 \|R_2 q_k\|_{L^2}^2 \right) \\ &\leq c (\langle \mathbf{D} \vec{\alpha}, \vec{\alpha} \rangle + \langle \mathbf{D}_1 \vec{\beta}^{(1)}, \vec{\beta}^{(1)} \rangle + \langle \mathbf{D}_2 \vec{\beta}^{(2)}, \vec{\beta}^{(2)} \rangle) = c \langle \mathbf{D}_M \mathbf{z}, \mathbf{z} \rangle, \end{aligned}$$

with a constant c independent of h . Similarly, due to

$$\langle \mathbf{M} \mathbf{z}, \mathbf{z} \rangle = \|v\|_{L^2}^2 \geq (1 - c_{CS})(\|w\|_{L^2}^2 + \|w_1\|_{L^2}^2 + \|w_2\|_{L^2}^2),$$

and using the lower bounds in (7.122) and (7.123), we obtain $\langle \mathbf{M} \mathbf{z}, \mathbf{z} \rangle \geq c \langle \mathbf{D}_M \mathbf{z}, \mathbf{z} \rangle$ with a constant $c > 0$ independent of h . \square

The result in this theorem proves that the matrix $\mathbf{D}_M^{-1} \mathbf{M}$ has a spectral condition number that is uniformly (w.r.t. h) bounded. Note that the constants in the spectral condition number bounds are also independent of the supports of the basis functions $R_i q_k$, $k \in \mathcal{J}_i^{\Gamma_h}$. In other words, a simple scaling is sufficient to control the stability (in L^2) of the basis functions with “very small” supports. Furthermore, we note that in the analysis we did *not* assume quasi-uniformity of the family of triangulations.

Corollary 7.9.8 Since the reduced extended finite element space $\tilde{Q}_h^{\Gamma_h}$ is spanned by a subset of the basis functions in (7.117), a similar L^2 -stability result trivially holds for the basis in the space $\tilde{Q}_h^{\Gamma_h}$.

Remark 7.9.9 There are two canonical splittings of the XFEM space $Q_h^{\Gamma_h}$, namely the ones in (7.116) and in (7.112):

$$Q_h^{\Gamma_h} = Q_h \oplus V_1^{\Gamma_h} \oplus V_2^{\Gamma_h}, \quad Q_h^{\Gamma_h} = R_1 Q_h \oplus R_2 Q_h,$$

where R_i is the restriction operator as in (7.111), but now with respect to $\Omega_{i,h}$. In the analysis above we used the basis corresponding to the first splitting, cf. (7.117):

$$\{q_k\}_{1 \leq k \leq n} \cup \{R_1 q_k\}_{k \in \mathcal{J}_1^{\Gamma_h}} \cup \{R_2 q_k\}_{k \in \mathcal{J}_2^{\Gamma_h}}. \quad (7.124)$$

Let \mathcal{J}_i be the index set of all k such that $\text{supp}(q_k) \cap \Omega_{i,h} \neq \emptyset$ and define $V_i := \text{span}\{q_k : k \in \mathcal{J}_i\}$. Note that $V_i \subset Q_h$ and $R_i Q_h = R_i V_i$ holds. The linear mapping $J : V_1 \times V_2 \rightarrow Q_h^{\Gamma_h}$

$$J(v_1, v_2) = R_1 v_1 + R_2 v_2 \quad (7.125)$$

is *bijective*. The second splitting induces the basis

$$\{R_1 q_k\}_{k \in \mathcal{J}_1} \cup \{R_2 q_k\}_{k \in \mathcal{J}_2}. \quad (7.126)$$

Related to the representations in these two bases we note the following. Take $v \in Q_h^{\Gamma_h}$ and let $v_i \in V_i$ be such that $v = R_1 v_1 + R_2 v_2$. For the representation in the basis (7.124) we have

$$v = \sum_{k=1}^n \alpha_k q_k + \sum_{i=1}^2 \sum_{k \in \mathcal{J}_i^{\Gamma_h}} \beta_k^{(i)} R_i q_k,$$

with

$$\begin{aligned} \alpha_k &= v(x_k), \quad x_k \in \mathcal{V}, \quad k = 1, \dots, n, \\ \beta_k^{(i)} &= v_i(x_k) - v(x_k), \quad k \in \mathcal{J}_i^{\Gamma_h}. \end{aligned}$$

For the representation in the basis (7.126) we have

$$v = \sum_{i=1}^2 \sum_{k \in \mathcal{J}_i} \xi_k^{(i)} R_i q_k, \quad \text{with } \xi_k^{(i)} = v_i(x_k), \quad k \in \mathcal{J}_i.$$

LBB-stability

If the XFEM method is used for the discretization of the pressure variable in a two-phase flow problem, then the space $Q_h^{\Gamma_h}$ is combined with a finite element space for the velocity discretization. In this context the question of LBB-stability of the pair of spaces arises. As far as we know, this topic has not been investigated in the literature, yet. In our applications, for the velocity discretization we use the space \mathbf{V}_h of piecewise quadratics. The Hood-Taylor pair (\mathbf{V}_h, Q_h) is LBB-stable. If instead of Q_h we use the extended space $Q_h^{\Gamma_h}$ it is not known, whether the pair $(\mathbf{V}_h, Q_h^{\Gamma_h})$ is LBB-stable. Related to this we comment on results of a numerical experiment that are presented in Sect. 7.10.3. In this experiment it is observed that for the *reduced* XFEM space $\tilde{Q}_h^{\Gamma_h}$ the pair $(\mathbf{V}_h, \tilde{Q}_h^{\Gamma_h})$ has a (much) better LBB-stability property than the pair $(\mathbf{V}_h, Q_h^{\Gamma_h})$. Hence, at least in the model problem considered in Sect. 7.10.3, the concept of reduction of the original XFEM space appears to be important in view of LBB-stability. There is no theoretical analysis that explains this effect.

7.9.5 Numerical experiment with XFEM

In this experiment, for a given piecewise smooth function we compute best approximation errors for the spaces Q_h , Q_h^Γ and \tilde{Q}_h^Γ . The behavior of these approximation errors confirms the results of the theoretical analyses treated above.

We take $\Omega = (-1, 1)^3$ and a planar interface $\Gamma = \{(x, y, z) \in \Omega : y + z = 0.05\}$ and $\Omega_1 = \{(x, y, z) \in \Omega : y + z < 0.05\}$, $\Omega_2 = \Omega \setminus \Omega_1$. Let u be given by

$$u = \begin{cases} x^2 + y^2 + z^2 & \text{in } \Omega_1 \\ 3x^2 + y^2 + 2z^2 + 2 & \text{in } \Omega_2. \end{cases}$$

We use a *uniform* triangulation of Ω with tetrahedra, resulting in a family $\{\mathcal{T}_{h_i}\}_{i \geq 0}$ with mesh size parameter $h = h_i = 2^{-i-1}$, $i = 0, 1, 2, \dots$. The interface Γ and the triangulations are such that Γ is not aligned with the triangulation. Let Q_h be the space of continuous piecewise linear functions on \mathcal{T}_h and Q_h^Γ , \tilde{Q}_h^Γ the corresponding XFEM and reduced XFEM spaces, respectively. In the criterion (7.110) that is used in the construction of the space \tilde{Q}_h^Γ the parameters l , α and \hat{c} have to be chosen. We consider approximation errors in the L^2 -norm and therefore we take $l = 0$ and $\alpha = 2$. We present results for different values of the cut-off parameter \hat{c} . Note that for $\hat{c} = 0$ we have $\tilde{Q}_h^\Gamma = Q_h^\Gamma$ (all discontinuous basis functions are kept) and for a sufficiently large \hat{c} we have $\tilde{Q}_h^\Gamma = Q_h$ (all discontinuous basis functions are deleted). For $W_h \in \{Q_h, Q_h^\Gamma, \tilde{Q}_h^\Gamma\}$ we compute the best approximation of u in W_h , i.e. $u_h \in W_h$ such that

$$\|u - u_h\|_{L^2} = \inf_{w_h \in W_h} \|u - w_h\|_{L^2}.$$

Results for the approximation error $e_h := \|u - u_h\|_{L^2}$ are given in Table 7.9, Table 7.10. In the latter table we use the construction of the reduced space \tilde{Q}_h^Γ based on the criterion (7.110) ($l = 0$, $\alpha = 2$) with different constants $\hat{c} = 10, 1, 0.1$. One-dimensional profiles of $u_h \in Q_h$ and $u_h \in Q_h^\Gamma$ are shown in Fig. 7.14.

# ref	$W_h = Q_h$	order	$W_h = Q_h^\Gamma$	order
0	1.60 E+0	-	1.44 E-1	-
1	1.20 E+0	0.41	3.71 E-2	1.96
2	8.88 E-1	0.43	9.37 E-3	1.99
3	6.27 E-1	0.50	2.35 E-3	1.99
4	4.52 E-1	0.47	5.89 E-4	2.00

Table 7.9. Approximation errors e_h for Q_h and Q_h^Γ .

The observed numerical order of convergence is consistent with the theoretically predicted improvement from $p = 0.5$ to $p = 2$. Furthermore, a good

ref#	$\hat{c} = 10$	order	$\hat{c} = 1$	order	$\hat{c} = 0.1$	order
0	1.60 E+0	-	1.60 E+0	-	1.77 E-1	-
1	1.20 E+0	0.41	2.69 E-1	2.57	4.01 E-2	2.14
2	8.88 E-1	0.43	4.72 E-2	2.51	9.37 E-3	2.10
3	1.37 E-2	6.01	8.98 E-3	2.39	2.35 E-3	1.99
4	2.60 E-3	2.40	5.89 E-4	3.93	5.89 E-4	2.00

Table 7.10. Approximation errors e_h for \tilde{Q}_h^F .

approximation quality appears to be not very sensitive with respect to the choice of the parameter \hat{c} .

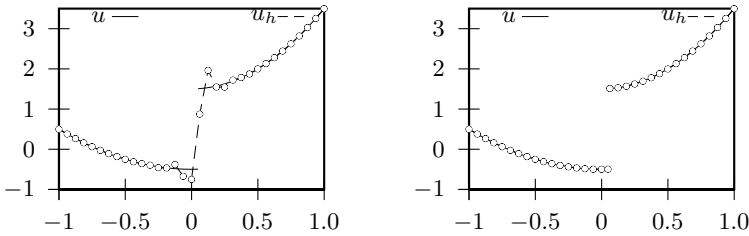


Fig. 7.14. 1D-profile of $u_h \in Q_h$ (left), $u_h \in Q_h^F$ (right) at $x = y = 0$, $h = 2^{-4}$.

The dimension of the space \tilde{Q}_h^F depends on the value for \hat{c} . These dimensions corresponding to the spaces used in Tables 7.9 and 7.10 are given in Table 7.11.

# ref.	$\hat{c} = \infty$	$\hat{c} = 10$	$\hat{c} = 1$	$\hat{c} = 0.1$	$\hat{c} = 0$
0	125	125	125	186	205
1	729	729	872	954	1017
2	4913	4913	5730	6001	6001
3	35937	39008	39103	40161	40161
4	274625	290878	291005	291005	291005

Table 7.11. Dimension of the space \tilde{Q}_h^F .

Note that for not too small refinement levels i the dimension of the (modified) XFEM space is only slightly larger than that of the standard finite element space.

7.10 Numerical experiments for a Stokes problem

Due to the Laplace-Young law, typically the pressure has a jump across the interface, when surface tension forces are present ($\tau \neq 0$), cf. Remark 1.1.5 and Remark 7.10.1 below. In numerical simulations, this discontinuity and inadequate approximation of the localized surface force term often lead to strong unphysical oscillations of the velocity \mathbf{u}_h at the interface, so called *spurious velocities* or *spurious currents*, cf. , e. g., [163, 111]. In this section we consider the relatively simple, but nevertheless interesting, test problem of a two-phase stationary Stokes problem (with $\mu_1 = \mu_2 = \mu$ in Ω) and investigate the discretization quality of the Laplace-Beltrami surface tension force approximation (Sect. 7.6) and of the extended finite element method for approximation of the pressure variable (Sect. 7.9.2). We will see that using the modified Laplace-Beltrami discretization \tilde{f}_{Γ_h} and the XFEM space results in a significant reduction of the spurious velocities compared to the case where one uses f_{Γ_h} and the standard FEM space Q_h . We emphasize that these improved methods are *not* restricted to this simplified problem but apply to the general Navier-Stokes model as well.

7.10.1 A stationary Stokes test problem

For a given sufficiently smooth interface Γ , we introduce the following Stokes problem. For $\mathbf{V}_0 := H_0^1(\Omega)^3$, $Q := L_0^2(\Omega)$, find $(\mathbf{u}, p) \in \mathbf{V}_0 \times Q$ such that

$$\begin{aligned} a(\mathbf{u}, \mathbf{v}) + b(\mathbf{v}, p) &= (\rho \mathbf{g}, \mathbf{v})_{L^2} + f_\Gamma(\mathbf{v}) && \text{for all } \mathbf{v} \in \mathbf{V}_0, \\ b(\mathbf{u}, q) &= 0 && \text{for all } q \in Q, \end{aligned} \quad (7.127)$$

where

$$\begin{aligned} a(\mathbf{u}, \mathbf{v}) &:= \int_{\Omega} \mu \nabla \mathbf{u} \cdot \nabla \mathbf{v} \, d\mathbf{x}, & b(\mathbf{v}, q) &= - \int_{\Omega} q \operatorname{div} \mathbf{v} \, d\mathbf{x}, \\ f_\Gamma(\mathbf{v}) &:= -\tau \int_{\Gamma} \kappa \mathbf{n} \cdot \mathbf{v} \, ds = -\tau \int_{\Gamma} \nabla_{\Gamma} \operatorname{id}_{\Gamma} \cdot \nabla_{\Gamma} \mathbf{v} \, ds, \end{aligned}$$

with a viscosity $\mu > 0$ that is constant in Ω . Recall that $f_\Gamma \in \mathbf{V}'_0$. Well-posedness of this variational problem follows from the same arguments as used for the *one*-phase stationary Stokes problem in Sect. 2.2.2. Theorem 15.3.1 can be applied and yields well-posedness of the variational problem (7.127). The unique solution of this problem is denoted by $(\mathbf{u}^*, p^*) \in \mathbf{V}_0 \times Q$.

Remark 7.10.1 Assume that the domain Ω is convex. Then the problem (7.127) has a *smooth* velocity solution $\mathbf{u}^* \in \mathbf{V}_0 \cap H^2(\Omega)^3$ and a *piece-wise smooth* pressure solution p with $p|_{\Omega_i} \in H^1(\Omega_i)$, $i = 1, 2$, which has a jump across Γ . These smoothness properties can be derived as follows. The curvature κ is assumed to be a smooth function (on Γ). Thus there exist

$\hat{p}_1 \in H^1(\Omega_1)$ such that $(\hat{p}_1)|_\Gamma = \kappa$ (in the sense of traces). Define $\hat{p} \in L^2(\Omega)$ by $\hat{p} = \hat{p}_1$ in Ω_1 , $\hat{p} = 0$ on Ω_2 . Note that for all $\mathbf{v} \in \mathbf{V}_0$,

$$\begin{aligned} f_\Gamma(\mathbf{v}) &= -\tau \int_\Gamma \kappa \mathbf{n}_\Gamma \cdot \mathbf{v} \, ds = -\tau \int_\Gamma \hat{p}_1 \mathbf{n}_\Gamma \cdot \mathbf{v} \, ds \\ &= -\tau \int_{\Omega_1} \hat{p}_1 \operatorname{div} \mathbf{v} \, d\mathbf{x} - \tau \int_{\Omega_1} \nabla \hat{p}_1 \cdot \mathbf{v} \, d\mathbf{x} \\ &= -\tau \int_\Omega \hat{p} \operatorname{div} \mathbf{v} \, d\mathbf{x} + \tau \int_\Omega \tilde{\mathbf{g}} \cdot \mathbf{v} \, d\mathbf{x}, \end{aligned}$$

with $\tilde{\mathbf{g}} \in L^2(\Omega)^3$ given by $\tilde{\mathbf{g}} = -\nabla \hat{p}_1$ in Ω_1 , $\tilde{\mathbf{g}} = 0$ on Ω_2 . Thus if (\mathbf{u}^*, p^*) is the solution of (7.127) then $(\mathbf{u}^*, p^* - \tau \hat{p})$ satisfies the standard Stokes equations

$$\begin{aligned} a(\mathbf{u}^*, \mathbf{v}) + b(\mathbf{v}, p^* - \tau \hat{p}) &= (\rho \mathbf{g} + \tau \tilde{\mathbf{g}}, \mathbf{v})_{L^2} \quad \text{for all } \mathbf{v} \in \mathbf{V}_0, \\ b(\mathbf{u}^*, q) &= 0 \quad \text{for all } q \in Q. \end{aligned} \tag{7.128}$$

From regularity results on Stokes equations and the fact that Ω is convex we conclude that $\mathbf{u}^* \in H^2(\Omega)^3 \cap H_0^1(\Omega)^3$ and $p^* - \tau \hat{p} \in H^1(\Omega)$. Thus $[p^* - \tau \hat{p}]_\Gamma = 0$ (a.e. on Γ) holds, which implies

$$[p^*]_\Gamma = \tau [\hat{p}]_\Gamma = \tau \kappa,$$

i.e., p^* has a jump across Γ of the size $\tau \kappa$.

Example 7.10.2 (Static Droplet) A simple example that is used in the numerical experiments in Sect. 7.10.3 is the following. Let $\Omega := (-1, 1)^3$ and Ω_1 a sphere with center at the origin and radius $r < 1$. We take $\mathbf{g} = 0$. In this case the curvature is constant, $\kappa = \frac{2}{r}$, and the solution of the Stokes problem (7.127) is given by $\mathbf{u}^* = 0$, $p^* = \tau \frac{2}{r} + c_0$ on Ω_1 , $p^* = c_0$ on Ω_2 with a constant c_0 such that $\int_\Omega p^* \, dx = 0$.

Discretization error bounds

We assume that a piecewise planar surface Γ_h is known, which is close to the interface Γ in the sense of (7.70). The induced polyhedral approximations of the subdomains are $\Omega_{1,h} = \operatorname{int}(\Gamma_h)$ (region in the interior of Γ_h) and $\Omega_{2,h} = \Omega \setminus \overline{\Omega_{1,h}}$. Furthermore, we define the piecewise constant approximation of the density by $\rho_h = \rho_i$ on $\Omega_{i,h}$. We assume that for $\mathbf{v}_h \in \mathbf{V}_h$ the integrals in

$$(\rho_h \mathbf{g}, \mathbf{v}_h)_{L^2} = \rho_1 \int_{\Omega_{1,h}} \mathbf{g} \cdot \mathbf{v}_h \, dx + \rho_2 \int_{\Omega_{2,h}} \mathbf{g} \cdot \mathbf{v}_h \, dx$$

can be computed with high accuracy. This can be realized efficiently in our implementation because if one applies the standard finite element assembling strategy by using a loop over all tetrahedra $T \in \mathcal{T}_h$, then $T \cap \Omega_{i,h}$ is either empty or T or a relatively simple polygonal subdomain (due to the construction of Γ_h). For more details we refer to Sect. 7.9.3.

The discretization of (7.127) is as follows: determine $(\mathbf{u}_h, p_h) \in \mathbf{V}_h \times Q_h$ such that

$$\begin{aligned} a(\mathbf{u}_h, \mathbf{v}_h) + b(\mathbf{v}_h, p_h) &= (\rho_h \mathbf{g}, \mathbf{v}_h)_{L^2} + f_{\Gamma_h}(\mathbf{v}_h) && \text{for all } \mathbf{v}_h \in \mathbf{V}_h, \\ b(\mathbf{u}_h, q_h) &= 0 && \text{for all } q_h \in Q_h. \end{aligned} \tag{7.129}$$

We do not restrict to a concrete pair of spaces (\mathbf{V}_h, Q_h) . For these spaces we (only) assume conformity $\mathbf{V}_h \subset \mathbf{V}_0$, $Q_h \subset Q$, and *LBB-stability* of the pair (\mathbf{V}_h, Q_h) . Approximations $f_{\Gamma_h}(\mathbf{v}_h)$ of $f_{\Gamma}(\mathbf{v}_h)$ are discussed in Sect. 7.6. Using standard finite element error analysis based on the Strang-lemma, cf. Sect. 15.4, we obtain the following discretization error bound.

Theorem 7.10.3 *Let (\mathbf{u}^*, p^*) , (\mathbf{u}_h, p_h) be the solution of (7.127) and (7.129), respectively. Then the error bound*

$$\begin{aligned} \mu \|\mathbf{u}_h - \mathbf{u}^*\|_1 + \|p_h - p^*\|_{L^2} &\leq c \left(\mu \inf_{\mathbf{v}_h \in \mathbf{V}_h} \|\mathbf{v}_h - \mathbf{u}^*\|_1 + \inf_{q_h \in Q_h} \|q_h - p^*\|_{L^2} \right. \\ &\quad + \sup_{\mathbf{v}_h \in \mathbf{V}_h} \frac{|(\rho \mathbf{g}, \mathbf{v}_h)_{L^2} - (\rho_h \mathbf{g}, \mathbf{v}_h)_{L^2}|}{\|\mathbf{v}_h\|_1} \\ &\quad \left. + \sup_{\mathbf{v}_h \in \mathbf{V}_h} \frac{|f_{\Gamma}(\mathbf{v}_h) - f_{\Gamma_h}(\mathbf{v}_h)|}{\|\mathbf{v}_h\|_1} \right) \end{aligned} \tag{7.130}$$

holds with a constant c independent of h , μ and ρ .

Remark 7.10.4 Assume Ω to be convex. Then the problem (7.128) is H^2 -regular and from a standard duality argument (and a scaling argument) it follows that

$$\|\mathbf{u}^* - \mathbf{u}_h\|_{L^2} \leq ch \left(\|\mathbf{u}^* - \mathbf{u}_h\|_1 + \frac{1}{\mu} \|p^* - p_h\|_{L^2} \right)$$

holds, with a constant c independent of μ and h .

Corollary 7.10.5 Let (\mathbf{u}^*, p^*) , (\mathbf{u}_h, p_h) be as in Theorem 7.10.3 and define

$$r_h := \sup_{\mathbf{v}_h \in \mathbf{V}_h} \frac{|(\rho \mathbf{g}, \mathbf{v}_h)_{L^2} - (\rho_h \mathbf{g}, \mathbf{v}_h)_{L^2}|}{\|\mathbf{v}_h\|_1} + \sup_{\mathbf{v}_h \in \mathbf{V}_h} \frac{|f_{\Gamma}(\mathbf{v}_h) - f_{\Gamma_h}(\mathbf{v}_h)|}{\|\mathbf{v}_h\|_1}.$$

The following holds:

$$\begin{aligned} \|\mathbf{u}_h - \mathbf{u}^*\|_1 &\leq c \left(\inf_{\mathbf{v}_h \in \mathbf{V}_h} \|\mathbf{v}_h - \mathbf{u}^*\|_1 + \frac{1}{\mu} \inf_{q_h \in Q_h} \|q_h - p^*\|_{L^2} + \frac{1}{\mu} r_h \right), \\ \|\mathbf{u}_h - \mathbf{u}^*\|_{L^2} &\leq ch \left(\inf_{\mathbf{v}_h \in \mathbf{V}_h} \|\mathbf{v}_h - \mathbf{u}^*\|_1 + \frac{1}{\mu} \inf_{q_h \in Q_h} \|q_h - p^*\|_{L^2} + \frac{1}{\mu} r_h \right), \\ \|p_h - p^*\|_{L^2} &\leq c \left(\mu \inf_{\mathbf{v}_h \in \mathbf{V}_h} \|\mathbf{v}_h - \mathbf{u}^*\|_1 + \inf_{q_h \in Q_h} \|q_h - p^*\|_{L^2} + r_h \right), \end{aligned}$$

with constants c independent of h , μ and ρ . We observe that if $\mu \ll 1$ then in the velocity error we have an error amplification effect proportional to $\frac{1}{\mu}$. This effect does not occur in the discretization error for the pressure.

We comment on the terms occurring in the bound in (7.130). We start with the velocity approximation error term $\mu \inf_{\mathbf{v}_h \in \mathbf{V}_h} \|\mathbf{v}_h - \mathbf{u}^*\|_1$. Assume a situation in which the solution \mathbf{u}^* of (7.127) is smooth: $\mathbf{u}^* \in H^2(\Omega)^3$. With standard finite element spaces \mathbf{V}_h for the velocity (e.g., P_1 or P_2) we then obtain

$$\inf_{\mathbf{v}_h \in \mathbf{V}_h} \|\mathbf{v}_h - \mathbf{u}^*\|_1 \leq ch.$$

If $\mathbf{u}^* \in H^3(\Omega)^3$, then with quadratic finite elements the upper bound can be improved to ch^2 .

Remark 7.10.6 Note that in Remark 7.10.1 the smoothness of \mathbf{u}^* was shown under the assumption of equal viscosity in both phases, i. e., $\mu_1 = \mu_2$. If μ is discontinuous across Γ , then the normal derivative of \mathbf{u}^* has a jump across Γ , which means that the velocity field \mathbf{u}^* has a kink at Γ . If the grid is not aligned to the interface, then the approximation of such functions in standard finite element spaces \mathbf{V}_h yields

$$\inf_{\mathbf{v}_h \in \mathbf{V}_h} \|\mathbf{v}_h - \mathbf{u}^*\|_1 \leq c\sqrt{h}.$$

In the case of large viscosity ratios $\max_{i=1,2} \mu_i / \min_{i=1,2} \mu_i$ (e. g., liquid-gas systems) the construction of specially adapted finite element spaces enabling first order convergence w.r.t. the H^1 -norm is required, cf. [66, 166]. However, for liquid-liquid systems with small viscosity ratios the influence of this error source turns out to be rather small compared to the pressure approximation error (second term in (7.130)).

Related to the third term in (7.130) we note the following. Due to (7.70a) we get $|\text{meas}_3(\Omega_i) - \text{meas}_3(\Omega_{i,h})| \leq ch_T^2$, $i = 1, 2$, and using this we obtain

$$\begin{aligned} |(\rho \mathbf{g}, \mathbf{v}_h)_{L^2} - (\rho_h \mathbf{g}, \mathbf{v}_h)_{L^2}| &\leq \sum_{i=1}^2 \rho_i \left| \int_{\Omega_i} \mathbf{g} \cdot \mathbf{v}_h \, dx - \int_{\Omega_{i,h}} \mathbf{g} \cdot \mathbf{v}_h \, dx \right| \\ &\leq c(\rho_1 + \rho_2) h_\Gamma \|\mathbf{v}_h\|_1, \end{aligned}$$

and thus an $\mathcal{O}(h_\Gamma)$ bound for the third term in (7.130).

The remaining two terms in (7.130) are less easy to handle. In Sect. 7.7 we treated the fourth term. It is shown that the approximation method based on the modified Laplace-Beltrami discretization f_{Γ_h} , cf. (7.60), results in a $\mathcal{O}(h_\Gamma)$ bound for this term whereas the Laplace-Beltrami approximation with f_{Γ_h} , cf. (7.54), only yields $\mathcal{O}(\sqrt{h_\Gamma})$.

The second term in (7.130) is treated in Sect. 7.9. It is shown that standard finite element spaces (e.g., P_0 or P_1) lead to a pressure discretization error $\inf_{q_h \in Q_h} \|q_h - p^*\|_{L^2} \sim \sqrt{h_\Gamma}$, and that for the extended finite element space (or its reduced variant) one has an L^2 -error bound proportional to h_Γ^2 .

Remark 7.10.7 Consider the problem as in Example 7.10.2. Then $\mathbf{u}^* = 0$, $\mathbf{g} = 0$ and the bound in (7.130) simplifies to

$$\begin{aligned} & \mu \|\mathbf{u}_h\|_1 + \|p_h - p^*\|_{L^2} \\ & \leq c \left(\inf_{q_h \in Q_h} \|q_h - p^*\|_{L^2} + \sup_{\mathbf{v}_h \in \mathbf{V}_h} \frac{|f_\Gamma(\mathbf{v}_h) - f_{\Gamma_h}(\mathbf{v}_h)|}{\|\mathbf{v}_h\|_1} \right). \end{aligned} \quad (7.131)$$

In the following sections we consider the Galerkin discretization (7.129) of the Stokes problem with $\mathbf{g} = 0$ in the cube $\Omega = (-1, 1)^3$. We assume constant viscosity $\mu = 1$. We will consider different interfaces Γ . The discrete problem is as follows: determine $\mathbf{v}_h \in \mathbf{V}_h$, $p_h \in Q_h$ such that

$$\begin{aligned} a(\mathbf{u}_h, \mathbf{v}_h) + b(\mathbf{v}_h, p_h) &= f_{\text{SF},h}(\mathbf{v}_h) \quad \text{for all } \mathbf{v}_h \in \mathbf{V}_h, \\ b(\mathbf{u}_h, q_h) &= 0 \quad \text{for all } q_h \in Q_h, \end{aligned} \quad (7.132)$$

where $f_{\text{SF},h} \in \mathbf{V}'_h$ are different approximations of f_Γ . We choose a uniform initial triangulation \mathcal{T}_0 of Ω where the vertices form a $5 \times 5 \times 5$ lattice and apply an adaptive refinement algorithm. Local refinement of the coarse mesh \mathcal{T}_0 in the vicinity of Γ yields the gradually refined meshes $\mathcal{T}_1, \mathcal{T}_2, \mathcal{T}_3, \mathcal{T}_4$ with local mesh sizes $h_\Gamma = h_i = 2^{-i-1}$, $i = 0, \dots, 4$, at the interface. For the discretization of velocity we choose the standard finite element space of piecewise quadratics:

$$\mathbf{V}_h := \{ \mathbf{v} \in C(\Omega)^3 : \mathbf{v}|_T \in \mathcal{P}_2 \text{ for all } T \in \mathcal{T}_h, \mathbf{v}|_{\partial\Omega} = 0 \}.$$

We consider different choices for the pressure finite element space, namely piecewise constant or continuous piecewise linear elements, i. e., the spaces Q_h^0 , Q_h^1 respectively, and the extended pressure space $Q_h^{\Gamma,h}$ introduced in Sect. 7.9.2. The discretization quality is quantified by computing norms of the errors

$$e_{\mathbf{u}} := \mathbf{u}^* - \mathbf{u}_h = -\mathbf{u}_h \quad \text{and} \quad e_p := p^* - p_h.$$

7.10.2 Test case A: Pressure jump at a planar interface

This simple test case is designed to examine interpolation errors of finite element spaces for the approximation of a discontinuous pressure variable. We consider two different interfaces Γ_1 and Γ_2 , which are both planes. Γ_1 is defined by

$$\Gamma_1 = \{ x \in \Omega : x_3 = 0 \}.$$

In this case the two subdomains are given by $\Omega_1 := \{ x \in \Omega : x_3 < 0 \}$ and $\Omega_2 := \Omega \setminus \overline{\Omega}_1$, cf. Fig. 7.15. Interface Γ_2 is defined by

$$\Gamma_2 = \{ x \in \Omega : x_2 + x_3 = 1 \},$$

and the corresponding subdomains are $\Omega_1 := \{ x \in \Omega : x_2 + x_3 < 0 \}$ and $\Omega_2 := \Omega \setminus \overline{\Omega}_1$, cf. Fig. 7.17.

Since for these planar interfaces Γ_1, Γ_2 the curvature is zero we introduce an artificial surface force f_{ASF} given by

$$f_{\text{ASF}}(\mathbf{v}) = -\sigma \int_{\Gamma} \mathbf{v} \cdot \mathbf{n} \, ds, \quad \mathbf{v} \in \mathbf{V},$$

with a constant $\sigma > 0$. Note that $f_{\text{ASF}} \in \mathbf{V}'$. The unique solution of (7.127), with $f_{\Gamma} = f_{\text{ASF}}$, is given by

$$\mathbf{u}^* = 0, \quad p^* = \begin{cases} C + \sigma & \text{in } \Omega_1, \\ C & \text{in } \Omega_2. \end{cases}$$

Here C is a constant such that $\int_{\Omega} p^* \, dx = 0$. In the experiments below we use $\sigma = 1$. For both interfaces *the interface approximation Γ_h is exact*, i. e., $\Gamma_h = \Gamma$, allowing an *exact discretization* of the interfacial force, i. e., $f_{\text{ASF},h} = f_{\text{ASF}}$.

Due to $\mathbf{g} = 0$, $\mathbf{u}^* \in \mathbf{V}_h$ and the fact that $\|f_{\text{ASF},h} - f_{\text{ASF}}\|_{\mathbf{V}'_h} = 0$ the error bound (7.130) simplifies to

$$\mu \|e_{\mathbf{u}}\|_1 + \|e_p\|_{L^2} \leq c \inf_{q_h \in Q_h} \|p^* - q_h\|_{L^2}. \tag{7.133}$$

Thus the errors in velocity and pressure are solely controlled by the approximation quality of the finite element space Q_h .

The number of velocity and pressure unknowns for the grids $\mathcal{T}_0, \dots, \mathcal{T}_4$ with different refinement levels are shown in Table 7.12. Note that $\dim Q_h^{\Gamma_h} > \dim Q_h^1$ due to the extended basis functions and that $\dim Q_h^0$ is even (much) larger.

interface	# ref.	$\dim \mathbf{V}_h$	$\dim Q_h^1$	$\dim Q_h^{\Gamma_h}$	$\dim Q_h^0$
$\Gamma = \Gamma_1$	0	1029	125	150	384
	1	6801	455	536	1984
	2	31197	1657	1946	8384
	3	131433	6235	7324	33984
	4	537717	24093	28318	136384
$\Gamma = \Gamma_2$	0	1029	125	190	384
	1	7749	543	768	2304
	2	42633	2313	3146	11556
	3	200469	9607	12808	52088
	4	871881	39229	51774	221796

Table 7.12. Dimensions of the finite element spaces for test case A.

We discuss the results obtained for the two cases $\Gamma = \Gamma_1$ and $\Gamma = \Gamma_2$.

Interface at $\Gamma = \Gamma_1$

For $\Gamma = \Gamma_1$, the interface Γ is *located at the element boundaries of tetrahedra* intersected by Γ , i. e., for each tetrahedron T intersecting Γ we have that $\Gamma \cap T$ is equal to a face of T .

In this special situation, the discontinuous pressure p^* can be represented exactly in the finite element space Q_h^0 of piecewise constants, thus the finite element solution $(\mathbf{u}_h, p_h) \in \mathbf{V}_h \times Q_h^0$ is equal to (\mathbf{u}^*, p^*) . This is confirmed by the numerical results: the exact solution (\mathbf{u}^*, p^*) fulfills the discrete equations (up to rounding errors). The same holds for the extended finite element space $Q_h^{\Gamma_h}$.

For the space of continuous piecewise linear finite elements we have $p^* \notin Q_h^1$. The grid \mathcal{T}_3 and the corresponding pressure solution are shown in Figs. 7.15 and 7.16. The error norms for different grid refinement levels are shown in Table 7.13. The L^2 -error of the pressure shows a decay of $\mathcal{O}(h^{1/2})$. This confirms the theoretical results for the approximation error $\min_{q \in Q_h^1} \|p^* - q_h\|_{L^2}$, cf. Sect. 7.9.1 and (7.133). The velocity error in the H^1 -norm shows the same $\mathcal{O}(h^{1/2})$ behavior, whereas in the L^2 -norm the error behaves like $\mathcal{O}(h^{3/2})$.

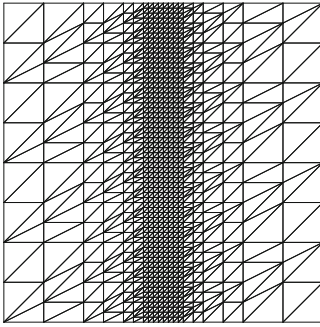


Fig. 7.15. Slice of grid at $x_1 = 0$ after 3 refinements for $\Gamma = \Gamma_1$.

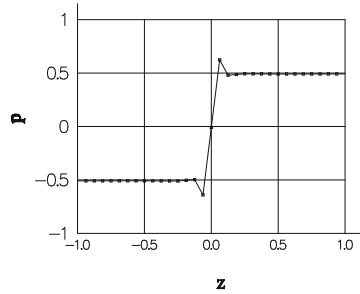


Fig. 7.16. 1D-profile of pressure jump at $x_1 = x_2 = 0$ for $p_h \in Q_h^1$. 3 refinements, $\Gamma = \Gamma_1$.

# ref.	$\ e_{\mathbf{u}}\ _{L^2}$	order	$\ e_{\mathbf{u}}\ _1$	order	$\ e_p\ _{L^2}$	order
0	4.26 E-2	–	4.26 E-1	–	5.32 E-1	–
1	1.85 E-2	1.2	3.41 E-1	0.32	3.78 E-1	0.49
2	7.09 E-3	1.38	2.55 E-1	0.42	2.68 E-1	0.5
3	2.60 E-3	1.45	1.85 E-1	0.46	1.90 E-1	0.5
4	9.37 E-4	1.47	1.33 E-1	0.48	1.34 E-1	0.5

Table 7.13. Errors for the (\mathbf{V}_h, Q_h^1) finite element pair, $\Gamma = \Gamma_1$.

Interface at $\Gamma = \Gamma_2$

We now consider the case $\Gamma = \Gamma_2$. This problem corresponds to the 2D problem discussed in Sect. 7.9.1, cf. Fig. 7.10. Γ is chosen such that $\Gamma \cap F \neq F$ for all faces of the triangulations $\mathcal{T}_0, \mathcal{T}_1, \mathcal{T}_2, \mathcal{T}_3$. As a consequence, $p^* \notin Q_h^0$ and $p^* \notin Q_h^1$, but $p^* \in Q_h^{I_h}$. We checked that the finite element solution $(\mathbf{u}_h, p_h) \in \mathbf{V}_h \times Q_h^{I_h}$ is indeed equal to (\mathbf{u}^*, p^*) (up to machine accuracy).

We first discuss results for P_1 finite elements. The grid \mathcal{T}_3 , obtained after 3 times refinement, and the corresponding pressure solution for P_1 finite elements are shown in Figs. 7.17 and 7.18. The error norms for different grid refinement levels are shown in Table 7.14. The same convergence orders as for the case $\Gamma = \Gamma_1$ are obtained, cf. Table 7.13.

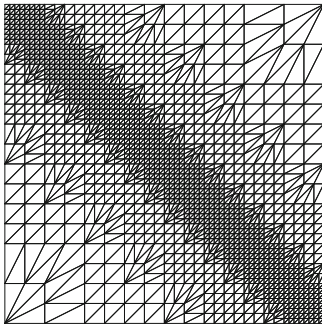


Fig. 7.17. Slice of grid at $x_1 = 0$ after 3 refinements for $\Gamma = \Gamma_2$.

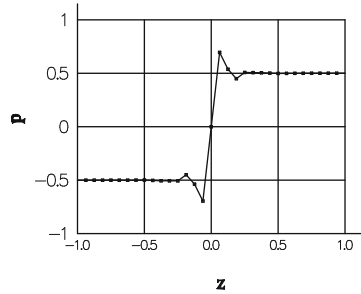


Fig. 7.18. 1D-profile of pressure jump at $x_1 = x_2 = 0$ for $p_h \in Q_h^1$. 3 refinements, $\Gamma = \Gamma_2$.

# ref.	$\ e_{\mathbf{u}}\ _{L^2}$	order	$\ e_{\mathbf{u}}\ _1$	order	$\ e_p\ _{L^2}$	order
0	2.53 E-2	–	2.56 E-1	–	5.44 E-1	–
1	1.24 E-2	1.02	2.25 E-1	0.18	3.99 E-1	0.45
2	5.03 E-3	1.31	1.75 E-1	0.36	2.88 E-1	0.47
3	1.89 E-3	1.41	1.29 E-1	0.44	2.06 E-1	0.48
4	6.88 E-4	1.46	9.35 E-2	0.47	1.46 E-1	0.49

Table 7.14. Errors for the (\mathbf{V}_h, Q_h^1) finite element pair, $\Gamma = \Gamma_2$.

Results for the P_0 finite elements are shown in Table 7.15. Compared to P_1 finite elements, the errors are slightly larger but show similar convergence orders, i. e., $\mathcal{O}(h^{1/2})$ for the pressure L^2 -error and velocity H^1 -error, and $\mathcal{O}(h^{3/2})$ for the velocity L^2 -error.

# ref.	$\ e_{\mathbf{u}}\ _{L^2}$	order	$\ e_{\mathbf{u}}\ _1$	order	$\ e_p\ _{L^2}$	order
0	3.98 E-2	–	3.49 E-1	–	7.30 E-1	–
1	1.64 E-2	1.28	2.75 E-1	0.35	4.89 E-1	0.58
2	6.14 E-3	1.41	2.04 E-1	0.43	3.35 E-1	0.54
3	2.22 E-3	1.47	1.48 E-1	0.46	2.34 E-1	0.52
4	7.92 E-4	1.49	1.06 E-1	0.48	1.65 E-1	0.51

Table 7.15. Errors for the (\mathbf{V}_h, Q_h^0) finite element pair, $\Gamma = \Gamma_2$.

7.10.3 Test case B: Static droplet

In this test case (cf. Example 7.10.2) we consider a static droplet $\Omega_1 = \{x \in \mathbb{R}^3 : \|x\| \leq r\}$ in the cube $\Omega = (-1, 1)^3$ with $r = 2/3$. We assume that surface tension is present, i. e., $f_{\text{SF}} = f_\Gamma$ with $\tau = 1$. This problem has the unique solution

$$\mathbf{u}^* = 0, \quad p^* = \begin{cases} c_0 + \kappa & \text{in } \Omega_1, \\ c_0 & \text{in } \Omega_2. \end{cases}$$

Since $\kappa = 2/r$, the pressure jump is equal to $[p^*]_\Gamma = 3$. A 2D variant of this test case is presented in [111, 115, 226].

In this problem the errors in velocity and pressure are influenced by *two error sources*, namely the approximation error of the discontinuous pressure p^* in Q_h (as in test case A) and errors induced by the discretization of the surface force f_Γ , cf. (7.131).

The number of velocity and pressure unknowns for the grids $\mathcal{T}_0, \dots, \mathcal{T}_4$ with different refinement levels are shown in Table 7.16. Note that $\dim Q_h^{\Gamma_h}$ is significantly larger than $\dim Q_h^1$, but that $\dim Q_h^{\Gamma_h} \ll \dim \mathbf{V}_h$.

# ref.	test case B		
	$\dim \mathbf{V}_h$	$\dim Q_h^1$	$\dim Q_h^{\Gamma_h}$
0	1029	125	176
1	5523	337	533
2	30297	1475	2295
3	139029	6127	9413
4	569787	24373	37355

Table 7.16. Dimensions of the finite element spaces for test case B.

We consider test case B for two different approximations of the surface tension functional f_Γ , namely the Laplace-Beltrami discretization f_{Γ_h} as in (7.54) and the modified Laplace-Beltrami discretization \tilde{f}_{Γ_h} as in (7.60). For the pressure space we choose $Q_h = Q_h^1$ and $Q_h = Q_h^{\Gamma_h}$. We do not present results for the space Q_h^0 because these are similar to those for Q_h^1 . Table 7.17 shows the decay

of the pressure L^2 -norm for the four different experiments. We observe poor $\mathcal{O}(h^{1/2})$ convergence in the cases where $p_h \in Q_h^1$ or when the surface tension force f_Γ is discretized by f_{Γ_h} . For the L^2 and H^1 -norm of the velocity error the convergence orders are $\mathcal{O}(h^{3/2})$ and $\mathcal{O}(h^{1/2})$, respectively, which is similar to the results in test case A.

We emphasize that only for the *combination* of the extended pressure finite element space $Q_h^{\Gamma_h}$ with the improved approximation \tilde{f}_{Γ_h} we achieve $\mathcal{O}(h^\alpha)$ convergence with $\alpha \geq 1$ for the pressure L^2 -error. The velocity error in the H^1 -norm shows a similar behavior (at least first order convergence), in the L^2 -norm we even have second order convergence, cf. Table 7.18.

For the improved Laplace-Beltrami discretization \tilde{f}_{Γ_h} the corresponding pressure solutions $p_h \in Q_h^1$ and $p_h \in Q_h^{\Gamma_h}$ are shown in Fig. 7.19. For the standard pressure space Q_h^1 we observe oscillations of the pressure at the interface inducing large spurious velocities in that region as shown in Fig. 7.20. For the XFEM pressure space $Q_h^{\Gamma_h}$ the pressure jump can be accurately resolved leading to a very large reduction of spurious velocities. In Fig. 7.21, on the left we illustrate these spurious velocities on the same scale as in Fig. 7.20 and on the right multiplied by a factor 20.

# ref.	$\ e_p\ _{L^2}$ for $p_h \in Q_h^1$				$\ e_p\ _{L^2}$ for $p_h \in Q_h^{\Gamma_h}$			
	f_{Γ_h}	order	\tilde{f}_{Γ_h}	order	f_{Γ_h}	order	\tilde{f}_{Γ_h}	order
0	1.60 E+0	–	1.60 E+0	–	3.12 E-1	–	1.64 E-1	–
1	1.07 E+0	0.57	1.07 E+0	0.57	1.00 E-1	1.64	4.97 E-2	1.73
2	8.23 E-1	0.38	8.23 E-1	0.38	6.24 E-2	0.68	1.66 E-2	1.58
3	5.80 E-1	0.51	5.80 E-1	0.51	4.28 E-2	0.54	7.16 E-3	1.22
4	4.13 E-1	0.49	4.13 E-1	0.49	2.95 E-2	0.54	2.83 E-3	1.34

Table 7.17. Pressure errors for the (\mathbf{V}_h, Q_h^1) and $(\mathbf{V}_h, Q_h^{\Gamma_h})$ finite element pair and different discretizations of f_Γ .

# ref.	$\ e_u\ _{L^2}$	order	$\ e_u\ _1$	order
0	7.16 E-3	–	1.10 E-1	–
1	1.57 E-3	2.19	4.26 E-2	1.37
2	3.25 E-4	2.28	1.70 E-2	1.33
3	8.57 E-5	1.92	7.43 E-3	1.19
4	1.75 E-5	2.29	2.40 E-3	1.63

Table 7.18. Errors and numerical order of convergence for the $(\mathbf{V}_h, Q_h^{\Gamma_h})$ finite element pair and improved Laplace-Beltrami discretization \tilde{f}_{Γ_h} .

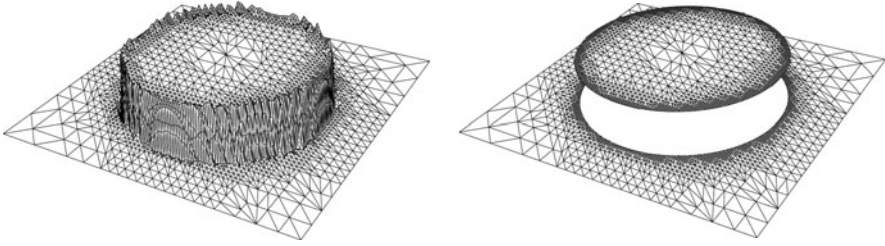


Fig. 7.19. Finite element pressure solution $p_h \in Q_h^1$ (left) and $p_h \in Q_h^{\Gamma_h}$ (right), visualized on slice at $x_3 = 0$.

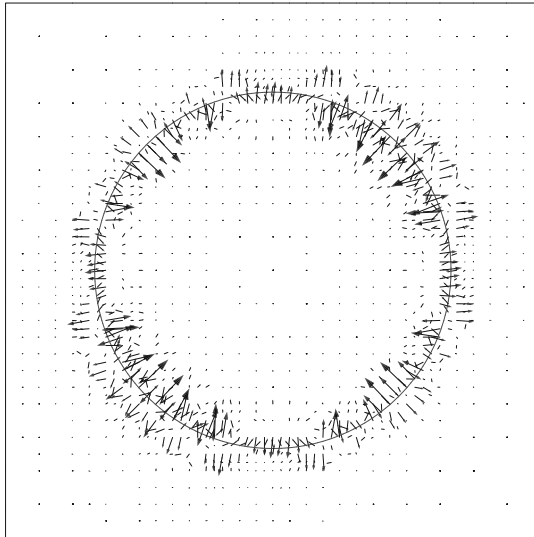


Fig. 7.20. Velocity \mathbf{u}_h for the case $p_h \in Q_h^1$, visualized on slice at $x_3 = 0$.

μ -dependence of the errors

We repeated the computations of $(\mathbf{u}_h, p_h) \in \mathbf{V}_h \times Q_h^{\Gamma_h}$ for the improved Laplace-Beltrami discretization \tilde{f}_{Γ_h} on the fixed grid \mathcal{T}_3 varying the viscosity μ . The errors are given in Table 7.19. We clearly observe that the velocity errors are proportional to μ^{-1} whereas the pressure error is independent of μ . This confirms the bound in (7.131).

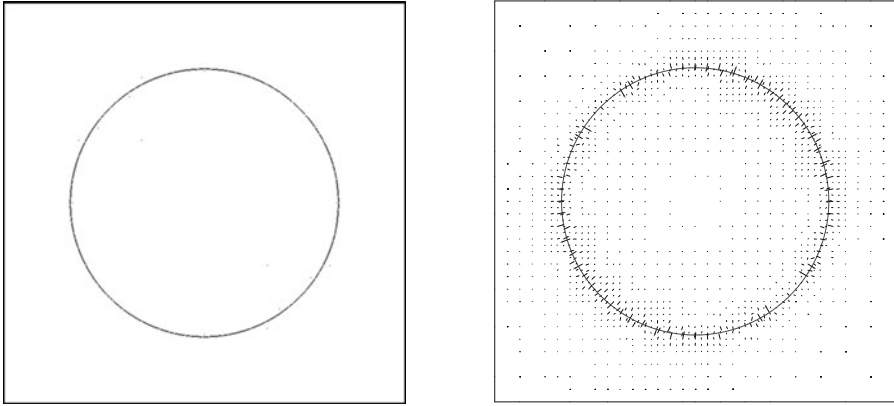


Fig. 7.21. Velocity \mathbf{u}_h for the case $p_h \in Q_h^{\Gamma_h}$ (left) and magnified by a factor 20 (right), visualized on slice at $x_3 = 0$.

μ	$\ e_{\mathbf{u}}\ _{L^2}$	$\ e_{\mathbf{u}}\ _1$	$\ e_p\ _{L^2}$
10	8.62 E-6	7.51 E-4	8.71 E-3
1	8.57 E-5	7.43 E-3	7.16 E-3
0.1	8.58 E-4	7.44 E-2	6.87 E-3
0.01	8.57 E-3	7.44 E-1	6.88 E-3
0.001	8.57 E-2	7.43 E+0	7.16 E-3

Table 7.19. Errors for the $(\mathbf{V}_h, Q_h^{\Gamma_h})$ finite element pair and improved Laplace-Beltrami discretization \tilde{f}_{Γ_h} on T_3 for different viscosities μ .

Condition numbers of scaled mass matrix

We consider the XFEM space $Q_h^{\Gamma_h}$, $h = h_i = 2^{-i-1}$, $i = 0, \dots, 4$, used in the static droplet example from above. For this space we determined the mass matrix \mathbf{M}_h . With $\mathbf{D}_h := \text{diag}(\mathbf{M}_h)$ we computed the spectral condition number of $\mathbf{D}_h^{-1}\mathbf{M}_h$, i.e., $\text{cond}(\mathbf{D}_h^{-1}\mathbf{M}_h) = \lambda_{\max}(\mathbf{D}_h^{-1}\mathbf{M}_h)/\lambda_{\min}(\mathbf{D}_h^{-1}\mathbf{M}_h)$. For $h = h_i$, $i = 0, \dots, 4$, the results are given in Table 7.20.

i	$\text{cond}(\mathbf{D}_h^{-1}\mathbf{M}_h)$
0	16.16
1	11.24
2	12.08
3	12.93
4	12.98

Table 7.20. Spectral condition number of the scaled XFEM mass matrix.

These results clearly show the uniform boundedness of the spectral condition number of the scaled mass matrix, as proved in Theorem 7.9.7.

LBB-stability

In the theoretical analysis, in particular in Theorem 7.10.3, we assume that the pair of spaces that is used is LBB-stable. The standard P_2 - P_1 Hood-Taylor pair (\mathbf{V}_h, Q_h^1) is known to be LBB-stable. An obvious question is what happens with stability if for the pressure instead of Q_h^1 we take the (larger) space \tilde{Q}_h^Γ . We do not have a satisfactory theoretical analysis of this stability issue, yet. Here we present results of a numerical experiment for the static droplet example from above. We consider this problem with the discretization pair $(\mathbf{V}_h, \tilde{Q}_h^{\Gamma_h})$. The matrix representation of this discrete problem leads to a symmetric saddle point problem of the form

$$\mathbf{K}_h = \begin{pmatrix} \mathbf{A}_h & \mathbf{B}_h^T \\ \mathbf{B}_h & 0 \end{pmatrix}.$$

Recall that $h = h_i = 2^{-i-1}$, $i = 0, \dots, 4$. The Schur complement matrix is given by $\mathbf{S}_h = \mathbf{B}_h \mathbf{A}_h^{-1} \mathbf{B}_h^T$. The LBB-constant for the $(\mathbf{V}_h, \tilde{Q}_h^{\Gamma_h})$ pair with $h = h_i$ is given by

$$C_{LBB}(i) = \inf_{p_h \in \tilde{Q}_h^{\Gamma_h,*}} \sup_{\mathbf{v} \in \mathbf{V}_h} \frac{(\operatorname{div} \mathbf{v}_h, p_h)_{L^2}}{\|\nabla \mathbf{v}_h\|_{L^2} \|p_h\|_{L^2}},$$

where $\tilde{Q}_h^{\Gamma_h,*}$ contains all functions from $\tilde{Q}_h^{\Gamma_h}$ that are L^2 -orthogonal to the constant. Let \mathbf{M}_h be the mass matrix in $\tilde{Q}_h^{\Gamma_h}$ and $m = m_i = \dim(\tilde{Q}_h^{\Gamma_h})$. Define $\mathbb{R}^{m,*} = \{\mathbf{y} \in \mathbb{R}^m : \langle \mathbf{y}, \mathbf{M}_h \mathbf{e} \rangle = 0\}$, with $\mathbf{e} := (1, 1, \dots, 1)^T$. The LBB constant can also be represented as follows, cf. (5.106),

$$C_{LBB}^2(i) = \inf_{\mathbf{y} \in \mathbb{R}^{m,*}} \frac{\langle \mathbf{S}_h \mathbf{y}, \mathbf{y} \rangle}{\langle \mathbf{M}_h \mathbf{y}, \mathbf{y} \rangle}, \tag{7.134}$$

and thus $C_{LBB}^2(i)$ is the smallest nonzero eigenvalue of $\mathbf{M}_h^{-1} \mathbf{S}_h$. Due to the fact that \mathbf{M}_h is uniformly spectrally equivalent to its diagonal \mathbf{D}_h we can instead consider the smallest nonzero eigenvalue of $\mathbf{D}_h^{-\frac{1}{2}} \mathbf{S}_h \mathbf{D}_h^{-\frac{1}{2}}$ which is denoted by $\lambda_{\min}^*(\mathbf{D}_h^{-1} \mathbf{S}_h)$. This eigenvalue can be approximated accurately using, for example, an inverse power iteration. In each iteration of this method the linear systems with matrix $\mathbf{D}_h^{-\frac{1}{2}} \mathbf{S}_h \mathbf{D}_h^{-\frac{1}{2}}$ can be solved using a CG method. We implemented this and computed (with sufficiently high accuracy) this smallest eigenvalue for several mesh sizes and for different values of the ‘‘cut-off’’ parameter \hat{c} used in the definition of $\tilde{Q}_h^{\Gamma_h}$, cf. (7.110). The resulting values are presented in Table 7.21. Note that $\hat{c} = \infty$ corresponds to the space $Q_h = Q_h^1$. The rather irregular behavior in the columns in Table 7.21 may be caused by the fact that we compute the smallest nonzero eigenvalue of $\mathbf{D}_h^{-1} \mathbf{S}_h$ and not

of $\mathbf{M}_h^{-1}\mathbf{S}_h$. We observe that for the full extended space $Q_h^{\Gamma_h}$, which coincides with $\tilde{Q}_h^{\Gamma_h}$ for $\hat{c} = 10^{-4}$, the LBB quantity $C_{LBB}^2(i)$ strongly deteriorates if i is increased. Hence, we conclude that with respect to LBB-stability it seems to be important (at least in this experiment) to use the *reduced* XFEM space $\tilde{Q}_h^{\Gamma_h}$ with a not too small parameter \hat{c} .

i	$\hat{c} = \infty$	$\hat{c} = 10$	$\hat{c} = 1$	$\hat{c} = 0.1$	$\hat{c} = 0.01$	$\hat{c} = 0.0001$
0	9.53 E-2	9.53 E-2	9.53 E-2	4.65 E-2	1.43 E-2	1.43 E-2
1	2.53 E-2	2.53 E-2	2.53 E-2	2.53 E-2	1.53 E-2	6.49 E-3
2	3.22 E-2	3.22 E-2	3.22 E-2	2.97 E-2	1.07 E-2	1.97 E-4
3	2.58 E-2	2.58 E-2	2.58 E-2	2.16 E-2	3.17 E-3	3.37 E-5
4	9.17 E-2	9.17 E-2	5.91 E-2	1.12 E-3	1.60 E-3	1.32 E-5

Table 7.21. Estimates of smallest nonzero eigenvalue of preconditioned Schur complement $\mathbf{D}_h^{-1}\mathbf{S}_h$.

7.11 Finite element discretization of two-phase flow problem

7.11.1 Spatial finite element discretization

In this section we combine the methods described in the previous sections to obtain a *semi*-discretization of a two-phase flow model. We recall the model given in (6.59): Find $\mathbf{u}(t) = \mathbf{u}(\cdot, t) \in \mathbf{V}_D$, $p(t) = p(\cdot, t) \in Q$, $\phi(t) = \phi(\cdot, t) \in W_{\mathbf{u},D}$ such that for almost all $t \in [0, T]$

$$\begin{aligned}
 & m\left(\frac{\partial \mathbf{u}}{\partial t}, \mathbf{v}\right) + a(\mathbf{u}, \mathbf{v}) \\
 & + c(\mathbf{u}; \mathbf{u}, \mathbf{v}) + b(\mathbf{v}, p) = (\rho \mathbf{g}, \mathbf{v})_{L^2} + f_\Gamma(\mathbf{v}) \text{ for all } \mathbf{v} \in \mathbf{V}_0, \\
 & b(\mathbf{u}, q) = 0 \text{ for all } q \in Q,
 \end{aligned} \tag{7.135}$$

$$\left(\frac{\partial \phi}{\partial t}, v\right)_{L^2} + (\mathbf{u} \cdot \nabla \phi, v)_{L^2} = 0 \text{ for all } v \in L^2(\Omega),$$

together with initial conditions $\mathbf{u}(0) = \mathbf{u}_0$, $\phi(0) = \phi_0$ in Ω . The notation is as in Sect. 6.3:

$$\begin{aligned}
 \mathbf{V} & := H^1(\Omega)^3, \\
 \mathbf{V}_0 & := \{ \mathbf{v} \in \mathbf{V} : \mathbf{v} = 0 \text{ on } \partial\Omega_D \}, \\
 \mathbf{V}_D & := \{ \mathbf{v} \in \mathbf{V} : \mathbf{v} = \mathbf{u}_D \text{ on } \partial\Omega_D \}, \\
 Q & := L_0^2(\Omega) = \left\{ q \in L^2(\Omega) : \int_\Omega q \, dx = 0 \right\}, \\
 W_{\mathbf{u},D} & := \{ w \in L^2(\Omega) : \mathbf{u} \cdot \nabla w \in L^2(\Omega), w|_{\partial\Omega_{in}} = \phi_D \},
 \end{aligned}$$

and

$$\begin{aligned}
 m(\mathbf{u}, \mathbf{v}) &:= \int_{\Omega} \rho \mathbf{u} \mathbf{v} \, dx, \\
 a(\mathbf{u}, \mathbf{v}) &:= \frac{1}{2} \int_{\Omega} \mu \operatorname{tr}(\mathbf{D}(\mathbf{u})\mathbf{D}(\mathbf{v})) \, dx, \\
 b(\mathbf{v}, q) &:= - \int_{\Omega} q \operatorname{div} \mathbf{v} \, dx, \\
 c(\mathbf{u}; \mathbf{v}, \mathbf{w}) &:= \int_{\Omega} \rho(\mathbf{u} \cdot \nabla \mathbf{v}) \mathbf{w} \, dx, \\
 f_{\Gamma}(\mathbf{v}) &:= -\tau \int_{\Gamma} \kappa \mathbf{n} \cdot \mathbf{v} \, ds.
 \end{aligned}$$

For the spatial discretization of this model we use the following methods:

- We construct *nested tetrahedral triangulations* $\{\mathcal{T}_h\}$ in the same way as for the one-phase flow problem, cf. Sect. 3.1.
- We apply streamline diffusion discretization of the level set equation, cf. Sect. 7.2.2, with piecewise *quadratic* finite elements. The space of piecewise quadratics is denoted by V_h .
- A polyhedral approximation Γ_h of Γ is constructed, as described in Sect. 7.3.
- For discretization of the velocity variable \mathbf{u} we use the standard FE space of piecewise quadratics. The spaces are denoted by \mathbf{V}_h ($\mathbf{v}_h = 0$ on $\partial\Omega_D$) and $\mathbf{V}_{D,h}$ ($\mathbf{v}_h =$ interpolation of \mathbf{u}_D on $\partial\Omega_D$).
- Discretization of f_{Γ} by \tilde{f}_{Γ_h} as explained in Sect. 7.6.
- For the discretization of the pressure variable p we use the extended finite element space $\tilde{Q}_h^{\Gamma_h}$, cf. Sect. 7.9.2. Default we use the variant in which new basis functions with “very small” support are deleted from the extended space (Sect. 7.9.3).

For the Galerkin discretization of the problem in (7.135) we proceed in the same way as for the one-phase Navier-Stokes equation. The semi-discretization reads as follows: Find $\mathbf{u}_h(t) \in \mathbf{V}_{D,h}$, $p_h(t) \in \tilde{Q}_h^{\Gamma_h}$ and $\phi_h(t) \in V_h(\phi_D)$ such that for $t \in [0, T]$:

$$\begin{aligned}
 m\left(\frac{\partial \mathbf{u}_h}{\partial t}(t), \mathbf{v}_h\right) + a(\mathbf{u}_h(t), \mathbf{v}_h) + c(\mathbf{u}_h(t); \mathbf{u}_h(t), \mathbf{v}_h) \\
 + b(\mathbf{v}_h, p_h(t)) = m(\mathbf{g}, \mathbf{v}_h) + \tilde{f}_{\Gamma_h}(\mathbf{v}_h) \quad \forall \mathbf{v}_h \in \mathbf{V}_h, \\
 b(\mathbf{u}_h(t), q_h) = 0 \quad \forall q_h \in Q_h^{\Gamma_h}, \tag{7.136} \\
 \sum_{T \in \mathcal{T}_h} \left(\frac{\partial \phi_h}{\partial t}(t) + \mathbf{u}_h(t) \cdot \nabla \phi_h(t), v_h + \delta_T \mathbf{u}_h(t) \cdot \nabla v_h\right)_{L^2(T)} = 0 \quad \forall v_h \in V_h.
 \end{aligned}$$

Clearly, this is a method of lines approach. The finite element spaces \mathbf{V}_h and V_h used for discretization of the velocity and of the level set function can be considered to be *independent* of t . The level set function trial space $V_h(\phi_D)$ depends on t if the inflow boundary data ϕ_D depend on t . If at a certain time $t = T_0 > 0$ the triangulation is adapted (local refinement and/or coarsening), the computed discrete solutions at $t = T_0$ are interpolated on the new triangulations. Then the next time interval $[T_0, T_1]$ can be treated by the method of lines with fixed discretization spaces \mathbf{V}_h and V_h , that differ from those used on the previous interval $[0, T_0]$. If in the two-phase flow problem the interface is *stationary* then the pressure discretization space $\tilde{Q}_h^{\Gamma_h}$ can also be considered to be *independent* of t . In the more interesting case in which there is an evolving interface there is a strong *dependence* of $\tilde{Q}_h^{\Gamma_h}$ on t . In that case a method of lines discretization as in (7.136) induces difficulties regarding the time discretization and it is more natural to use a Rothe approach, cf. Remark 4.2.2. We come back to this issue in Sect. 8.1.2.

Let $\{\boldsymbol{\xi}_j\}_{1 \leq j \leq N}$, $\{\psi_j\}_{1 \leq j \leq K}$ and $\{\xi_j\}_{1 \leq j \leq L}$ be (nodal) bases of \mathbf{V}_h , $\tilde{Q}_h^{\Gamma_h}$ and V_h , respectively. We emphasize again, that in case of an evolving interface we have $\tilde{Q}_h^{\Gamma_h} = \tilde{Q}_h^{\Gamma_h}(t)$ and thus in particular $K = K(t)$. The bases induce corresponding representations of the finite element functions in vector form. Functions $\mathbf{u}_h(t) \in \mathbf{V}_h$, $p_h(t) \in Q_h$ and $\phi_h(t) \in V_h$ can be represented as:

$$\begin{aligned} \mathbf{u}_h(t) &= \sum_{j=1}^N u_j(t) \boldsymbol{\xi}_j, & \vec{\mathbf{u}}(t) &:= (u_1(t), \dots, u_N(t)), \\ p_h(t) &= \sum_{j=1}^K p_j(t) \psi_j, & \vec{\mathbf{p}}(t) &:= (p_1(t), \dots, p_K(t)), \\ \phi_h(t) &= \sum_{j=1}^L \phi_j(t) \xi_j + b_h(t), & \vec{\boldsymbol{\phi}}(t) &:= (\phi_1(t), \dots, \phi_L(t)), \end{aligned}$$

with $b_h(t) \in V_h(\phi_D)$ such that $b_h(t)(x) = \phi_D(x, t)$ for all $x \in \mathcal{V}(\partial\Omega_{in})$ and $b_h(t)(x) = 0$ for all other vertices x , cf. (7.15). For $\phi_h \in V_h(\phi_D)$ and $\mathbf{u}_h \in \mathbf{V}_h$ (or $\mathbf{V}_{D,h}$) we introduce the following (mass and stiffness) matrices:

$$\begin{aligned}
 \mathbf{M}(\phi_h) &\in \mathbb{R}^{N \times N}, & \mathbf{M}(\phi_h)_{ij} &= \int_{\Omega} \rho(\phi_h) \boldsymbol{\xi}_i \cdot \boldsymbol{\xi}_j \, dx, \\
 \mathbf{A}(\phi_h) &\in \mathbb{R}^{N \times N}, & \mathbf{A}(\phi_h)_{ij} &= \frac{1}{2} \int_{\Omega} \mu(\phi_h) \operatorname{tr}(\mathbf{D}(\boldsymbol{\xi}_i) \mathbf{D}(\boldsymbol{\xi}_j)) \, dx, \\
 \mathbf{B}(\phi_h) &\in \mathbb{R}^{K \times N}, & \mathbf{B}(\phi_h)_{ij} &= - \int_{\Omega} \psi_i \operatorname{div} \boldsymbol{\xi}_j \, dx, \\
 \mathbf{N}(\phi_h, \mathbf{u}_h) &\in \mathbb{R}^{N \times N}, & \mathbf{N}(\phi_h, \mathbf{u}_h)_{ij} &= \int_{\Omega} \rho(\phi_h) (\mathbf{u}_h \cdot \nabla \boldsymbol{\xi}_j) \cdot \boldsymbol{\xi}_i \, dx, \\
 \mathbf{E}(\mathbf{u}_h) &\in \mathbb{R}^{L \times L}, & \mathbf{E}(\mathbf{u}_h)_{ij} &= \sum_{T \in \mathcal{T}_h} \int_T \xi_j (\xi_i + \delta_T \mathbf{u}_h \cdot \nabla \xi_i) \, dx, \\
 \mathbf{H}(\mathbf{u}_h) &\in \mathbb{R}^{L \times L}, & \mathbf{H}(\mathbf{u}_h)_{ij} &= \sum_{T \in \mathcal{T}_h} \int_T (\mathbf{u}_h \cdot \nabla \xi_j) (\xi_i + \delta_T \mathbf{u}_h \cdot \nabla \xi_i) \, dx.
 \end{aligned}$$

We also need the following vectors:

$$\begin{aligned}
 \vec{\mathbf{g}}(\phi_h) &\in \mathbb{R}^N, & \vec{\mathbf{g}}(\phi_h)_i &= \int_{\Omega} \rho(\phi_h) \mathbf{g} \cdot \boldsymbol{\xi}_i \, dx, \\
 \vec{\mathbf{f}}_{\Gamma_h}(\phi_h) &\in \mathbb{R}^N, & \vec{\mathbf{f}}_{\Gamma_h}(\phi_h)_i &= \vec{f}_{\Gamma_h}(\boldsymbol{\xi}_i), \\
 \mathbf{b}(\mathbf{u}_h) &\in \mathbb{R}^L, & \mathbf{b}(\mathbf{u}_h)_i &= \sum_{T \in \mathcal{T}_h} \int_T \left(\frac{\partial b_h}{\partial t} + \mathbf{u}_h \cdot \nabla b_h \right) (\xi_i + \delta_T \mathbf{u}_h \cdot \nabla \xi_i) \, dx.
 \end{aligned}$$

Below we write $\vec{\mathbf{M}}(\vec{\phi}(t)) := \mathbf{M}(\phi_h)$, and similarly for other matrices and vectors. Using these notations we obtain the following equivalent formulation of the coupled system of ordinary differential equations (7.136), where for simplicity we assumed $\mathbf{u}_D = 0$: Find $\vec{\mathbf{u}}(t) \in \mathbb{R}^N$, $\vec{\mathbf{p}}(t) \in \mathbb{R}^K$ and $\vec{\phi}(t) \in \mathbb{R}^L$ such that for all $t \in [0, T]$

$$\begin{aligned}
 \vec{\mathbf{M}}(\vec{\phi}(t)) \frac{d\vec{\mathbf{u}}}{dt}(t) + \vec{\mathbf{A}}(\vec{\phi}(t)) \vec{\mathbf{u}}(t) + \vec{\mathbf{N}}(\vec{\phi}(t), \vec{\mathbf{u}}(t)) \vec{\mathbf{u}}(t) + \vec{\mathbf{B}}(\vec{\phi}(t))^T \vec{\mathbf{p}}(t) \\
 = \vec{\mathbf{g}}(\vec{\phi}(t)) + \vec{\mathbf{f}}_{\Gamma_h}(\vec{\phi}(t)), \tag{7.137a}
 \end{aligned}$$

$$\vec{\mathbf{B}}(\vec{\phi}(t)) \vec{\mathbf{u}}(t) = 0, \tag{7.137b}$$

$$\vec{\mathbf{E}}(\vec{\mathbf{u}}(t)) \frac{d\vec{\phi}}{dt}(t) + \vec{\mathbf{H}}(\vec{\mathbf{u}}(t)) \vec{\phi}(t) = -\mathbf{b}(\vec{\mathbf{u}}(t)). \tag{7.137c}$$

In addition we have initial conditions for $\vec{\mathbf{u}}$ and $\vec{\phi}$.

7.11.2 Numerical experiment with a two-phase flow problem

In Sect. 1.3.1 we presented simulation results of a rising butanol droplet in water, which is a system with a rather small surface tension coefficient

$\tau = 1.63 \cdot 10^{-3} \text{ N/m}$. In this section we consider a similar rising droplet example, but now for a toluene-water system, where the surface tension coefficient is about 20 times larger. Hence, compared to the butanol-water system the numerical simulation of the fluid dynamics in the toluene-water system is (much) more challenging for the applied numerical methods. Below we compare the numerical results obtained by applying the reduced XFEM pressure space $\tilde{Q}_h^{\Gamma_h}$ and the standard FEM pressure space Q_h^1 of piecewise linears.

We use the standard two-phase model described in (7.135). Consider a single toluene droplet with an initial spherical shape with radius $r = 10^{-3} \text{ m}$ inside a rectangular tank $\Omega = [0, 12 \cdot 10^{-3}] \times [0, 30 \cdot 10^{-3}] \times [0, 12 \cdot 10^{-3}] \text{ m}^3$ filled with water, cf. Fig. 1.8. The material properties of this two-phase system are given in Table 7.22. Note that the properties of water slightly differ from those in Table 1.1 which is due to the fact that in the real experiment the water was saturated with toluene at an equilibrium state to avoid any mass transfer between the droplet and the ambient phase. Gravitation acts in negative x_2 -direction, i. e., $\mathbf{g} = (0, -9.81, 0) \text{ m/s}^2$. Initially at rest ($\mathbf{u}_0 = 0 \text{ m/s}$) the bubble starts to rise in x_2 -direction due to buoyancy effects.

quantity (unit)	toluene	water
$\rho \quad (\text{kg/m}^3)$	867.5	998.8
$\mu \quad (\text{kg/m s})$	$5.96 \cdot 10^{-4}$	$1.029 \cdot 10^{-3}$
$\tau \quad (\text{N/m})$	$34.31 \cdot 10^{-3}$	

Table 7.22. Material properties of the system toluene/water.

For the initial triangulation \mathcal{T}_0 the domain Ω is subdivided into $4 \times 10 \times 4$ sub-cubes each consisting of 6 tetrahedra. Then the grid is refined four times in the vicinity of the interface Γ . As time evolves the grid is adapted to the moving interface. The velocity space \mathbf{V}_h consists of piecewise quadratics and the pressure is either discretized using the reduced XFEM space $\tilde{Q}_h^{\Gamma_h}$ with $\tilde{c} = 1$ or the standard finite element space Q_h^1 consisting of piecewise linears. The surface tension force term is discretized using the modified Laplace-Beltrami discretization \tilde{f}_{Γ_h} as in (7.60). The level set function is discretized by piecewise quadratics and streamline-diffusion stabilization. A re-initialization $\text{ReInit}(\phi_h)$ is performed as defined in (7.44) with $c = 10$. Mass conservation is forced in each time step as described in Sect. 7.4.2. For time discretization the decoupled implicit Euler scheme is applied with $\Delta t = 5 \cdot 10^{-4}$, cf. (8.23).

Figure 7.22 shows the initial shape of the droplet and the droplet shapes after 10 time steps for the cases $Q_h = \tilde{Q}_h^{\Gamma_h}$ and $Q_h = Q_h^1$, respectively. While the interface is smooth using the extended pressure finite element space, it shows many “spikes” in the case of the standard pressure space. These spikes are of course non-physical and only caused by numerical oscillations at the interface,

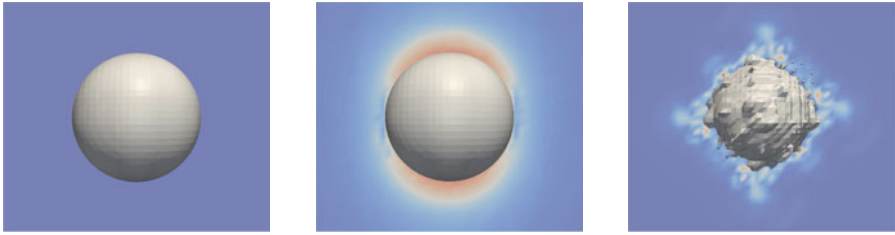


Fig. 7.22. Initial droplet shape (left) and after 10 time steps for the XFEM case (middle) and the standard FEM case (right).

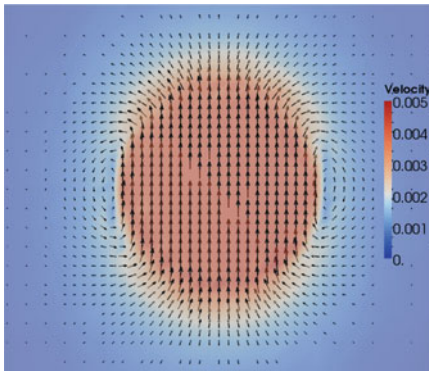


Fig. 7.23. Velocity field at interface for the XFEM case.

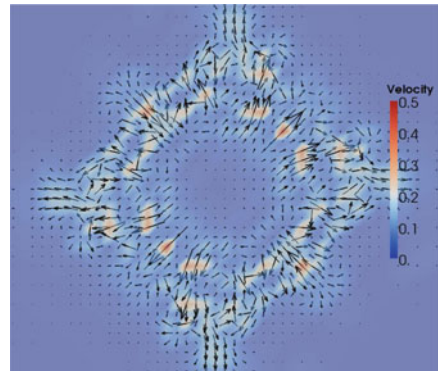


Fig. 7.24. Velocity field at interface for the standard FEM case.

so-called *spurious velocities*, which are shown in Fig. 7.24. The velocity field for the XFEM case $Q_h = \tilde{Q}_h^{\Gamma_h}$ is smooth showing the characteristic vortices, cf. Fig. 7.23. Note that the scaling of the color coding in both figures is very different, with a maximum velocity of $5 \cdot 10^{-3} m$ for the extended pressure space compared to $5 \cdot 10^{-1} m$ for the standard pressure space. These results clearly show, that for this realistic two-phase flow example the standard pressure space Q_h^1 is not suitable, whereas the (reduced) extended pressure space $\tilde{Q}_h^{\Gamma_h}$ yields satisfactory results.